

Use of Sodium Sulfate Separated from Agricultural Drainage Water in Glass Making

Final Report

June 2006

Prepared for
Department of Water Resources
California

TASK ORDER T04
Interagency Agreement B81907 (4600000543-01)

P. Thy¹ and B.M. Jenkins²

¹Department of Geology

²Department of Biological and Agricultural Engineering
University of California at Davis



UC DAVIS
UNIVERSITY OF CALIFORNIA

Addresses:

P. Thy¹

B.M. Jenkins²

¹ Department of Geology

² Department of Biological and Agricultural Engineering

University of California

One Shields Avenue

Davis CA 95616

thy@geology.ucdavis.edu (P. Thy)

bmjenkins@ucdavis.edu (B.M. Jenkins)

The illustration on front is a typical window glass produced from using sodium carbonate as source for sodium. Fired for 6 hours at 1300 °C. Container is 40 mm in diameter (10 ml) (SNC-E-18).



Frontispiece. Glass batch made from 3 kg flat glass mixture based on purified natural sodium sulfate as source of sodium. Fired for 4 days at 1300 °C. The container is 12 cm in diameter and 15.5 cm deep and filled to 2 cm from the top rim.

Acknowledgements

We are grateful to the California Department of Water Resources and the US EPA for funding this study. We have received generous help and access to software and instruments from the NEAT-ORU, Thermochemistry Facility and the Microprobe Laboratory, Department Geology, University of California, Davis. Dae Hyun Kim and Matt Yore, Department of Biological and Agricultural Engineering provided purified salt.

Disclaimer. Publication of any finding or recommendation in this report should not be construed as representing the opinion or conclusion of the California Department of Water Resources. Also, mention of trade names or commercial products does not constitute endorsement or recommendation on the part of the University of California or the California Department of Water Resources.

Table of Contents

	Page
Abstract -----	4
Introduction -----	7
Glass Making -----	7
Raw Materials and Melting -----	7
Sodium Sulfate in Glass Making -----	9
Sodium Sulfate used in this Study -----	11
Decomposition and Melting of Sulfates and Carbonates -----	17
Calcium Carbonate -----	17
Sodium Carbonate -----	18
Sodium Sulfate -----	19
Silicate Melt -----	20
Thermodynamic Modeling of Glass Melting -----	21
Experimental Procedures -----	26
Experimental Methods -----	26
Analytical Procedures -----	27
Preparation of Glass Mixtures -----	28
Experimental Results -----	30
Predicted Melting Temperature -----	30
Exploratory Experiments -----	31
Container and Container Volume -----	33
Melting Temperature -----	34
Effect of Composition -----	35
Heterogeneity of Glass Mixture -----	38
Cooling Rate Effects -----	38
Melting Duration -----	39
Crystallization and Devitrification -----	42
Reaction with Container -----	52
Sodium Sulfate Coating -----	53
Sodium Loss -----	58
Physical Properties of Molten Glass and Sodium Sulfate -----	60
Discussion -----	62
Formation of Sulfate Coating -----	62
Crystallization and Devitrification -----	65
Optimal Conditions for Glass Formation -----	66
Summary and Conclusions -----	68
References -----	69

List of Tables

Table 1. Typical flat glass composition -----	9
Table 2. Composition of pond evaporite (Rainbow Ranch) -----	11
Table 3. Interpretation of X-ray diffraction pattern for evaporite pond salt -----	13
Table 4. Interpretation of X-ray diffraction pattern mirabilite and thenardite mixture -----	15
Table 5. Mixtures used for thermodynamic modeling -----	21
Table 6. Chemical components used for producing mixtures -----	28

Table 7. Summary of mixtures of sulfate based ‘window’ glass -----	29
Table 8. Compositions of mixtures based on natural evaporation pond salt -----	29
Table 9. Experimental results -----	31
Table 10. Average glass compositions -----	37
Table 11. Interpretation of X-ray diffraction pattern for devitrified glass -----	43
Table 12. Effect of devitrification on glass composition-----	47
Table 13. Effect of reaction with container-----	52
Table 14. Interpretation of X-ray diffraction pattern for sulfate coating -----	55
Table 15. Mineralogy of sulfate coating (SNC-I-26) -----	58
Table 16. Estimated losses of sulfur and sodium (SNC-I-26) -----	59

List of Figures

Figure 1. Part of the ternary system $\text{Na}_2\text{O}-\text{CaO}-\text{SiO}_2$ of interest to glass making -----	9
Figure 2. X-ray diffraction pattern for evaporation salts -----	12
Figure 3. X-ray diffraction pattern for a mixture of mirabilite and thenardite -----	14
Figure 4. Summary decomposition equilibria of carbonates and sulfate -----	16
Figure 5. Release of CO_2 as a function of time from firing calcium carbonate-----	17
Figure 6. Release of CO_2 as a function of time from firing sodium carbonate -----	18
Figure 7. Release of SO_2 as a function of time from firing sodium sulfate. -----	19
Figure 8. Sodium sulfate coating after firing sodium sulfate -----	19
Figure 9. Release of SO_2 and CO_2 as a function of time from firing typical glass mixture -----	20
Figure 10. Phase equilibria predicted by FactSage modeling -----	22
Figure 11. Composition of sulfate (solid and melt) as a function of temperature -----	23
Figure 12. Liquidus depression as a function of sodium sulfate in mixture -----	23
Figure 13. Composition of the gas phase as a function of fraction of sodium sulfate -----	24
Figure 14. Silicate liquid composition as a function of temperature and sulfate fraction -----	25
Figure 15. Thermocraft furnace used in the experimental work -----	26
Figure 16. Glass mixtures plotted in the ternary $\text{SiO}_2-\text{CaO}-\text{Na}_2\text{O}$ system -----	30
Figure 17. Glass produced from standard window glass composition without sodium sulfate---	32
Figure 18. Glass produced from standard window glass composition with sodium sulfate-----	32
Figure 19. Unmelted glass batch in thick-walled container-----	33
Figure 20. Mixture C melted in small containers -----	34
Figure 21. Second remelting at 1450°C of unmelted product-----	35
Figure 22. Set of experiments done at same temperature and duration-----	36
Figure 23. Temperature as a function of duration cooling rate-----	39
Figure 24. Effect of melting duration -----	40
Figure 25. Accumulative effect of remelting-----	41
Figure 26. BSE images of experimental product of SNC-C-16 -----	42
Figure 27. X-ray diffraction pattern for SNC-C-16-----	43
Figure 28. BSE Image of tridymite growth forms in SNC-H-23-----	44
Figure 29. Experimental product of SNC-H-25-----	45
Figure 30. Cross section of partially devitrified glass in SNC-H-25 -----	46
Figure 31. BSE close-up of the devitrified spheres in SNC-H-25 -----	47
Figure 32. BSE close-ups of devitrified spheres in SNC-H-25-----	48
Figure 33. Cross section of SNC-D-17-----	50
Figure 34. Composition of interstitial glass in SNC-D-17 -----	50

Figure 35. Variation in major oxides for SNC-H-22 -----	51
Figure 36. Variation in major oxides for SNC-H-23 -----	51
Figure 37. BSE image of SNC-C-23 showing reaction with container-----	52
Figure 38. Sulfate Coating on SNC-I-27c -----	53
Figure 39. Sulfate Coating on SNC-C-16-----	54
Figure 40. X-Ray Diffraction Pattern for Sulfate Coating on SNC-C-16 -----	54
Figure 41. X-Ray Diffraction Pattern for Sulfate Coating on SNC-I-26 -----	56
Figure 42. BSE Image and X-Ray Elemental Dot Maps for Sulfate Coating on SNC-I-26-----	56
Figure 43. Energy Dispersive Spectra of Bulk Sulfate and anhydrite Residual Grain-----	57
Figure 44. Anhydrite Grain -----	57
Figure 45. Loss of Na ₂ O from glass as a function of original sodium sulfate content -----	59
Figure 46. Density of molten sodium sulfate -----	60
Figure 47. Summary of calculated physical properties (density and surface tension) of glass ---	61
Figure 48. Part of ternary system with target and resultant compositions of glass-----	67

ABSTRACT

Industrial container and flat glasses are typically made using sodium carbonate as a source for sodium with the other components being quartz sand and calcite (calcium carbonate). We have investigated the effects of substituting natural and synthetic sodium sulfate for sodium carbonate in a typical soda-lime glass recipe.

The principal motivation has been to utilize sodium sulfate and other salts separated from agricultural drainage water in the San Joaquin Valley of California. Two sources of salt were used in the experiments and modeling described here: 1) a natural evaporation pond salt composed of 85 % (by weight) of thenardite (Na_2SO_4) and minor amounts of blodite ($\text{Na}_2\text{Mg}[\text{SO}_4]_2 \cdot 4\text{H}_2\text{O}$), and halite (NaCl), and 2) a purified sodium sulfate separated from agricultural drainage water using a pilot solar concentration and salt crystallization system. Precipitated salt from a solute is composed of relatively pure mirabilite ($\text{Na}_2\text{SO}_4 \cdot 10\text{H}_2\text{O}$) that during drying easily decomposes to thenardite. One of the outcomes of this study has been that it is essential that sodium sulfate (natural or precipitated) is thoroughly dried to remove water of crystal hydration and adsorbed water before use. Particularly, crystal bound water in sodium sulfate may adversely affect the composition of the product glass as well as its physical properties.

Small amounts (<2 %) of sodium sulfate have traditionally been used in glass making to enhance quartz sand dissolution and fining (removal of gas bubbles). However, use of large amounts of sodium sulfate has not previously been attempted undoubtedly because of the added complexity of dealing with the gaseous release of SO_2 in addition to CO_2 . Sodium sulfate decomposes in silicate melts by reacting with SiO_2 to form soda-lime-silica melt and SO_2 (or SO_3) and O_2 with SO_3 dominantly stable at relatively low temperatures.

We have investigated the release of CO_2 and SO_2 from pure sulfate and carbonates as well as from a sulfate based glass mixture. The decomposition and release of CO_2 from calcium carbonate and sodium carbonate occur at nearly similar temperatures of about 800 °C. In contrast, sodium sulfate appears to be stable as a melt to very high temperatures with appreciable decomposition from about 1300 °C. Mixtures of calcium carbonate, sodium sulfate, and silica representing a standard flat glass composition clearly show that carbonate decomposes at about 800 °C and sulfate at 1200-1300 °C. The formation of a sulfate melt and its preservation to high temperatures has been substantiated by thermochemical modeling showing that sodium sulfate melt is stable between 875-1200 °C. While sodium carbonate decomposes at approximately the same temperatures as calcium carbonate, sodium sulfate is stable with a silicate melt to relatively high temperatures within the melting interval of typical soda-lime glasses. Sulfur, in contrast to carbon, is also relatively soluble in silicate melt. The result is that the melting behavior, melt compositions, and physical melt properties during reaction and melting in soda-lime glasses depends on whether sulfate or carbonate is used as source for sodium. These striking differences in the behavior of sodium sulfate and sodium carbonate warrant direct experimental investigations.

We conducted melting experiments of a mixture of pure reagents of silica, calcium carbonate, sodium carbonate, and sodium sulfate as well as natural pond or precipitated sodium sulfate salt. The target composition for most experiments was 76.5 wt. % SiO_2 , 9.8 wt. % CaO , and 13.7 wt. % Na_2O , corresponding to a typical industrial flat glass composition. For some experiments, CaO and/or Na_2O were increased relative to SiO_2 to test compositional effects. The experiments were conducted in a large volume furnace controlled and monitored by $\text{Pt}^{90}\text{Pt}^{10}\text{Rh}$ thermocouples and used variously

sized alumina sample containers. The majority of experiments was conducted with a heating rate of 10 °C/min to a maximum of 1300 °C and was maintained at 1300 °C for 6 to 100 hours. The experiments were mostly terminated by shutting of the power to the furnace resulting in a cooling rate of about 90 °C/min. Tests were made to examine the effect of melting duration and cooling rate. It was shown that duration below 72-100 hours often would result in variable amounts of devitrification on the surface of the glass and along container contacts in extreme cases producing a massive milky white translucent glass. Duration above 72-100 hours in most cases would result in clear transparent glass. The observation that devitrification dominantly occurs on surfaces, container walls, and on preexisting unmelted grains suggest that nucleation occurs heterogeneously and that the studied compositions readily form glass upon cooling. We further tested the effect of cooling rates between 90 and 6 °C/min on the ability to form a glass without observing indications of nucleation and crystallization. Products melted for only a short duration often easily devitrified during cooling. Scanning electron microscope investigations suggest that for many of these, the devitrification occurred on preexisting crystalline grains. An increase of melting duration and/or temperature can be predicted to eliminate or reduce devitrification effects.

The chosen maximum melting temperature of 1300 °C was predicted to be well above liquidus conditions of about 1000-1100 °C for most glass mixtures. Despite this, some products showed crystallization and/or abundant devitrification resulting in a translucent white mixture composed of glass and tridymite crystals. The presence of tridymite was unexpected since the starting compositions were predicted to be saturated liquidus conditions in Ca-Na silicates and not in tridymite. This would suggest a major change in the starting composition during heating and melting, such as a partial loss in Na₂O in addition to SO₂ and CO₂. Direct analyses of glass products show that up to 60 % of the original content of Na₂O may have been lost during melting.

The experimental results clearly show that mixtures with high sodium sulfate often form a coating on glass surface. This coating is composed of a mixture of thenardite and glauberite (Na₂Ca[SO₄]₂) suggesting crystallization and low temperature exsolution from an original sulfate melt. Although we have no direct observations, we attribute this to gravity segregation of a sulfate melt from the silicate and accumulation on the surface. The calculated lower density and surface tension of sulfate melt compared to silicate melt as well as the thermodynamic observations support this. The sulfate coating appears in some experiments with above 25-28 wt. % sodium sulfate in the original glass mixture. The preservation of the sulfate coating is controlled by the rate of decomposition that can be increased by a flow of air through the furnace as well as by the shape of container. Strong circulation and replenishment of the furnace gas along the melt surface will increase decomposition rate of sodium sulfate with the result that the sodium sulfate coating may be reduced or not preserved.

Our study shows that sodium sulfate (natural, purified, or synthetic) can be use as the source for sodium in a standard flat glass composition. Sodium sulfate in the glass mixture decomposes at 1200-1300 °C and the silicate melt readily forms a glass upon cooling. Devitrification during cooling occurs sometimes on surfaces and unmelted grains. Melting duration of 100 hours at 1300 °C appears to be sufficient to avoid devitrification in many cases. An increase in melting temperature to 1500 °C, as often used in gas-fired glass furnaces, may markedly reduce the required duration. Our experiments suggest that for glass mixtures with above 25-30 % sodium sulfate, a sulfate melt can form and segregate from the silicate melt and accumulate on surfaces. This effectively changes the melt composition and its physical properties and results in crystallization of tridymite producing a massive translucent milky white glass.

The ease with which devitrification occurs suggests that interaction between sodium sulfate melt and crystalline grains during melting may severely restrict dissolution and thus promotes nucleation during cooling. Devitrification may thus be a fundamental property of sulfate-rich glass mixtures that should be further explored. It is possible that properties of the glass ceramic material for some applications might be advantageous.

INTRODUCTION

The principal motivation for this study has been the desirability of utilizing salts separated from agricultural drainage waters and other related salts for practical purposes, including salts from evaporation ponds (USDOI/CRA, 1990; Cervinka et al., 1999; SJVDIP, 2000; Tanji et al., 1992; Jenkins et al., 2003). In a previous study, we explored the use of natural sodium sulfate from evaporated drainage water together with rice straw ash for making glass (Jenkins et al., 1998). This attempt was successful although the addition of potassium and the introduction of other elements from the ash may not be desirable in terms of the physical properties and the long-term durability of the glass.

In this study we focus on producing soda-lime glasses using natural evaporation sodium sulfate from the San Joaquin Valley of California as complete or partial source for sodium in a standard, industrial flat glass composition. We also use a large volume, box furnace instead of the vertical quench furnace used in our previous study. This allows us to produce larger volumes of glass than the drop-sized glasses produced with the quench furnace. We utilize standard techniques developed for industrial glass making (Morey, 1954; Babcock, 1977; Copper, 1986; Doremus, 1994) with necessary exceptions such as volume and temperature constraints imposed by the available melting furnace and melting containers as well as safety considerations in a small non-industrial laboratory setting.

The sodium sulfate utilized in this study is in most experiments either natural evaporation pond salt or anhydrous certified sodium sulfate reagent. The natural sulfate salt comes from an evaporation pond of the southern San Joaquin Valley, Southern California (Rainbow Ranch, now Andrews Ag). We also used purified natural salt separated from agricultural drainage water using a pilot solar concentration system operated at Red Rock Ranch, Five Points, in the central San Joaquin Valley.

The effects of substituting sodium sulfate, natural or synthetic, for sodium carbonate as commonly used in glass production was systematically examined. Although intuitively it should be possible to use sodium sulfate for making glass, the behavior of sulfate and carbonate in silicate melts are sufficiently different to warrant direct theoretical and experimental investigations. The potential for the release of SO_2 in addition to CO_2 during glass melting also causes added engineering and environmental concerns relating to the need to control corrosion, atmospheric pollution, and acid deposition.

The behavior of sodium and calcium sulfates and carbonates are first evaluated as pure components and in silicate mixtures. Thermochemical modeling is then applied to predict the behavior of adding sodium sulfate to a typical window glass composition. Background detail and literature surveys are included in an earlier report (Jenkins et al., 1998).

GLASS MAKING

Raw Materials and Melting

Glass is solid material formed by cooling a silicate melt in such a way that crystallization and other phase separations do not occur or are restricted (Jones, 1956; Rekhson, 1986; Doremus, 1994). The silicate melt is formed from melting mixtures of silicate and carbonate minerals at high

temperatures. Soda-lime glass, composed mainly of Si-Ca-Na-O, is the most common glass type used for windows and containers (Doremus, 1994; Bansal and Doremus, 1986). Pressing and blowing hot glass blobs produce containers. A float process developed in the 1950s whereby molten glass is floated onto a molten tin bath, pulled off, and cooled under controlled conditions is used to make flat or window glass.

The raw materials for soda-lime glass are typically quartz sand consisting of at least 99 % pure natural quartz (SiO_2) to which is added limestone (CaCO_3) and sodium carbonate or soda ash (Na_2CO_3). The calcium source is high purity natural limestone. The Solvay process whereby salt, limestone, and ammonia are reacted to produce sodium carbonate is commonly used to manufacture soda ash. Other minor components may be added to the raw glass batch such as alumina in the form of feldspar and magnesia in the form of dolomite to improve glass properties. For the experimental products discussed in this report, a small amount of alumina is added through reactions with containers. Small amounts of magnesia are added when natural sodium sulfate is utilized in the experiments.

A soda-lime glass is composed of a random polymerized, oxygen-bonded, silica network where each silica atom is surrounded by oxygen anions (Wicks, 1986; Doremus, 1994). Alumina may substitute for silica in the silica-oxygen network. Modifying cations such as calcium and sodium break the silica-oxygen bonding. As long as the total of the modifying Na_2O and CaO units are in less than one-to-one ratio to the number of SiO_2 units, the silicon-oxygen network is preserved because each silicon tetrahedron is linked to at least three other tetrahedrons thus retaining the glass forming tendency (Doremus, 1994). The proportion of modifying cations determines the extent of polymerization, such that the ratio of network forming to network modifying cations is a measure of polymerization.

Glass is made from mixing the raw components in the desired proportions (Table 1) and firing the mixture to 1200-1500 °C well above liquidus (or full melting point) temperatures. A typical soda-lime glass mixture will melt between 950 and 1150 °C according to the pure ternary system Na_2O - CaO - SiO_2 (Morey and Bowen, 1925; Morey, 1930) (Figure 1). The composition of the glass mixture strongly influences the melting point (Figure 1). Increasing the CaO content at constant SiO_2 will systematically raise the complete melting point (liquidus) to higher temperatures. In contrast, increasing the Na_2O content at constant SiO_2 will significantly lower the melting point down to as low as the ternary eutectic at 725 °C. The melt composition at this ternary is SiO_2 73.5, Na_2O 21.3, and CaO 5.2 wt. % and the coexisting crystalline phases are SiO_2 , $\text{Na}_2\text{O} \cdot 2\text{SiO}_2$, and $\text{Na}_2\text{O} \cdot 3\text{CaO} \cdot 6\text{SiO}_2$ (Morey and Bowen, 1925).

Glass may separate into two melts (liquid immiscibility) at high temperature or as a result of heat treatments. Such separation may result in uniform crystallization in a matrix melt enriched in sodium and calcium because of the formation of a silica-rich immiscible melt. The addition of small amounts of alumina is known to reduce the tendency for phase separation. Burnett and Douglas (1970) have demonstrated that for typical soda-lime glasses, the immiscibility field is suppressed to below the liquidus. Liquid separation is furthermore restricted to above 580 °C because of slow cation diffusion.

The cooling of a melt below its melting point may result in the separation of a crystalline (or melt) nucleus with critical size. Prolonged undercooling will lead to crystal growth. Crystallization (or devitrification) is an important problem in glass making. The separation of crystals will change (for

better or worse) glass properties such as viscosity, thermal expansion, and optical properties. Thus crystallization is often not desired in glasses. The exceptions are some glass-ceramic materials (Corning Glass) for which uniform crystallization has been shown to result in superior properties such as high strength and impact resistance, low electrical conductivity, chemical reactivity, and thermal expansion, and opaque to white optical properties (Stookey and Maurer, 1962).

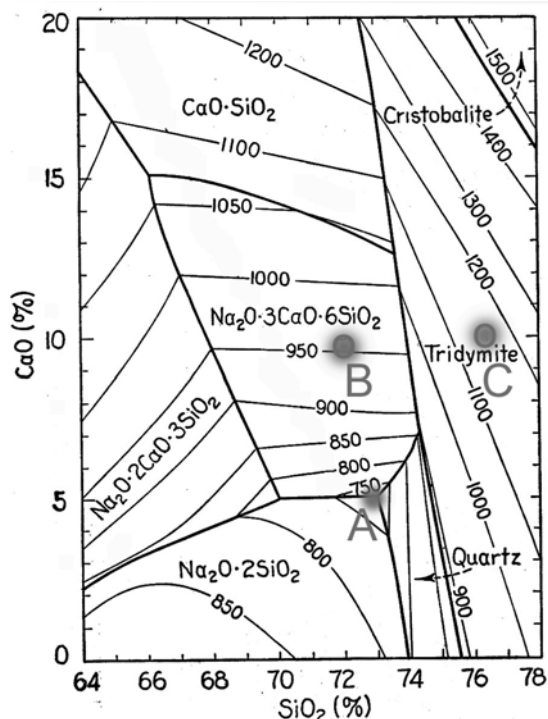


Figure 1. Ternary system $\text{Na}_2\text{O}-\text{CaO}-\text{SiO}_2$ (part) of interest to glass making (wt. % oxides). Dots are the typical flat glass composition used as the starting point in this study as well as the ternary eutectic composition (Table 1).

Figure 1. Typical Flat Glass Composition

	A	B	C
SiO_2	73.5	72.5	76.5
Al_2O_3		1.5	
Fe_2O_3		0.1	
MgO		3.0	
CaO	5.2	9.3	9.8
Na_2O	21.3	13.0	13.7
K_2O		0.3	
Total	100.0	99.7	100.0

SiO_2	60.9
CaCO_3	25.1
Na_2SO_4	14.0
Total	100.0

A. Melt composition at the eutectic point in the ternary system ($\text{CaO}-\text{Na}_2\text{O}-\text{SiO}_2$). B. Typical plate glass after Zarzycki (1991). C. Column (B) calculated to the ternary system together with the required mixture of components.

Sodium Sulfate in Glass Making

Sodium sulfate is used in glass making in relatively small quantities to facilitate dissolution of quartz grains and fining of the melt (removal of air bubbles) (Swartz, 1986). During melting, gases are released as CO_2 , SO_2 , N_2 , and O_2 and other components dependent on the purity of the initial mixture and the amount of trapped air. Oxygen from trapped air reacts readily with reduced components from melting and dissolves into the melt. Nitrogen forms bubbles that float in the silicate melt. The CO_2 gas is released during decomposition of carbonates used as the sources for the modifying cations (Ca, Na). Sulfur containing gas species are present when sodium sulfate is added to speed up melting and fining. Air bubbles rise in the melt ideally to be eliminated by flotation from the melt.

Factors that can control the ease with which such gas bubbles are removed are the viscosity of the melt (or composition), temperature (high temperature reduces viscosity), and duration. Increased size of bubbles will also enhance removal by flotation. Gas bubbles retained in the glass after quenching are rarely desired except perhaps in some artistic applications.

Reboil is another way that gas bubbles can form in a previous bubble-free melt. Reboil is caused by changes in CO₂ and/or SO₂ saturation in the melt such as during an enhanced dissociation of quartz grains (change of composition) as well as by changes in furnace gas composition that affect the solubility of CO₂ and/or SO₂ in the melt. Bubble formation can also result from reactions with furnace containers.

The addition of a fining agent such as sodium sulfate increase bubble formation and bubble size and, thereby, increase bubble rise velocity and separation. Combined with efforts to regulate the melt viscosity by raising temperature, fining agents are thus often used in glass making.

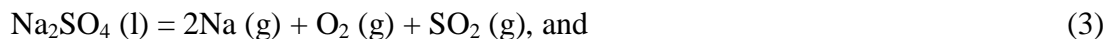
The amount of sodium sulfate added is typically 1-2 % of the total batch glass mixture, well below the amounts we use in this study. The addition of sodium sulfate reduces melting temperature, homogenizes the melt, eliminates fine bubble seeds, and helps to reduce unmelted quartz grains (silica stone or foam) (Swartz, 1986).

Pure anhydrous sodium sulfate melts at 884 °C (Lide, 1991) and remains in its molten stage until decomposition is initiated at 1100 °C. Complete decomposition occurs at temperatures well above 2000 °C (Samadhi et al., 2001). The decomposition of sodium sulfate has been suggested to occur according to the following reactions (see Samadhi et al., 2001, for a review):

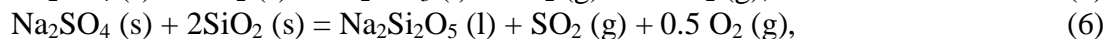
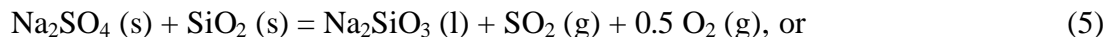


Reaction (1) is believed to occur between 1100 and 1200 °C with reaction (2) being the rate-controlling step. The Na₂O either remains in the melt or forms a volatile phase.

The presence of volatile metallic Na has been disputed and alternative reactions have been proposed based on observations from particulate matter and direct mass spectrometry. These includes:



The behavior of Na₂O in silicate melts is uncertain since this species may either remain in the melt or form a volatile species. Sodium sulfate may react with silica in silicate melts commonly proposed to occur at temperatures above 1000 °C according to the reactions:



The decomposition of sodium sulfate in glass batches occurs at significantly lower temperatures of about 1200-1300 °C in glass batches compared to decomposition of pure sodium sulfate (Samadhi et al., 2001).

Because of the molten stage of sodium sulfate to fairly high temperatures during glass melting, sulfate melt can accumulate as a melt film on the surface of molten glass or around quartz grains. Such melt films may expedite quartz grain dissolution and bubble release from the melt surface. Excess sodium sulfate, however, may accumulate on glass batches as thick layers that may inhibit fining.

SODIUM SULFATE USED IN THIS STUDY

Part of the experimental modeling summarized in this report was conducted using a natural evaporation pond salt from the Rainbow Ranch (now Andrews Ag), San Joaquin Valley, California. The composition of this salt is given in Table 2 as wt. % components. If it is assumed that the deficiency relative to 100 % total is water of hydration (not analyzed), we can recast the analyses into reasonable ideal mineral components. Magnesium is assumed to form blodite (or bloedite) ($\text{Na}_2\text{Mg}[\text{SO}_4]_2 \cdot 4\text{H}_2\text{O}$); boron is assumed to form borax ($\text{Na}_2\text{B}_4\text{O}_7 \cdot 10\text{H}_2\text{O}$), and all chlorite together with potassium and, if required, sodium are calculated as halite with small amounts of sylvite ($[\text{K},\text{Na}]\text{Cl}$).

The calculations suggest that thenardite (Na_2SO_4) constitutes about 85 % by weight of the salt (Table 2). The remaining is gypsum, halite, blodite, borax, and water, with blodite and halite being the dominating minor minerals.

Table 2. Composition of Pond Precipitate (Rainbow Ranch)

	Wt.%	Components	Mol.%	Wt.%
Na	29.90	Na_2SO_4	77.36	85.49
Ca	0.14	$\text{CaSO}_4 \cdot 2\text{H}_2\text{O}$	0.44	0.58
Mg	0.68	(K.Na)Cl	5.19	2.37
K	0.039	$\text{Na}_2\text{Mg}(\text{SO}_4)_2 \cdot 4\text{H}_2\text{O}$	3.60	9.37
B	0.037	$\text{Na}_2\text{B}_4\text{O}_7 \cdot 10\text{H}_2\text{O}$	0.11	0.33
Cl	1.43	H_2O	13.30	1.86
SO_4	63.50	Total	100.00	100.00
NO_3	nd			
Se	0.0003	Residual (atomic fractions):		
Total	95.72	H	0.0129	
H_2O	4.28	S	-0.0001	

H_2O has been calculated as the deficiency in the total.

Reasonable minerals and their compositions are assumed.

nd - not detected.

This mineralogy is reasonable considering mineralogical studies of salt deposits (Tanji et al, 1992) who observed that the dominating minerals in San Joaquin Valley evaporation ponds were halite and thenardite. The latter mineral easily hydrates to mirabilite ($\text{Na}_2\text{SO}_4 \cdot 10\text{H}_2\text{O}$) at a temperature below 32 °C. Particularly along the margins of ponds was found gypsum ($\text{CaSO}_4 \cdot 2\text{H}_2\text{O}$) and blodite. The presence of carbon may variously stabilize calcite (CaCO_3), burkeite ($\text{Na}_6\text{CO}_3[\text{SO}_4]_2$), and nahcolite (NaHCO_3). It is interesting that a double salt like glauberite ($\text{Na}_2\text{Ca}[\text{SO}_4]_2$) has not been detected in the natural salts.

The evaporation salt utilized in this study represent a marginal part of an evaporation pond and may contain relatively higher impurities such as magnesium compared to more centrally formed salt although the latter tends to contain more chloride. It may also contain a small amount of crystal-bound water in blodite.

The mineralogy of the salt was examined using X-ray diffraction techniques. A desktop Rigaku Miniflex diffractometer using Cu K_α radiation was utilized for this purpose. Peak identification and search was made using the MCI JADE software package and the PDF diffraction database. The

diffraction pattern for the evaporation salt is illustrated in Figure 2 as intensity (counts) versus 2θ (two-Theta, degrees). The obtained results are listed in Table 3 as 2θ , intensity, and calculated d-spacing in Ångstrom ($1 \text{ Å} = 10^{-10} \text{ m}$). The three major phases described above are present in the evaporation pond salt (blodite, thenardite, halite). The interpretation of the diffraction pattern is given in Table 3.

Thenardite is identified by the major peaks $d=2.646 \text{ Å}$ ($2\theta=33.84$), $d=2.798 \text{ Å}$ ($2\theta=31.96$), $d=4.678 \text{ Å}$ ($2\theta=18.95$), $d=3.080 \text{ Å}$ ($2\theta=28.96$) listed in order of decreasing intensity (Table 3). These d-spacings define the crystalline surfaces (022), (311), (111), and (040), respectively, reflecting an orthorhombic dipyramidal habit (Palache et al., 1951).

Bloedite (or blodite) is identified by the major peaks $d=4.583 \text{ Å}$ ($2\theta=19.35$), $d=3.296 \text{ Å}$ ($2\theta=27.02$), $d=2.966 \text{ Å}$ ($2\theta=31.10$), and $d=2.738 \text{ Å}$ ($2\theta=32.68$) listed in order of decreasing intensity (Table 3). These d-spacings define the crystalline surfaces (210), (021), (-221), and (400), respectively, reflecting a monoclinic prismatic habit (Palache et al., 1951).

Halite is identified by the major peaks $d=2.835 \text{ Å}$ ($2\theta=31.52$) and $d=1.632 \text{ Å}$ ($2\theta=56.32$) although it is possible that the most intensive peak at 2θ of 31.52 may be an overlap with a bloedite peak.

The ease with which thenardite hydrates to mirabilite ($\text{Na}_2\text{SO}_4 \cdot 10\text{H}_2\text{O}$) or mirabilite dehydrates to thenardite, makes it essential that sulfate salt is stored dry before and between uses. Mirabilite contains about 56 % water by weight. Thus the identification of highly hydrated minerals in salt used for glass making is critical since the presence of water strongly biases the batch composition by reducing sodium. The X-ray diffraction pattern shown in Figure 3 and summarized in Table 4 illustrates the ease with which this transformation occurs. The original sample was a mirabilite stored in airtight container at temperatures below 10°C . The partial transformation occurred during preparation of the sample for X-ray diffraction analyses. Mirabilite is easily identified by the peaks $d=5.533 \text{ Å}$ ($2\theta=16.13$) and $d=3.5677 \text{ Å}$ ($2\theta=24.85$).

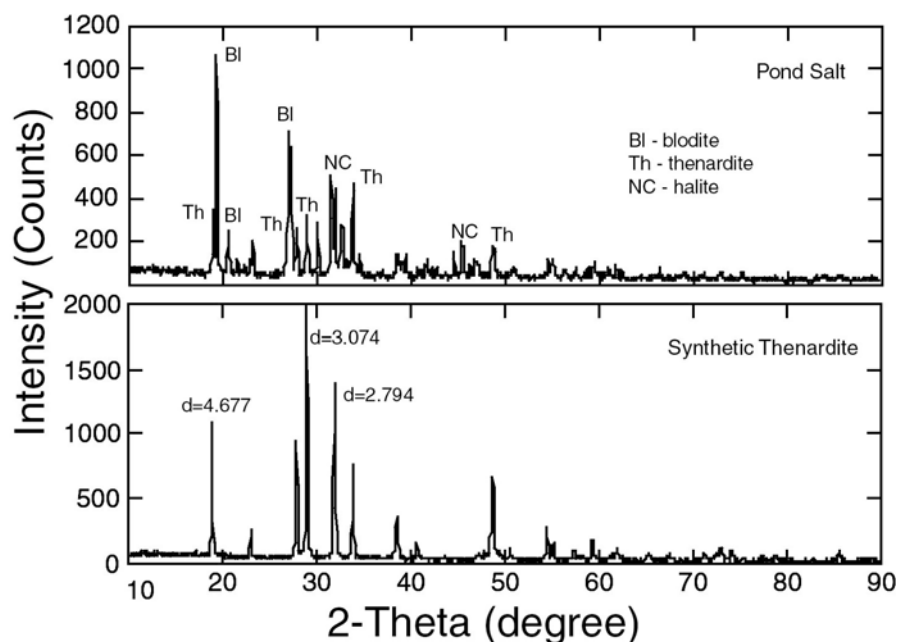


Figure 2. X-ray diffraction pattern for evaporation salts compared to synthetic sodium sulfate (thenardite).

Table 3. Interpretation of X-ray Diffraction Pattern for Evaporation Pond Salt

#	2-Theta	d(A)	I	I %	Mineral	d(A)	I %	2-Theta
1	18.956	4.678	294	29.3	Thenardite	4.659	71	19.035
2	19.351	4.583	1003	100.0	Blodite	4.555	95	19.472
3	20.639	4.300	190	18.9	Blodite	4.281	30	20.731
4	21.559	4.119	57	5.7				
5	22.327	3.979	34	3.4				
6	23.269	3.820	146	14.6	Blodite	3.800	25	23.390
7	27.029	3.296	637	63.5	Blodite	3.289	95	27.089
8	27.878	3.198	183	18.2	Thenardite	3.181	52	28.027
9	28.964	3.080	264	26.3	Thenardite	3.077	55	28.990
10	30.108	2.966	237	23.6	Blodite	2.971	40	30.053
11	31.527	2.835	463	46.2	Halite	2.821	100	31.692
12	31.960	2.798	373	37.2	Thenardite	2.784	100	32.123
13	32.680	2.738	181	18.0	Blodite	2.732	40	32.753
14	33.846	2.646	392	39.1	Thenardite	2.648	52	33.826
15	34.606	2.590	89	8.9	Blodite	2.586	20	34.659
16	37.087	2.422	28	2.8				
17	38.565	2.333	109	10.9	Thenardite	2.330	25	38.615
18	39.506	2.279	78	7.8	Blodite	2.276	20	39.563
19	41.629	2.168	78	7.8	Blodite	2.170	16	41.583
20	42.207	2.139	37	3.7				
21	42.709	2.115	42	4.2				
22	44.631	2.029	107	10.7	Blodite	2.025	30	44.715
23	45.450	1.994	165	16.5	Halite	1.994	55	45.449
24	46.283	1.960	46	4.6				
25	46.847	1.938	77	7.7				
26	48.759	1.866	135	13.5	Blodite	1.858	10	48.985
27	51.037	1.788	52	5.2				
28	54.647	1.678	79	7.9				
29	55.044	1.667	79	7.9				
30	56.321	1.632	43	4.3	Halite	1.628	15	56.477
31	57.548	1.600	45	4.5				
32	58.796	1.569	44	4.4				
33	59.473	1.553	64	6.4				

Obtained pattern compared to expected values for best fits for thenardite, blodite, and halite. d(A) - d-spacing in Angstrom; I - intensity in counts; I % - intensity in % relative to highest peak.

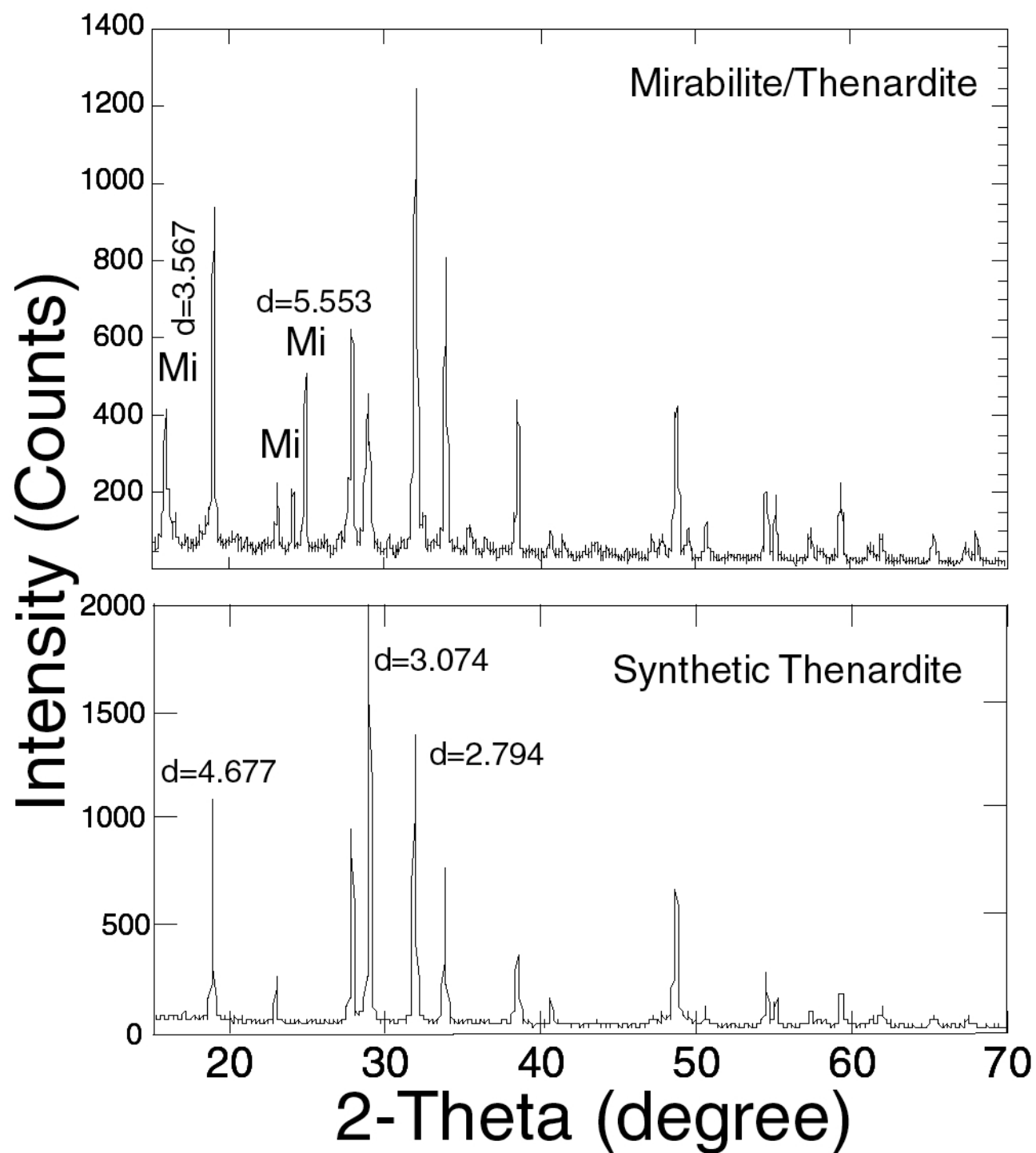


Figure 3. X-ray diffraction patterns for a mixture of mirabilite and thenardite and compared to synthetic sodium sulfate (thenardite).

Table 4. Interpretation of X-ray Diffraction Pattern for Mirabilite and Thenardite Mixture

#	2-Theta	d(A)	I	I %	Mineral	d(A)	I %	2-Theta
1	16.004	5.534	348	29.4	Mirabilite	5.490	100	16.131
2	16.537	5.356	64	5.4				
3	18.557	4.777	76	6.4				
4	19.040	4.657	870	73.6	Thenardite	4.659	71	19.035
5	20.272	4.377	39	3.3				
6	23.100	3.847	169	14.3	Thenardite	3.838	17	23.153
7	24.168	3.680	139	11.8	Mirabilite	3.670	7	24.231
8	27.878	3.568	443	37.5	Mirabilite	3.580	17	24.850
9	26.237	3.394	34	2.9	Thenardite	3.181	52	28.027
10	27.962	3.188	554	46.9				
11	29.081	3.068	391	33.1				
12	30.354	2.942	47	4.0	Thenardite	3.077	55	28.990
13	32.079	2.788	1182	100.0				
14	32.600	2.745	71	6.0				
15	33.980	2.636	750	63.5	Thenardite	2.648	52	33.826
16	35.463	2.529	66	5.6				
17	36.580	2.455	43	3.6				
18	37.022	2.426	34	2.9	Thenardite	2.330	25	38.615
19	38.643	2.328	388	32.8				
20	40.777	2.211	54	4.6				
21	41.576	2.170	45	3.8	Thenardite	1.865	36	48.780
22	43.623	2.073	34	2.9				
23	44.384	2.039	28	2.4				
24	47.261	1.922	56	4.7	Thenardite	1.865	36	48.780
25	47.921	1.897	52	4.4				
26	48.858	1.863	378	32.0				
27	49.602	1.836	67	5.7	Thenardite	1.681	13	54.553
28	50.700	1.799	94	8.0				
29	54.799	1.680	165	14.0				
30	55.177	1.663	162	13.7	Thenardite	1.663	8	55.202
31	57.438	1.603	75	6.3	Thenardite	1.553	10	59.473
32	58.093	1.587	28	2.4				
33	59.383	1.555	200	16.9				

Obtained pattern compared to expected values for best fits for thenardite, mirabilite, and halite. d(A) - d-spacing in Angstrom; I - intensity in counts; I % - intensity in % relative to highest peak.

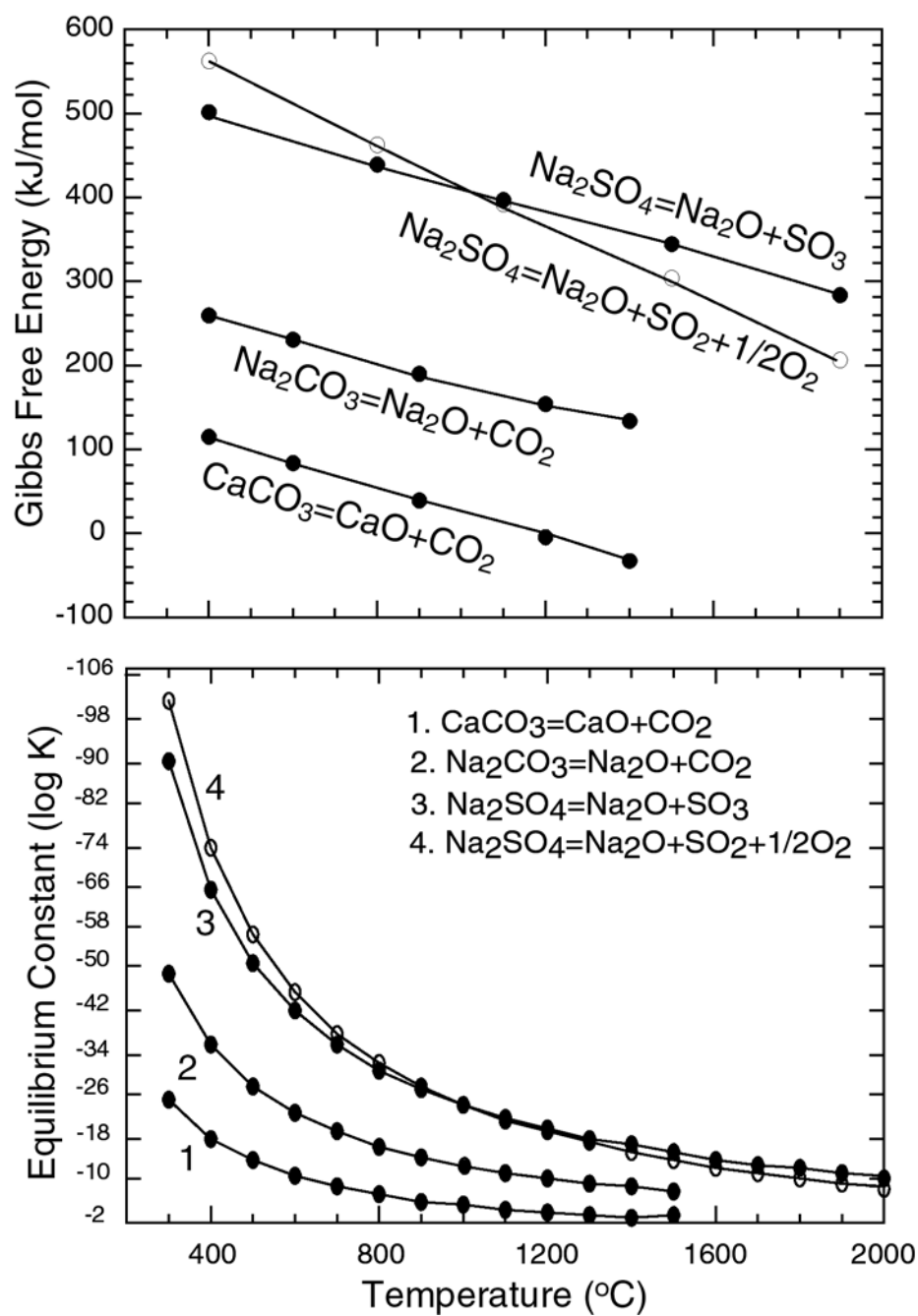


Figure 4. Summary decomposition equilibria of carbonates and sulfate of interest to glass making. Data from Stern (2001).

DECOMPOSITION AND MELTING OF SULFATES AND CARBONATES

Here we briefly review the behavior of the pure components used in the experimental and modeling work. We have conducted a series of tests on pure synthetic minerals and mixtures using the same furnace as for the main experiments of this study. Figure 4 summarizes the Gibbs free energy and equilibrium constants for the decomposition reactions of interest in this study (Stern, 2001).

The furnace was for the present tests operated without supplied air during melting. The furnace atmosphere was continuously analyzed with an on-line Horiba PG-250 portable gas analyzer calibrated for CO₂ on air. The components analyzed were NO, SO₂, CO, CO₂, and O₂. The delay in analyzer response was about 30 seconds. This method allows us to continuously monitor the furnace atmosphere and to evaluate the effects of temperature on release of SO₂ and CO₂ from pure reagents as well as mixtures of these.

Calcium Carbonate

A total of 2.5 g of calcium carbonate powder was heated to 1300 °C at a rate of 10 °C/min. The furnace was kept at the maximum temperature for 2 hours and was subsequently cooled as fast as possible by turning off the power to the furnace. The result for CO₂ is shown in Figure 5.

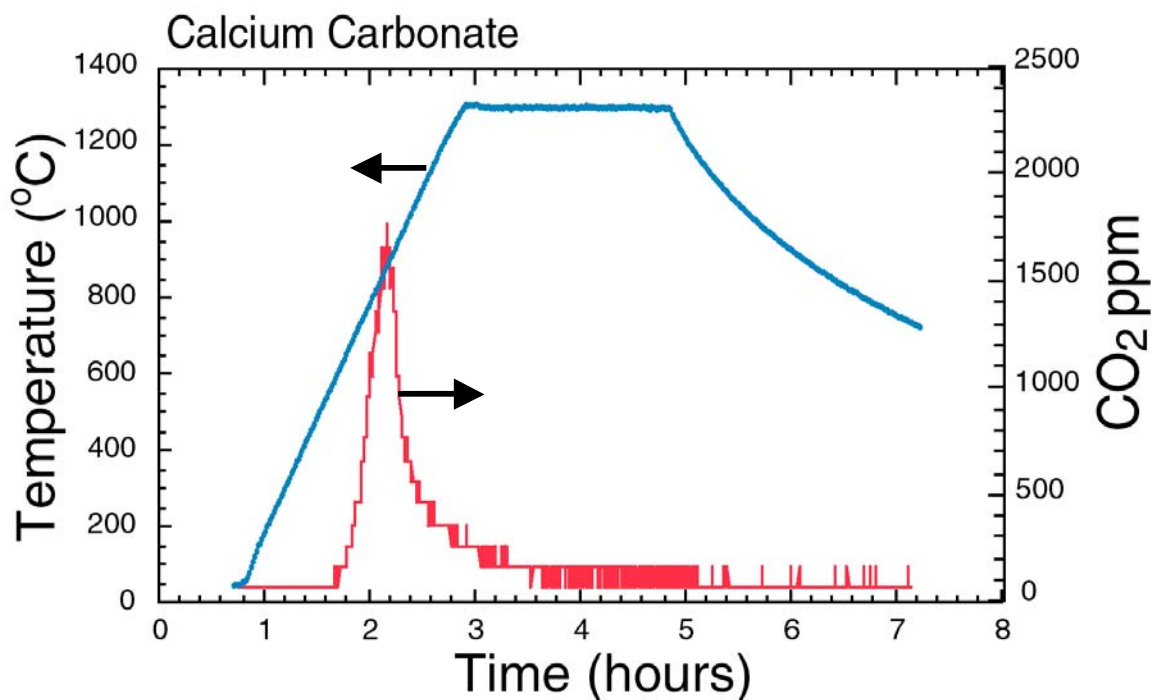


Figure 5. Release of CO₂ as a function of time from firing reagent grade calcium carbonate. For clarity, the minimum CO₂ concentration has been adjusted to 50 ppm. The arrows point toward the relevant scales.

The maximum release of CO₂ occurs between 850 and 900 °C bracketing the expected decomposition temperature of 899 °C (Lide, 1991). The observed weight loss during the experiment was 45 % that is very close the theoretical loss of 44 % from pure calcium carbonate. This test

confirms the expected breakdown of calcium carbonate to CO_2 and residual lime at temperatures just below 900°C .

Since glass mixtures commonly start melting at about 700°C and are fully melted at about 1100°C or lower, calcium carbonate decomposes during melting with the result that carbon is released to the gas and calcium incorporated into the melt.

Sodium Carbonate

The behavior of sodium carbonate is uncertain. Lide (1991) lists the melting point at 851°C and Stern (2001) as 857°C . Sodium carbonate shows appreciable decomposition from just above the melting point (Janz and Lorenz, 1961; Stern, 2001).

The firing test illustrated in Figure 6 used 3 g of pure sodium carbonate. Sodium dioxide is not a stable phase and reacts rather fast with air forming, for example, thermonatrite ($\text{Na}_2\text{CO}_3 \cdot \text{H}_2\text{O}$) that complicates mass balance calculations. It is possible that the wide CO_2 peak may be related to continuous reactions between sodium and atmospheric CO_2 and H_2 .

Despite the broad release peak, the maximum CO_2 release occurs at about 850°C closely corresponding to the expected temperature of $851-7^\circ\text{C}$. The present firing test thus suggests a decomposition reaction similar to that for calcium carbonate.

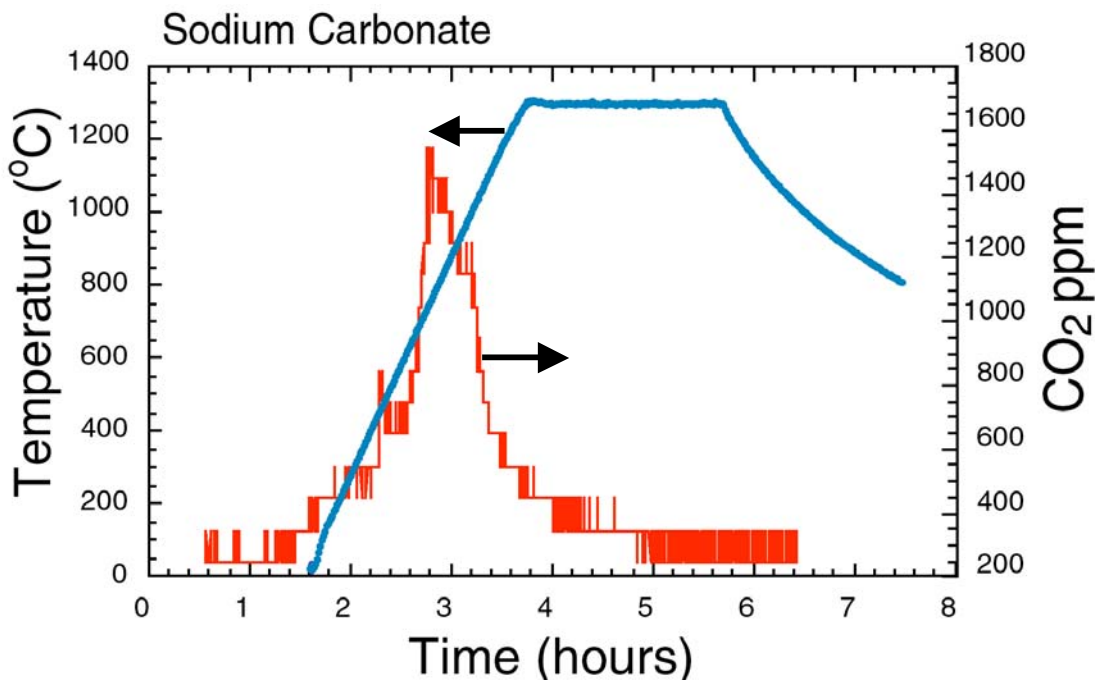


Figure 6. Release of CO_2 as a function of time from firing reagent grade sodium carbonate. For clarity, the minimum CO_2 concentration has been adjusted to 50 ppm. The arrows point toward the relevant scales.

This result suggests that sodium carbonate decomposes at temperatures about $40-50^\circ\text{C}$ lower than for calcium carbonate. Thus, sodium carbonate likely behaves similar to calcium carbonate during melting of glass mixes with CO_2 released to the gas phase and Na_2O incorporated into the melt.

Sodium Sulfate

Anhydrous sodium sulfate melts at 884 °C (Lide, 1991) and will upon heating form a melt prior to decomposition. Molten sodium sulfate shows significant decomposition from 1600-1700 °C based on thermodynamic modeling (Samadhi et al., 2002). This means that sodium sulfate may remain as a melt until well after the liquidus temperature of common glass mixtures.

The firing test illustrated in Figure 7 used 3 g of pure sodium sulfate. The observed weight loss of 15% was significantly below the total loss expected if all SO₂ was released during firing (56 %). Thus only a small amount of SO₂ is decomposed probably only sufficient to saturate the furnace gas. The majority of the sodium sulfate remains as a melt, or after cooling as a sulfate coating (Figure 8).

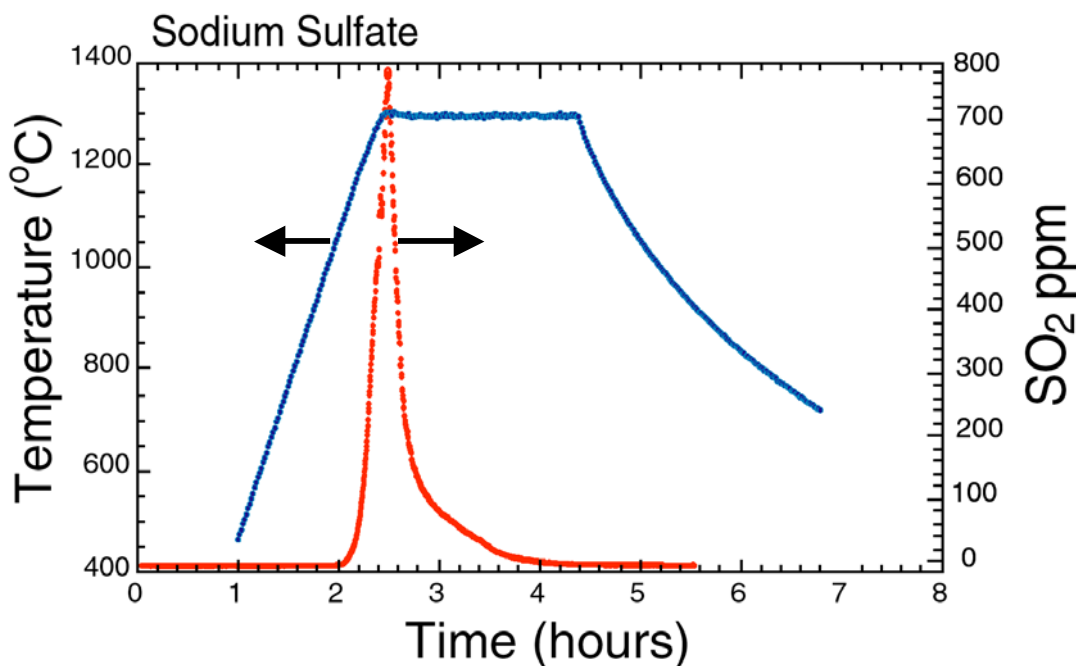


Figure 7. Release of SO₂ as a function of time from firing reagent grade sodium sulfate. The arrows point toward the relevant scales.

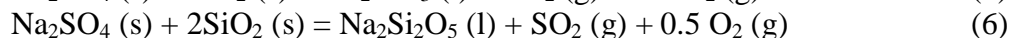


Figure 8. Sodium sulfate coating after firing sodium sulfate (see Figure 7).

Similar firing tests with the furnace gas continuously replenished by an inlet of air resulted in the complete loss of SO₂ from sodium sulfate at identical temperature conditions.

Silicate Melt

Sodium sulfate reacts with silica in silicate melts commonly proposed to occur at temperatures above 1000 °C according to the reactions:



It is, thus, expected that melting and decomposition of sulfate and carbonates in glass mixtures, containing silica, will differ from the observations based on pure components. We have tested this by preparing a glass mixture of silica (8.8 g), calcium carbonate (2.5 g), and sodium sulfate (3.0 g). The results of firing this mixture under the same conditions as done for the pure components are illustrated in Figure 9.

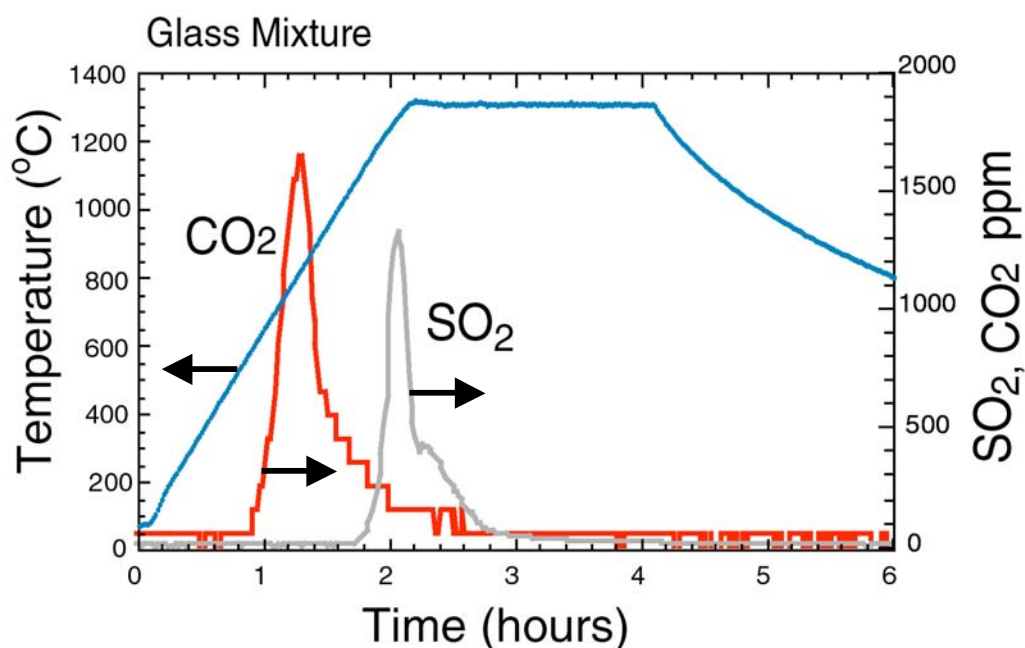


Figure 9. Release of SO₂ and CO₂ as a function of time from typical glass mixture prepared from reagent grade silica, sodium sulfate, and calcium carbonate. The arrows point toward the relevant scales.

A total of 14.2 g mixture was fired with a weight loss of 20 % that compares well to the expected loss of 19 % if all CO₂ and SO₂ are released. The maximum release temperatures read from Figure 9 are slightly, but significantly, lower than obtained for the pure components. The CO₂ is released at about 800 °C and SO₂ at about 1250 °C. This is likely to have been caused by the sulfate/carbonate interaction with the silicate in the melt. This suggests that sulfate melt decomposes fully just below a temperature of 1300 °C in a silicate melt in contrast to the behavior of pure sodium sulfate that may be stable as a melt to very high temperatures.

This brief survey suggests that there are marked differences in the way carbonates and sulfates of sodium behave in silicate melt. Calcium and sodium carbonates appear to decompose at temperatures below 900 °C. Sodium sulfate melts at fairly low temperature, but remains as a melt phase until high temperatures well above the liquidus conditions for typical glass mixtures where it starts to decompose at about 1300 °C for the present glass compositions.

THERMODYNAMIC MODELING GLAS MELTING

To examine the effect of substituting sodium sulfate for sodium carbonate, we calculated a series of theoretical glass mixtures using oxides, carbonates, and sulfates commonly used for making industrial glasses (Doremus, 1994). The series was constrained by the ratios of Na₂SO₄ and Na₂CO₃ on a weight basis going from 0.0 to 1.0 in constant steps of 0.1. Sulfate fraction of glass mixtures refers in this report to the Na₂SO₄/(Na₂SO₄+Na₂CO₃) weight ratio. The result is a series of compositions with constant SiO₂ and CaO and variable SO₃ and CO₂, while Na₂O only varies slightly with sodium sulfate fraction (Table 5). The glass mixtures are given in Table 5 in terms of mixing components (oxide, sulfate, and carbonate) and oxides (SiO₂, Na₂O, CaO, SO₃, and CO₂). The refractory glass compositions are calculated volatile free to 100 %. Because the mixtures were calculated on a weight basis, some variation is seen in refractory glass compositions (Table 5).

Table 5. Mixtures Used for Thermodynamical Modeling

Mixture ID**	0.0*	0.1	0.2	0.3	0.4	0.5	0.6	0.7	0.8	0.9	1.0
Mixing Component (wt. %)											
SiO ₂	61.30	61.30	61.30	61.30	61.30	61.30	61.30	61.30	61.30	61.30	61.30
CaCO ₃	17.70	17.70	17.70	17.70	17.70	17.70	17.70	17.70	17.70	17.70	17.70
Na ₂ SO ₄	0.00	2.10	4.20	6.30	8.40	10.50	12.60	14.70	16.80	18.90	21.00
Na ₂ CO ₃	21.00	18.90	16.80	14.70	12.60	10.50	8.40	6.30	4.20	2.10	0.00
Total	100.00	100.00	100.00	100.00	100.00	100.00	100.00	100.00	100.00	100.00	100.00
Mixture as Oxides (wt. %)											
SiO ₂	61.30	61.30	61.30	61.30	61.30	61.30	61.30	61.30	61.30	61.30	61.30
Na ₂ O	12.28	11.97	11.66	11.35	11.03	10.72	10.41	10.10	9.79	9.48	9.16
CaO	9.92	9.92	9.92	9.92	9.92	9.92	9.92	9.92	9.92	9.92	9.92
SO ₃		1.18	2.37	3.55	4.73	5.92	7.10	8.29	9.47	10.65	11.84
CO ₂	16.50	15.63	14.76	13.89	13.01	12.14	11.27	10.40	9.53	8.65	7.78
Sum	100.00	100.00	100.00	100.00	100.00	100.00	100.00	100.00	100.00	100.00	100.00
Refractory Composition (Glass)											
SiO ₂	73.42	73.69	73.97	74.25	74.53	74.81	75.10	75.39	75.68	75.97	76.26
Na ₂ O	14.71	14.39	14.07	13.74	13.41	13.09	12.75	12.42	12.08	11.74	11.40
CaO	11.88	11.92	11.97	12.01	12.06	12.10	12.15	12.20	12.24	12.29	12.34
Sum	100.00	100.00	100.00	100.00	100.00	100.00	100.00	100.00	100.00	100.00	100.00

* Similar to mixture E. ** The mixture ID gives the fraction of sodium sulfate (synthetic) in the sulfate of the mixture.

The phase proportions and compositions, using the glass mixes in Table 5, were modeled as a function of temperature and sulfate fraction based on Gibbs free energy minimization using the FactSage thermodynamic program package and database (Bale et al., 2002). The temperature was varied from 500 °C to 1600 °C in steps of 25 or 100 °C, dependent on the range of interest. The results shown in Figure 10 give the phase proportions as a function of temperature for selected sulfate fractions.

Sulfate liquid develops in mixtures with above 0.1 sodium sulfate fraction at a relatively constant temperature of about 900 °C, consistent with a melting temperature of pure sodium sulfate of 884 °C (Lide, 1991). The fraction of sulfate melt is proportional to the fraction of sulfate in the glass mixture (Table 5 and Figure 10). The temperature of start of decomposition (or dissociation to SO₂ and Na₂O) rise with the amount of sulfate fraction in the original mixture from about 900 to 1000 °C. Likewise, the sulfate melt is completely decomposed between 1000 and 1200 °C. The decomposition

temperatures for the glass mixtures are significantly lower than for pure sodium sulfate (1600-2000 °C; Samadhi et al., 2002). This reflects a marked freezing point depression for the multicomponent glass mixture.

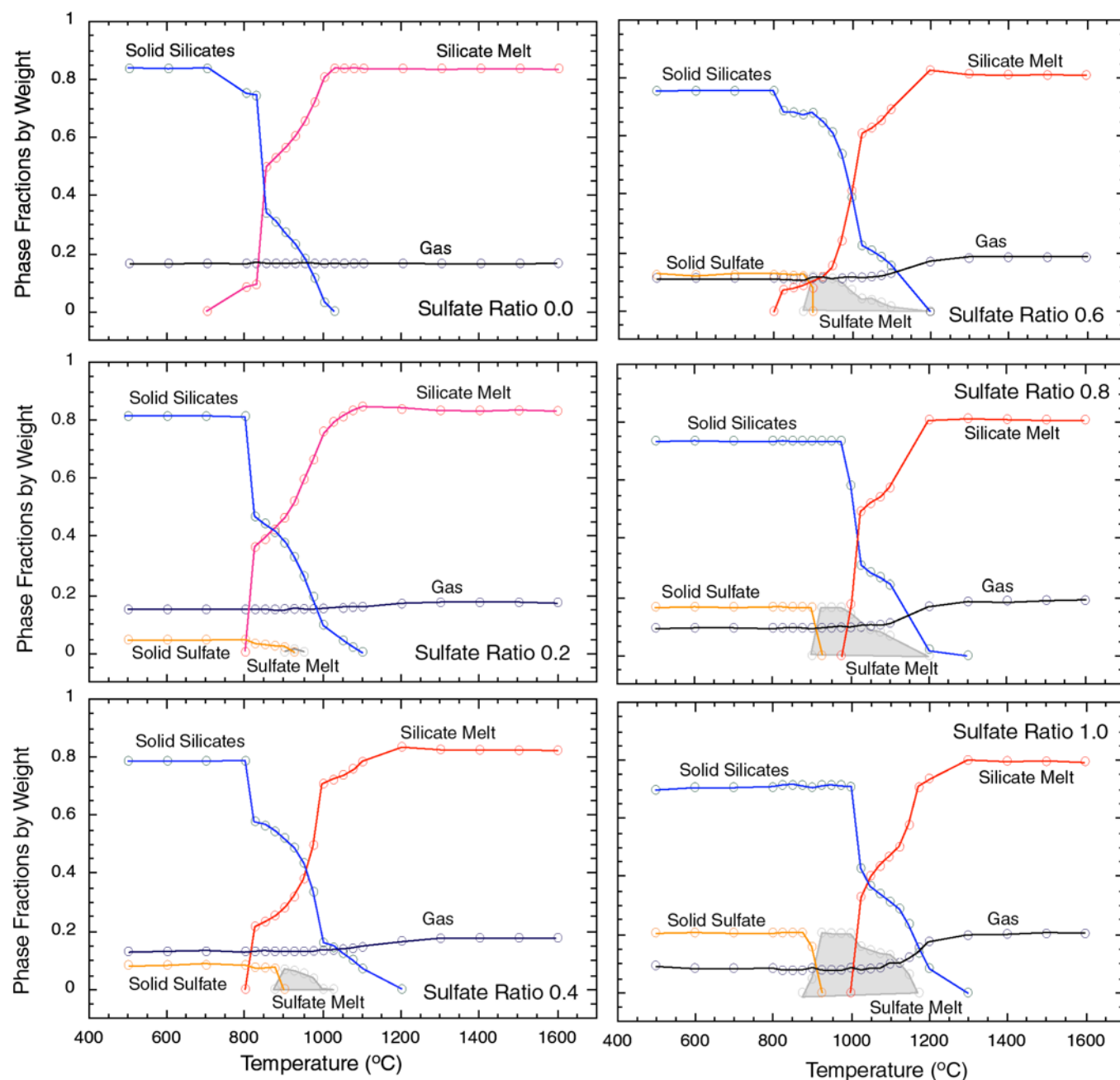


Figure 10. Predicted phase equilibria. Calculated on a weight fraction basis as a function of temperature and sulfate ratio (sulfate ratios 0.0 to 1.0, Table 5).

The calculated equilibrium composition of the solid sulfate is nearly pure Na_2SO_4 with little CaSO_4 in the solid solution for all original glass mixtures with sodium sulfate fractions below 0.8. For higher sulfate fractions, the CaSO_4 content of the sulfate solid solution strongly increases and reached 28 % for mixtures with high sulfate fraction. The CaSO_4 content remains relatively constant

during melting, but markedly decreases as the sulfate decomposes suggesting that initial decomposition is caused by the preferential dissociation of Na_2SO_4 over CaSO_4 (Figure 11).

The silicate phases during melting are relatively independent of the composition of the glass mixture. Quartz is present at temperatures below 800 °C and is replaced at higher temperature by tridymite. The only other important silicate phase predicted by FactSage is $\text{Na}_2\text{Ca}_3\text{Si}_6\text{O}_{12}$ or N3C6S (also known as ‘divitrite’ by glass makers) that is stable to 900 °C, above which tridymite is the liquidus silicate mineral. This is consistent with the $\text{CaO-Na}_2\text{O-SiO}_2$ liquidus phase diagram of Morey and Bowen (1925; Figure 1).

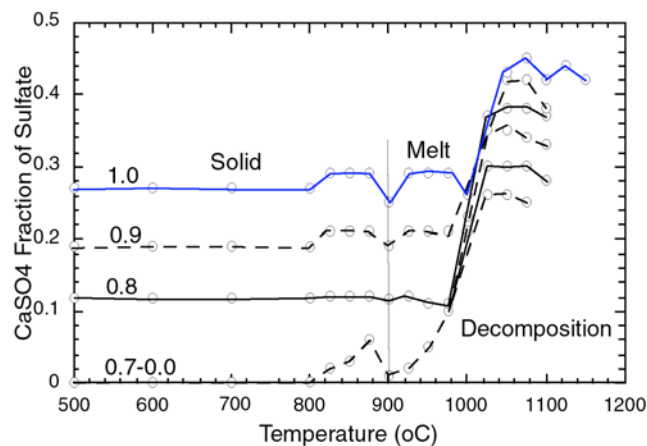


Figure 11. Composition of sulfate solid and melt as a function of temperature calculated using the FactSage database. CaSO_4 fraction is the $\text{CaSO}_4/(\text{CaSO}_4+\text{Na}_2\text{SO}_4)$ ratio of the solid solution, on a weight basis.

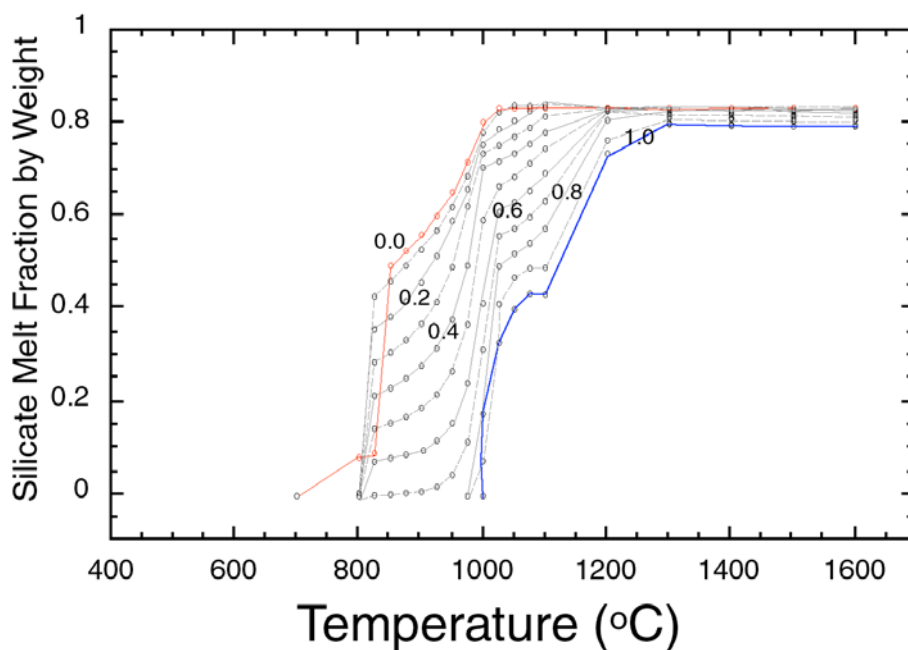


Figure 12. Liquidus depression as a function of fraction of sodium sulfate in mixture (MIX 0-1, Table 1) as predicted by FactSage.

Another interesting observation is that the liquidus is raised about 200 °C by replacing sodium carbonate with sulfate in the starting mixes (Figure 12). This is in part a result of the lowering of Na_2O and increase in SiO_2 in the glass mixtures with increasing weight fraction of sodium sulfate (Table 5).

The composition of the gas phase is markedly affected by release of SO_2 as a gas species from about 900 to 1000 °C (Figure 13). There is no indication that sodium (metallic or otherwise) appears as a significant gas species within the temperature interval investigated.

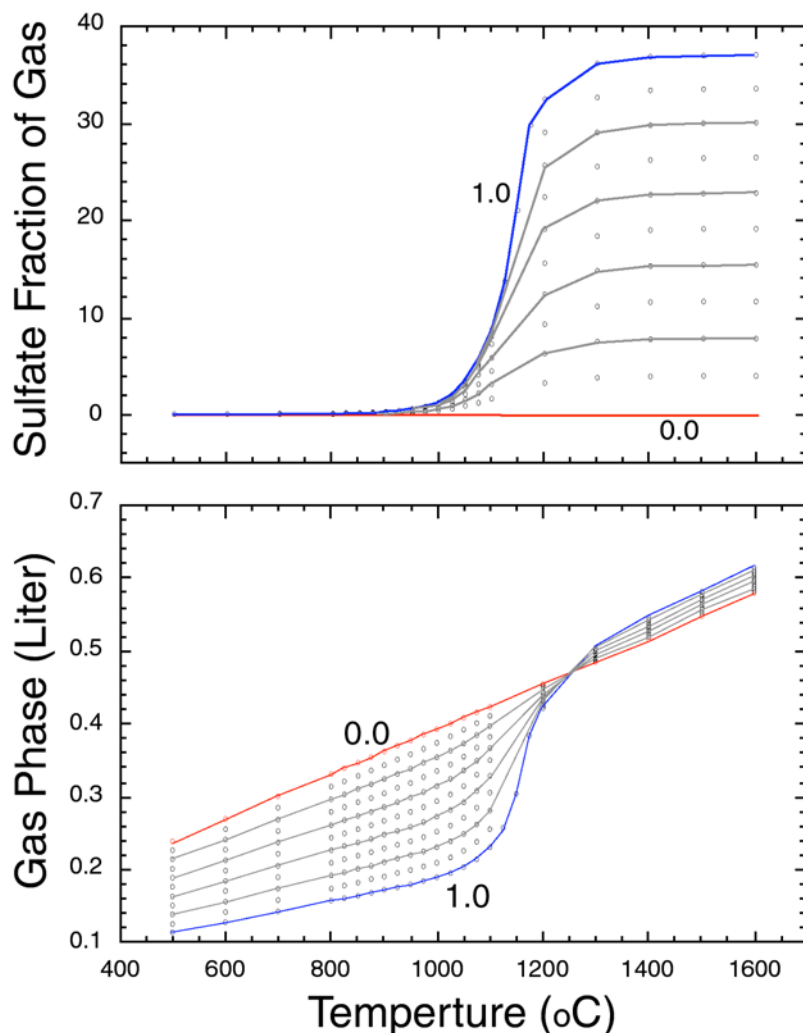


Figure 13. Composition of the gas phase as a function of fraction of sodium sulfate and temperature predicted by FactSage.

The variation in the refractory composition of the silicate melt phase is shown in Figure 14. Calcium increases markedly while sodium decreases during initial melting, but levels-out with high melt fractions and high temperature and closely approximates the concentrations in the bulk system. Sulfur and carbon are partitioned into the melt at low temperature and may reach total concentrations of 12 to 13 wt. % at 1000 °C, calculated as Na_2SO_4 and CaCO_3 . With increasing temperature above 1300 °C, sulfur and carbon are partially driven out of the melt and added to the gas.

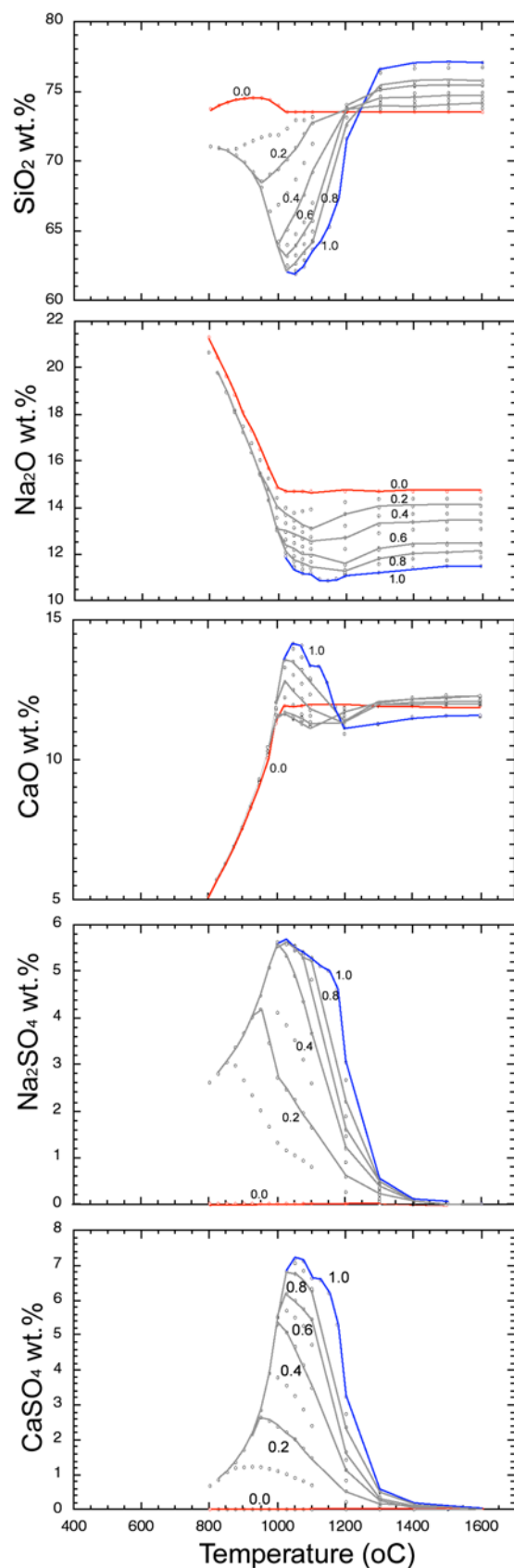


Figure 14. Silicate liquid composition as a function of temperature and sulfate fraction (MIX 0-1, Table 5) predicted by FactSage. Composition as wt. % oxides (SiO₂, CaO, Na₂O) and sulfates (Na₂SO₄, CaSO₄). The sulfur content of the melt is by convention given as sodium and calcium sulfate.

One of the important findings of this survey is that the replacement of sodium carbonate, commonly used for glass making, with sodium sulfate results in the development of a sulfate immiscible liquid during melting. This sulfate melt is stable to temperatures several hundred degrees above complete melting of the glass mixture. Potentially this molten sulfate may separate from the glass and form a coating stable to very high temperatures well above temperatures commonly used for glass making. Such sulfate separation will markedly reduce the sodium content of the refractory glass and thus raise its liquidus temperature and the ability to form glass during quenching.

EXPERIMENTAL PROCEDURES

Experimental Methods

A heavy duty, high temperature Thermcraft box melting furnace (Figure 15) was used to produce glass from pure materials and/or natural sulfate salt. The furnace control consists of a setpoint controller and a solid state power controller. The temperature is monitored by S-type thermocouples. The programmable setpoint controller allows the temperature to be ramped to a specific maximum temperature and maintained there for the duration of the experiment.



Figure 15. Thermcraft furnace used in the experimental work.

The temperature variation in the furnace was characterized by testing temperature control and variation. The temperature ramps to the maximum temperature with only an initial 2-3 °C overshooting of the target temperature. The temperature gradient in the furnace was determined from the melting point of gold to be less than a few °C.

Most experiments were performed with an air inlet maintained at 6 or 20 lpm and an open exhaust valve. A few experiments were done with continuous sampling and analyses of the furnace gas. These latter experiments are discussed in the section on 'Decomposition and melting of sulfates and carbonates.'

We selected a target glass composition (Table 1, Analysis C) representing a typical industrial type soda-lime glass. This composition was used as a starting point for the experimental program from which all other glass mixtures were prepared.

The experiments were performed in different types of containers. First, large volume, thick-walled, porous alumina containers were tested. These were shown to cause devitrification and to inhibit glass formation for short duration experiments, as discussed below. The following experiments were done in variously sized, thin-walled, high-temperature pressed alumina containers. These latter proved more useful with some limitations as discussed below.

The melting temperature was chosen at 1300°C for our initial experiments well above the expected liquidus temperature (Figure 1). The furnace was typically ramped to maximum temperature at 10 °C/min. Duration at the maximum temperature was selected between 2 and 200 hours. The experiments were either cooled as fast as permitted by the furnace (~100 °C/min) or controlled-cooled at 10 °C/min. In some cases, the experimental products were extracted directly from the furnace and cooled to ambient temperature (~1000 °C/min).

Analytical Procedures

All experimental products were extracted from the furnace and visually inspected after having cooled to ambient temperature. The physical characteristics were noted such as optical characteristics, crystallization/devitrification, cracking, reactions with container walls, and sulfate coatings. Selected products were sampled for thin section preparation and polishing. The thin sections were examined using optical and scanning electron microscopes. The glass and crystalline products were analyzed using the CAMECA SX100 electron beam microprobe at UC Davis Geology Department. The precision of the electron microprobe analyses is generally within 1-3 % for major elements and 5 % for minor elements. The oxides analyzed were SiO₂, TiO₂, Al₂O₃, Fe₂O₃, MnO, MgO, CaO, Na₂O, K₂O, and P₂O₅. The detection limit was taken to be 0.01 wt. % of the oxides. It is assumed that all iron occurs as Fe³⁺. Other elements, including Cl, were not present in sufficient amounts to be detected. Some products were examined using the scanning electron facility of the CAMECA SX100 electron microprobe.

Mineral phases were identified using X-ray diffraction techniques. A desktop Rigaku Miniflex diffractometer using Cu K_α radiation was utilized for this purpose. Peak identification and search was made using the MCI JADE software package and the PDF diffraction database.

Preparation of Glass Mixtures

The starting mixtures were prepared using silica floated powder, calcium carbonate powder; sodium carbonate powder, and sodium sulfate powder (Table 6). The sodium sulfate (synthetic and natural) was ground to fine powder in a ceramic mortar. All components were stored in airtight containers before and between use. The mixtures were prepared by thoroughly mixing the chemical components in proportions as given in Table 7. For the preliminary experiments, synthetic certified sodium sulfate was chosen to avoid the impurities present in the sodium sulfate from drainage water. Other experiments use a natural sulfate salt collected from a drainage pond in southern California (Table 2).

Table 6. Chemical components used for producing mixtures

Sodium sulfate: natural evaporation pond salt
Sodium sulfate: Fisher Certified A.C.S. (anhydrous)
Sodium carbonate: Fisher certified (anhydrous)
Calcium carbonate: Fisher certified A.C.S.
Silica dioxide: Fisher floated powder

A summary of the prepared mixtures is given in Table 7. Mixtures A to C were made with synthetic sodium sulfate. Mixture A was prepared to be identical to typical industrial plate or window glass (Table 1). Mixture C was prepared to be identical to that used for the ‘window glass’ experiment of Jenkins et al. (1998, table 10). Mixture B was an accidental mixture that we used to test the effect of high silica content. Mixtures D and F to H were based on the natural sodium sulfate as source for sodium. Mixture D was intended to be identical to C, except for the use of natural sodium sulfate. Mixture E was prepared to be identical to C, except that sodium carbonate was used as the source for sodium, as is typical for industrial glass production. Mixture J was identical to mixture C except that synthetic sodium sulfate was used. Mixtures 0.5 and 1.0 were prepared using synthetic sodium sulfate (see also Table 5) relatively similar to mixture C.

A series of mixtures was prepared to test the effect of variable sodium and calcium. Mixture F was prepared with 20 % higher sodium sulfate than used for C. Mixture G was prepared with 20 % higher calcium carbonate than used for F. Mixture H was prepared with 10 % higher calcium carbonate than used for F. Finally, Mixture I was prepared to compensate for the observed loss of sodium when using Mixture H. This was done by increasing the sodium sulfate content to an appropriate level.

The compositions of the mixtures utilizing the natural sulfate salt have been recalculated in Table 8, taking into account that minor amounts of sodium, magnesium, and chloride is included in the natural salt. Other components in the natural salt are below detection limit (potassium, boron, and selenium). It is seen that the glass compositions using the natural sodium sulfate for practical purposes are nearly identical to compositions based on pure synthetic sulfate. The differences are only small amounts of MgO and Cl. It should, however, be noted that later analytical work has demonstrated that the MgO content of the natural sulfate salt is grossly underestimated (see later discussion).

Use of Sodium Sulfate Separated from Agricultural Drainage Water in Glass Making

Table 7. Summary of mixtures of sulfate based 'window' glass (wt. %)

Target A		Mixture A		Target G		Mixture G	
SiO ₂	75.11	SiO ₂	60.9	SiO ₂	69.49	SiO ₂	52.5
CaO	7.54	CaCO ₃	25.1	CaO	13.94	CaCO ₃	18.8
Na ₂ O	17.35	Na ₂ SO ₄ (s)	14.0	Na ₂ O	16.57	Na ₂ SO ₄ (n)	28.7
	100.00		100.0		100.00		100.0
Target B		Mixture B		Target H		Mixture H	
SiO ₂	84.91	SiO ₂	73.5	SiO ₂	68.22	SiO ₂	51.2
CaO	7.69	CaCO ₃	11.9	CaO	15.45	CaCO ₃	20.7
Na ₂ O	7.40	Na ₂ SO ₄ (s)	14.7	Na ₂ O	16.33	Na ₂ SO ₄ (n)	28.1
	100.00		100.0		100.00		100.0
Target C		Mixture C		Target I		Mixture I	
SiO ₂	73.47	SiO ₂	57.3	SiO ₂	60.29	SiO ₂	41.2
CaO	11.86	CaCO ₃	16.5	CaO	9.83	CaCO ₃	12.0
Na ₂ O	14.67	Na ₂ SO ₄ (s)	26.2	Na ₂ O	29.88	Na ₂ SO ₄ (n)	46.8
	100.00		100.0		100.00		100.0
Target D		Mixture D		Target J		Mixture J	
SiO ₂	73.47	SiO ₂	57.3	SiO ₂	73.47	SiO ₂	57.3
CaO	11.86	CaCO ₃	16.5	CaO	11.86	CaCO ₃	16.5
Na ₂ O	14.67	Na ₂ SO ₄ (n)	26.2	Na ₂ O	14.67	Na ₂ SO ₄ (s)	26.2
	100.00		100.0		100.00		100.0
Target E		Mixture E		Target 1.0		Mixture 1.0	
SiO ₂	73.47	SiO ₂	61.4	SiO ₂	76.26	SiO ₂	61.3
CaO	11.86	CaCO ₃	17.7	CaO	12.34	CaCO ₃	17.7
Na ₂ O	14.67	Na ₂ CO ₃	21.0	Na ₂ O	11.40	Na ₂ SO ₄ (s)	21.0
	100.00		100.0		100.00		100.0
Target F		Mixture F		Target 0.5		Mixture 0.5	
SiO ₂	70.44	SiO ₂	53.2	SiO ₂	74.81	SiO ₂	61.3
CaO	11.39	CaCO ₃	15.4	CaO	12.10	CaCO ₃	17.7
Na ₂ O	18.17	Na ₂ SO ₄ (n)	31.4	Na ₂ O	13.09	Na ₂ SO ₄ (s)	10.5
	100.00		100.0			Na ₂ CO ₃ (s)	10.5
					100.00		100.00

Prepared by mixing silica, carbonate, and synthetic (s) or natural (n) sodium sulfate or sodium carbonate powders in weight proportions as specified

Table 8. Compositions of mixtures based on natural evaporation pond salt

Mixture	Sulfate salt	D	F	G	H	I
SiO ₂		57.3	53.2	52.5	51.2	41.2
CaCO ₃		16.5	15.4	18.8	20.7	12.0
Na ₂ SO ₄ (n)	100.00	26.2	31.4	28.7	28.1	46.8
SiO ₂	0.00	73.21	70.09	69.19	67.90	59.71
Na ₂ O	41.99	14.04	17.36	15.88	15.65	28.48
CaO	0.20	11.87	11.44	13.94	15.45	10.01
MgO	1.18	0.39	0.49	0.44	0.44	0.80
Cl	1.49	0.49	0.62	0.55	0.56	1.00
CO ₂						
SO ₃	55.14					
	100.00	100.00	100.00	100.00	100.00	100.00

n, see footnote, Table 7.

EXPERIMENTAL RESULTS

The melting experiments were performed with different batch compositions, melting temperatures, durations, and in different types of containers. The experiments are summarized in Table 9 giving the starting mixtures, containers, and experimental conditions (temperature, duration, and cooling rate) together with the main experimental results. Our exploratory experiments were done without monitoring sulfur release to the furnace atmosphere during melting. Tests of volatile release are presented in the section on ‘Decomposition and melting of sulfates and carbonates.’

Predicted Melting Temperatures

The various glass mixtures tested in the investigation are plotted in the ternary SiO_2 - CaO - Na_2O system (Figure 16; Morey and Bowen, 1925). Mixtures A-E and J are located near or above the ternary eutectic minimum point suggesting melting temperatures of 700-1000 °C. The mixtures with elevated CaO or Na_2O (F-I) suggest higher melting temperatures of 1050-1150 °C. Mixture B that accidentally was prepared with too high SiO_2 plots well within the tridymite field suggesting very high melting temperatures of above 1300 °C. Mixtures 0.5 and 1.0 are relatively similar to mixture C.

The melting temperature chosen for most of the experiments was 1300 °C. This temperature is well above the inferred melting temperature from thermodynamic modeling (Figures 10 and 12) as well as from simplified phase diagrams (Figure 16).

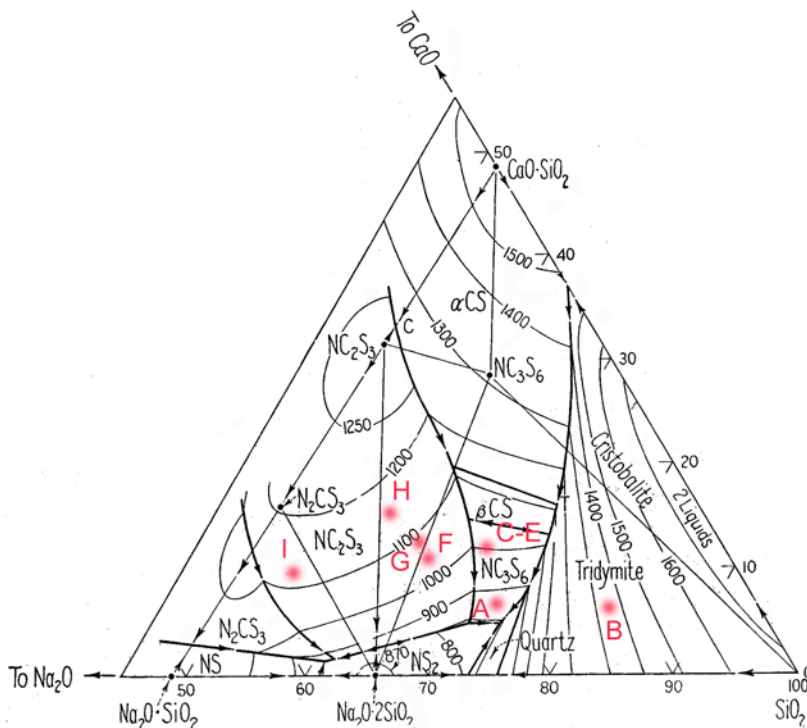


Figure 16. Glass mixtures tested in this investigation (Tables 7 and 8) plotted in the ternary SiO_2 - CaO - Na_2O system (Morey and Bowen, 1925). Compositions J, 0.5, and 1.0 are similar to C.

Use of Sodium Sulfate Separated from Agricultural Drainage Water in Glass Making

Table 9. Experimental results

ID no.	container	Mix	Na source	ramp oC/min	dwell oC	time hrs	cool oC/min	Weight before (g)	Weight after (g)	Loss %	Sulfate Coat (g)	Devitrification	Glass	Comments
SNC-A-1	large container (1)	A	synthetic sulfate	10	1300	3	100	146.5	119.0	19		completely		
SNC-A-5	large container	A	synthetic sulfate	10	1350	3	100					completely		rerun of #1
SNC-A-6	large container	A	synthetic sulfate	10	1400	3	100					partial	glass during remelting	rerun of #2
SNC-B-7	large container	B	synthetic sulfate	10	1300	6	100	137.0	119.0	13		complete		
SNC-B-8	large container	B	synthetic sulfate	10	1350	6	100					complete		rerun of #7
SNC-B-9	large container	B	synthetic sulfate	10	1450	2	100					partial	glass at base	rerun of #8
SNC-C-11	small dish (2)	C	synthetic sulfate	10	1300	6	100						glass	
SNC-C-12	small dish	C	synthetic sulfate	10	1300	6	10						glass	
SNC-C-13	large container	C	synthetic sulfate	10	1300	6	10					complete	glass at base	
SNC-C-14	small dish	C	synthetic sulfate	10	1300	6	10						glass	with #13
SNC-C-15	large container	C	synthetic sulfate	10	1300	24	10					complete		rerun of #13
SNC-C-16	intermediate dish (3)	C	synthetic sulfate	10	1300	6	10	139.9	119.0	15	Yes	complete		
SNC-D-17	cylinder (4)	D	natural sulfate	10	1300	6	10				Yes	complete		sulfate on top and in vesicles pulled out from 1300 oC
SNC-D-19	intermediate dish	D	natural sulfate	10	1300	1.8	1000	54.3	41.8	23		partial	partial glass	
SNC-E-18	intermediate dish	E	sodium carbonate	10	1300	6	100	91.5	74.0	19			glass	spiral crack
SNC-F-20	intermediate dish	F	natural sulfate	10	1300	6	100	106.8	77.7	27		surface	glass	
SNC-G-21	intermediate dish	G	natural sulfate	10	1300	6	100	100.3	71.7	29	Yes	surface	glass	Sulfate coat in 1.5 cm circular patch
SNC-H-22	intermediate dish	H	natural sulfate	10	1300	6	10	102.7	74.7	27		incipient marginal surface complete	glass	6 lpm air flow
SNC-H-23	large container	H	natural sulfate	10	1300	6	10							6 lpm air flow
SNC-H-24	intermediate dish	H	natural sulfate	10	1300	6	100	106.1	77.3	27		incipient marginal surface	glass	6 lpm air flow
SNC-H-25	tall large dish (5)	H	natural sulfate	10	1300	6	100	613.1	459.7	25		partial	glass	6 lpm air flow
SNC-I-26	tall large dish (5)	I	natural sulfate	10	1300	48	100	600.3	528.3	12	172.6 (32.7%)		glass	no airflow
SNC-I-27a	intermediate dish	I	natural sulfate	10	1300	12	100	99.1	84.4	15	31.5 (37.3%)	partial	glass	no airflow
SNC-I-27b	intermediate dish	I	natural sulfate	10	1300	12	100	103.9	88.1	15	32.0 (36.3%)	partial	glass	20 lpm air flow
SNC-I-27c	intermediate dish	I	natural sulfate	10	1300	48	100	107.2	90.1	17	36.5 (40.5%)		glass	20 lpm air flow
SNC-I-27d	cylinder	I	natural sulfate	10	1300	12	100	62.0	54.0	13	Yes	partial	turbulent mixture of glass and sulfate	20 lpm air flow
SNC-1.0-28	intermediate dish	1.0	synthetic sulfate	10	1300	100	100	95.1	76.0	20			glass	20 lpm air flow
SNC-0.5-29	intermediate dish	0.5	synthetic sulfate	10	1300	100	100	105.8	87.2	18			glass	20 lpm air flow
SNC-1.0-30	intermediate dish	1.0	synthetic sulfate	10	1300	100	100	103.9	85.1	18		minor surface devitrification	glass	20 lpm air flow heterogeneous powder
SNC-J-31	intermediate dish	J	synthetic sulfate	10	1300	100	100	99.3	77.8	22			glass	20 lpm air flow

1. Thick (10 ml) porous walled, rectangular container (inner dimensions 75 x 50 x 25 mm).
2. Small pressed walled, 40 mm diameter and 10 mm deep circular dish (AD-998 high alumina).
3. Intermediate pressed walled, 70 mm diameter, 22 mm deep circular dish (AD-998 high alumina).
4. Tall cylindrical pressed walled, 35 mm diameter, 100 mm deep container (AD-998 high alumina).
5. Tall pressed large diameter container, 120 mm in diameter and 120 mm tall (AD-998 high alumina).

Exploratory Experiments

Experiment SNC-E-18 was done without sodium sulfate using a composition very similar to a standard soda-lime window glass with an estimated liquidus temperature of about 1000 °C. The source of sodium in the mixture was sodium carbonate. The mixture was melted for 6 hours at a maximum temperature of 1300 °C. The ternary phase diagram predicts a 1000 °C liquidus temperature for this composition. The product is a clear transparent glass with a spiral crack along the base of the glass (Figure 17). This result demonstrates that standard glass compositions are easily produced using the chosen experimental setup and procedures.

Experiments SNC-C-16 and SNC-D-19 were similar to SNC-E-18 both in terms of batch compositions and in melting conditions as well as predicted liquidus temperature. The only difference was that sodium sulfate was used as the source for sodium instead of sodium carbonate (synthetic sodium sulfate in SNC-C-16 and natural sodium sulfate in SNC-D-19). It was, thus, expected that these two sets of exploratory experiment would produce similar results. Despite this expectation, the results are strikingly different. While the sodium sulfate-free mixture produced a

clear transparent glass, the sodium sulfate-based mixtures produced semitransparent to translucent glasses (Figure 18). Experiment SNC-C-16 resulted in a translucent milky white glass (see subsequent discussion). Experiment SNC-D-19 resulted in a mixture of semitransparent and translucent glass. The bulk compositions recalculated on a volatile-free basis, melting conditions, duration, and container were all similar to the experiment on the carbonate-based glass (Figure 17), with the exception that SNC-D-19 was melted for only 1.8 hours instead of the normally used 6 hours. Another unexpected result for SNC-C-16 was a 2-3 mm thick coating of sodium sulfate on the top surface of the glass (to be discussed later).



Figure 17. Glass produced from standard window glass composition without adding sodium sulfate (SNC-E-18). Melted at 1300 °C for 6 hours. Container is 77 mm in diameter and 26 mm deep (100 ml).



Figure 18. Glass produced from standard window glass composition with synthetic sodium sulfate (SNC-C-16) or natural sodium sulfate (SNC-D-19) instead of sodium carbonate. Melted at 1300 °C for 6 and 1.8 hours, respectively. The container is 77 mm in diameter and 26 mm deep (100 ml).

Container and Container Volume

The first set of experiments produced conflicting results. Thick-walled, porous alumina, 100 ml containers appeared to inhibit glass formation (Figure 19) forming milky white mixture of glass and crystals (see subsequent discussion of devitrification). The result using thin walled containers suggest partial melting (see surface of SNC-C-16; Figure 18) and/or near complete devitrification (see SNC-D-19; Figure 18). Using basically the same glass mixtures, but smaller and thin-walled containers (10 ml), resulted in clear glass without crystallization (Figure 20).



Figure 19. This experiment used the same batch composition as SNC-C-16 and the same melting conditions at 1300 °C. The melting time was increased from 6 hrs to 24 hrs. The upper image shows the product as extracted from the furnace only partially melted. The lower image shows the same product with the crust removed revealing glass formed at the base of the container. Dimension of container is 77 x 98 mm and 36 mm deep (outer measurements).



Figure 20. Mixture C melted in small containers (10 ml) forming clear glass in contrast to the results using larger containers (Figure 19). The differences between three experiments are that SNC-C-11 were cooled faster (~ 100 $^{\circ}\text{C}/\text{min}$) than SNC-C-12 and SNC-C-14 that both were cooled slower (50 $^{\circ}\text{C}/\text{min}$). Synthetic sulfate was used for all three experiments. The container is 44 mm in diameter and 10 mm deep (10 ml).

We attribute these somehow anomalous and unexpected results to several factors. There appears to be an apparent negative correlation between container size and ease of melting and glass formation. It is plausible that small containers with small glass volumes will heat faster and thereby remain above the liquidus for a longer duration compared to larger sized containers. This may result in early establishment of convection in the melt that more efficiently dissolves quartz-grains and also enhances fining of the melt. A consequence may also be a more efficient destruction of potential nucleation sites in the melt. This effect could in combination with a faster cooling for small containers result in a tendency to preserve glass in these compared to the larger volume containers.

Based on these observations, we increased melting duration significantly in some of the subsequent experiments. It is also possible that increasing the melting temperature also can counteract the apparent container volume effect.

The experiments show that crystals appear either as a result of crystallization during cooling (devitrification) as shown in Figure 18 or because the glass mixture does not completely melt during heating. The latter is best illustrated by experiment SNC-C-15 where the top surface appears relatively unmelted as indicated by retention of markings in the original powder surface ('3' shaped suture, Figure 19, upper).

Melting Temperature

We performed a few experiments to examine the effect of increasing the melting temperature above 1300 $^{\circ}\text{C}$ for some experiments performed in the larger-sized and thick-walled containers. Because the furnaces available for the experiments were designed for a maximum temperature of 1500 $^{\circ}\text{C}$, only a few 1350 - 1450 $^{\circ}\text{C}$ experiments were conducted.

The expectations are that an increase in melting temperature will increase the amount of glass in the products. Experiments SNC-A-1 and SNC-B-7 were remelted at increasingly higher temperatures of 1350 , 1400 , and 1450 $^{\circ}\text{C}$ with an increase of melt fraction in the products as expected. This is particularly seen for SNC-B-7 that was done on a mixture with a melting point above 1300 $^{\circ}\text{C}$ (Figure 21).



Figure 21. Second remelting at 1450 °C of completely devitrified experiment originally conducted at 1300 °C (SNC-B-7). First remelting was done at 1350 °C (SNC-B-8). The accumulated melting duration was 14 hours. Dimension of container is 77 x 98 mm and 36 mm deep (outer measurements).

Effect of Composition

A set of experiments was conducted to test the effect of increasing the fraction of network modifying elements beyond the 1:2 (CaO+Na₂O):SiO₂ ratio of typical industrial window glass. The experiments were conducted at identical conditions (1300 °C for 6 hrs.), in the same size containers (thin-walled, 100 ml), and using natural sodium sulfate. The first experiment (SNC-F-20) was done with a glass mixture prepared by increasing the fraction of calcium carbonate in the typical industrial glass mixture C by 20 %. The product illustrated in Figure 22 shows a partial devitrified surface (SNC-F-20). The next experiments were done with a mixture produced by increasing calcium carbonate by 20 % compared to mixture F. The product illustrated in Figure 22 shows partial, but relatively restricted devitrification (SNC-G-21). The next mixture was prepared by increasing the fraction of calcium carbonate by 10 % compared to mixture F. The products made by melting this glass mixture are illustrated in Figure 22 (SNC-H-22, SNC-H-24). The results were clearly a reduction in the amount of devitrification on the surface. Two different cooling rates were used for these latter experiments. SNC-H-22 cooled by shutting off the power to the furnace (fast cooling), while SNC-H-24 was cooled at a rate of 50 °C/min. The effects of these different cooling rates are only apparent in the fracturing of the glass masses.

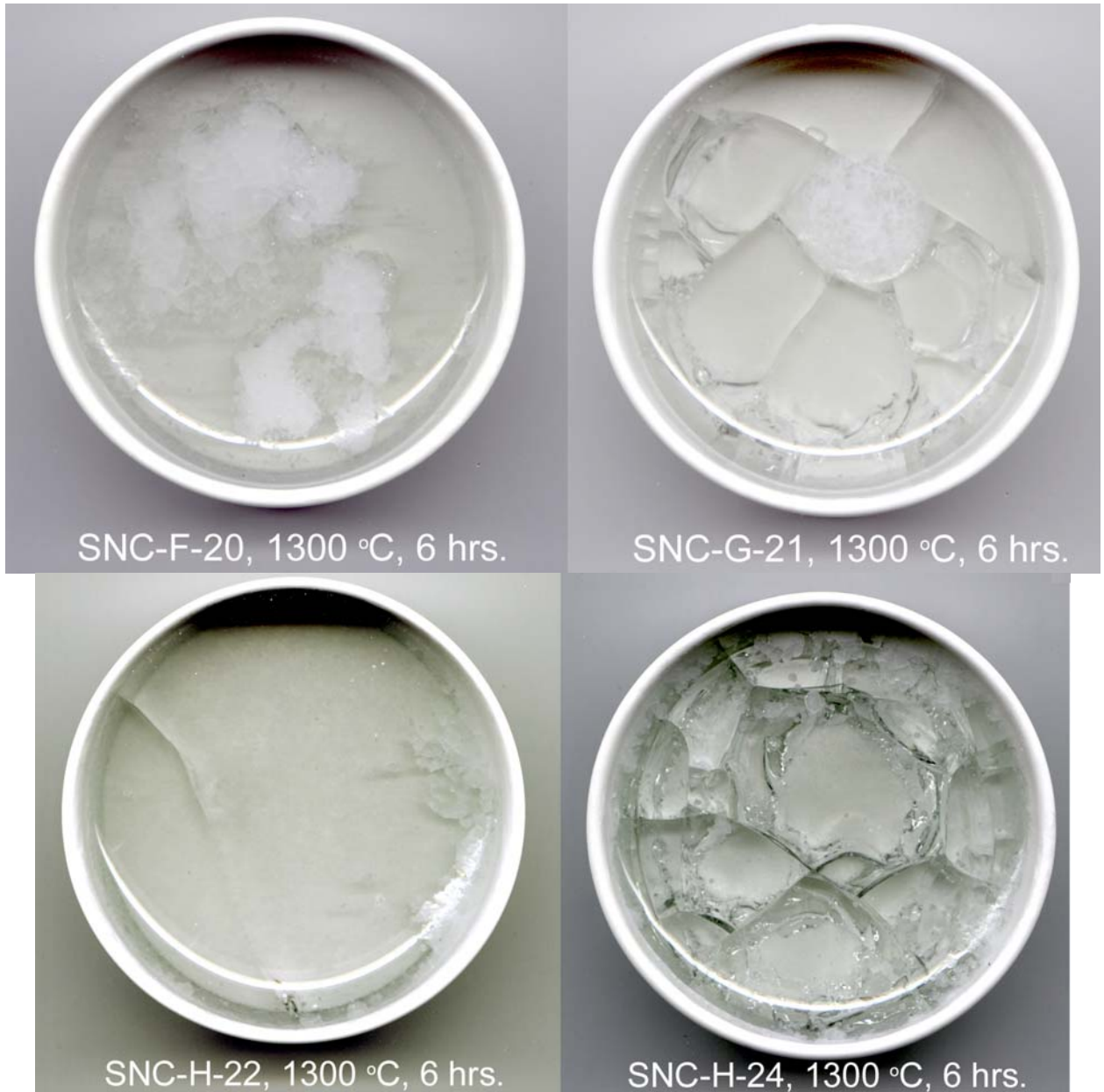


Figure 22. Set of experiments done at same temperature (1300 °C) and duration (6 hrs), but with variable composition. Composition SNC-F was prepared by increasing sodium sulfate in the mixture. Compositions SNC-G and SNC-H were prepared by increasing calcium carbonate in the mixtures. The container is 77 mm in diameter and 26 mm deep (100 ml).

Table 10 gives a summary of electron microscope analyses of the experimental glasses. These are given as the average of several point-analyses, standard deviation, normalization to 100 %, and comparison to the target composition of the glasses. The most important observation from comparing the target compositions with the resultant compositions of the experimental glasses is that significant amounts of sodium were being lost during firing and melting.

Use of Sodium Sulfate Separated from Agricultural Drainage Water in Glass Making

Table 10. Average glass compositions

Oxides	SNC-D-17 Average	N=36 SD	SNC-D-17	Mixture D	SNC-E-18 average	N=7 SD	SNC-E-18	Mixture E	SNC-F-20 average	N=7 SD	SNC-F-20	Mixture F
SiO ₂	68.33	1.9	67.61	73.47	70.77	0.32	71.77	73.47	74.23	0.49	75.06	70.09
Al ₂ O ₃	0.34	0.2	0.34		0.25	0.04	0.25		0.31	0.04	0.31	
MgO	4.09	0.28	4.05		0.10	0.03	0.10		3.36	0.08	3.40	0.49
CaO	15.78	1.54	15.61	11.86	13.22	0.14	13.41	11.86	10.69	0.39	10.81	11.44
Na ₂ O	11.54	1.35	11.42	14.67	14.19	0.14	14.39	14.67	9.95	0.40	10.06	17.36
SO ₂	0.71	0.26	0.70		0.05	0.03	0.05		0.32	0.10	0.32	
Cl	0.28	0.15	0.28		0.03	0.01	0.03		0.04	0.01	0.04	0.62
Total	101.07		100.00	100.00	98.61		100.00	100.00	98.90		100.00	100.00
CaO/Na ₂ O	1.37		20 % Tridymite (*)	0.81	0.93			0.81	1.07			0.66
% Na ₂ O loss			38% (*)				2%				42%	
Oxides	SNC-G-21 average	N=7 SD	SNC-G-21	Mixture G	SNC-H-22 Average	N=10 SD	SNC-H-22	Mixture H	SNC-H-23 Average	N=29 SD	SNC-H-23	Mixture H
SiO ₂	66.54	0.42	67.66	69.19	68.72	0.59	70.49	68.22	65.86	0.05	66.71	68.22
Al ₂ O ₃	0.83	0.04	0.84		0.46	0.09	0.47		0.38	0.05	0.38	
MgO	3.48	0.12	3.54	0.44	3.33	0.13	3.42		4.79	0.46	4.85	
CaO	16.61	0.25	16.89	13.94	15.03	0.41	15.42	15.45	18.12	0.81	18.35	15.45
Na ₂ O	10.06	0.07	10.23	15.88	9.16	0.08	9.40	16.33	9.05	0.31	9.17	16.33
SO ₂	0.8	0.05	0.81		0.71	0.04	0.73		0.47	0.25	0.48	
Cl	0.03	0.01	0.03	0.55	0.08	0.03	0.08		0.05	0.02	0.05	
Total	98.35		100.00	100.00	97.49		100.00	100.00	98.72		100.00	100.00
CaO/Na ₂ O	1.65			0.88	1.64			0.95	2.00			0.95
% Na ₂ O loss			36%				42%				44%	
Oxides	SNC-H-24 average	N=7 SD	SNC-H-24	Mixture H	SNC-H-25 average	N=5 SD	SNC-H-25	Mixture H	SNC-I-26 average	N=10 SD	SNC-I-26	Mixture I
SiO ₂	68.29	0.26	69.70	67.9	69.98	0.32	71.01	67.90	68.95	0.28	71.08	59.71
Al ₂ O ₃	0.69	0.07	0.70		1.06	0.20	1.08		0.73	0.12	0.75	
MgO	3.02	0.11	3.08	0.44	3.37	0.07	3.42	0.44	6.21	0.08	6.40	0.80
CaO	15.93	0.32	16.26	15.45	15.04	0.67	15.26	15.45	9.28	0.32	9.57	10.01
Na ₂ O	9.16	0.14	9.35	15.65	8.07	0.76	8.19	15.65	11.06	0.17	11.40	28.48
SO ₂	0.81	0.10	0.83		0.83	0.04	0.84		0.67	0.08	0.69	
Cl	0.08	0.02	0.08	0.56	0.2	0.02	0.20	0.56	0.11	0.02	0.11	1.00
Total	97.98		100.00	100.00	98.55		100.00	100.00	97.01		100.00	100.00
CaO/Na ₂ O	1.74			0.95	1.86			0.95	0.84			0.35
% Na ₂ O loss			40%				48%				60%	
Oxides	SNC-I-27a average	N=7 SD	SNC-I-27a	Mixture I	SNC-I-27c average	N=7 SD	SNC-I-27c	Mixture I	SNC-I-27g average	N=7 SD	SNC-I-27g	Mixture I
SiO ₂	66.14	0.66	67.31	59.71	68.00	0.5	68.67	59.71	76.42	0.92	78.00	59.71
Al ₂ O ₃	4.81	1.62	4.90		0.39	0.02	0.39		0.84	0.09	0.86	
MgO	1.66	0.17	1.69	0.80	1.73	0.06	1.75	0.80	1.57	0.08	1.60	0.80
CaO	13.22	1.48	13.45	10.01	13.12	0.35	13.25	10.01	8.35	0.44	8.52	10.01
Na ₂ O	11.71	0.23	11.92	28.48	14.95	0.13	15.10	28.48	10.35	0.36	10.56	28.48
SO ₂	0.7	0.03	0.71		0.81	0.14	0.82		0.43	0.09	0.44	
Cl	0.02	0.01	0.02	1.00	0.02	0.01	0.02	1.00	0.01	0	0.01	1.00
Total	98.26		100.00	100.00	99.02		100.00	100.00	97.97	1.98	100.00	100.00
CaO/Na ₂ O	1.13			0.35	0.88			0.35	0.81			0.35
% Na ₂ O loss			58%				47%				63%	
Oxides	SNC-1-28 average	N=7 SD	SNC-1-28	Mixture 1	SNC-0.5-29 average	N=7 SD	SNC-0.5-29	Mixture 0.5	SNC-1-30 average	N=8 SD	SNC-1-30	Mixture 1
SiO ₂	69.27	0.42	70.40	76.26	71.15	0.44	72.07	74.81	67.81	1.07	69.63	74.81
Al ₂ O ₃	3.36	0.5	3.41		2.75	0.14	2.79		3.77	0.41	3.87	
MgO	0.12	0.03	0.12		0.09	0.02	0.09		0.16	0.03	0.16	
CaO	13.79	0.68	14.01	12.34	12.3	0.14	12.46	12.10	14.67	0.47	15.06	12.10
Na ₂ O	11.27	0.2	11.45	11.40	11.94	0.09	12.09	13.09	10.14	0.18	10.41	13.09
SO ₂	0.57	0.07	0.58		0.46	0.05	0.47		0.83	0.14	0.85	
Cl	0.02	0.01	0.02		0.03	0.01	0.03		0.01	0.00	0.01	
Total	98.4		100.00	100.00	98.72		100.00	100.00	97.39		100.00	100.00
CaO/Na ₂ O	1.22			1.08	1.03			0.92	1.44			0.92
% Na ₂ O loss			0%				8%				20%	
Oxides	SNC-J-31 average	N=7 SD	SNC-J-31	Mixture J								
SiO ₂	69.05	0.52	70.00	73.47								
Al ₂ O ₃	3.04	0.12	3.08									
MgO	0.11	0.02	0.11									
CaO	12.56	0.27	12.73	11.86								
Na ₂ O	13.28	0.18	13.46	14.67								
SO ₂	0.58	0.06	0.59									
Cl	0.02	0.01	0.02									
Total	98.64		100.00	100.00								
CaO/Na ₂ O	0.95			0.81								
% Na ₂ O loss			8%									

It is notable that sodium loss is strongly reduced from all experiments based on the standard industrial, window glass composition. This includes the completely sodium carbonate based experiment (SNC-E-18), partial sodium carbonate based experiment (SNC-0.5-29), and completely sodium sulfate based experiments (SNC-SNC-1.0-28, SNC-1.0-30, and SNC-J-31). These all show relatively low sodium loss ($<20\%$) and are all based on the standard window glass composition.

It is equally notable that all experiments for which the standard industrial glass composition was modified to contain higher amounts of calcium and sodium show strong sodium losses. Experiment SNC-F-20 was prepared by increasing sodium sulfate and results in marked sodium loss of about 40% of the original sodium content (as wt. % oxide). Experiments SNC-G-21, SNC-H-22, SNC-H-23, SNC-H-24, and SNC-H-25 were done on mixtures containing higher calcium compared to SNC-F-20. These experiments indicate a similar sodium loss of $40\text{--}50\%$ (wt. % oxide).

There appears to be one exception. Experiment SNC-D-17 was made on a typical window glass composition. The product was strongly devitrified. Mixing calculations using the glass composition obtained with the microprobe and the target composition (Table 10) estimated about 20% tridymite and a Na_2O loss of 38% (wt. %).

A series of experiments were based on a composition for which the sodium content was increased by 40% in order to counteract the effects of the observed sodium loss. These experiments were SNC-I-26 and SNC-I-27. The result was an even stronger loss of sodium of $40\text{--}60\%$ (wt. % oxide).

Heterogeneity of Glass Mixture

The possibility that some of the adverse effects observed could be related to incomplete mixing of the components made us test a simple 'layered cake' configuration of the starting powder. The overall composition was composition 1.0, similar to a typical window glass (Table 7). Sodium sulfate was placed at the bottom, calcium carbonate in the middle, and silica at top of the 'cake' in the container. Melting conditions were similar to previous experiments, except that the melting duration was 100 hours.

The product showed nearly complete melting and glass-formation with the exception of a few millimeter-sized, devitrification patches on the surface of the glass. This result led us to conclude that heterogeneity in the glass mixture will have only minor effect on glass formation and stability during quenching for sufficiently long melting intervals.

Cooling Rate Effects

The abundant devitrification observed in many experiments led us to test the effect of cooling rate on the ease of crystallization. The overall composition and melting composition were as used for the other experiments reported here (mixture 1.0, Table 7). All tests were done with a $10^\circ\text{C}/\text{min}$ heating rate to 1300°C and 24 hrs duration at maximum temperature.

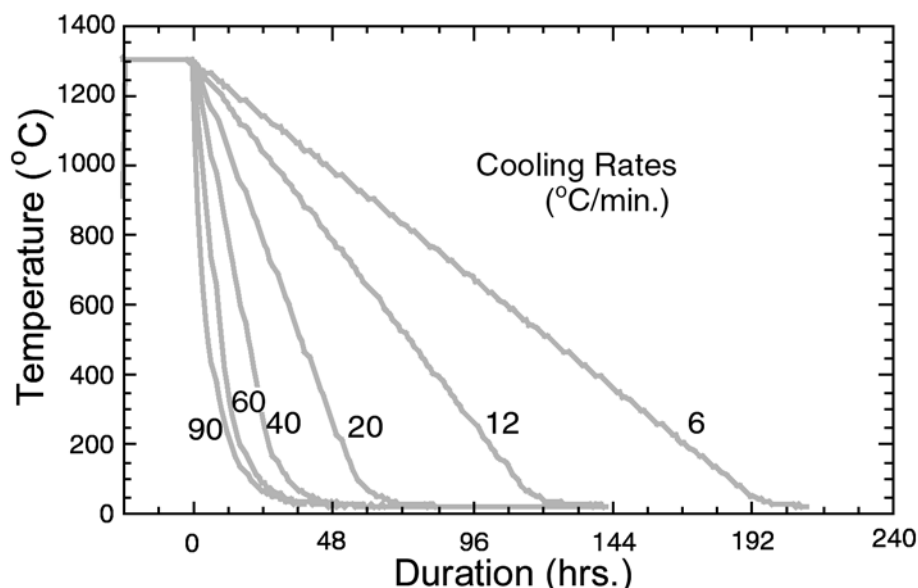


Figure 23. Temperature as a function of duration (hrs) for experiments testing glass formation. All cooling rates examined produced clear glass without crystallization.

The cooling rates examined are illustrated in Figure 23 and varied from 90 °C/min to 6 °C/min. The highest cooling rate was obtained by shutting off the power to the furnace. All tests produced glass without noticeable crystallization. It was expected that a crystal nucleation and growth field could have been intersected for the low cooling rate experiments of 6 °C/min. As this was not the case, the critical cooling rate for glass formation for the composition used in this study must be below 6 °C/min. This demonstrated the ease with which glass is formed for the present composition and that the cooling rate chosen in this study is sufficient to avoid homogeneous nucleation. These tests also allow us to conclude that the observed crystallization (or devitrification) is the result of heterogeneous nucleation during quenching.

Melting Duration

The final experiments were conducted to test the effect of melting duration. The same glass mixture as used above was selected (mixture 1.0, Table 7). The melting conditions were also similar to those used above except that the duration at maximum temperature (1300 °C) was varied from 1 to 48 hours. The products are illustrated in Figure 24. The product after 1 hour melting was composed of a mixture of glass and crystals. The overall result was a milky white mass with an irregular surface. The product after 12 hours melting revealed a proportion of glass with patches of clear glass. The product after 48 hours melting was a clear glass without crystallization.

Another observation was that remelting of the products in general resulted in higher glass fractions. Thus remelting the 12-hour melted product in Figure 25 for an additional 48 hours produced a significant increase in the proportion of glass. Further remelting for another 24 hours produced a glass with only a millimeter sized crystallized patch on the surface. Melting at an accumulated duration of 108 hours produced a clear glass without crystallization.

These results make us conclude that the melting duration may strongly affect the nature of the melting products. We suggest that the longer melting duration (1) increases the likelihood that all

quartz particles are completely disintegrated, (2) increases the disruption of the polymerized melt structure, and (3) results in complete destruction of quartz-like potential nucleation points of the melt. The overall effect of increasing melting duration may thus be to ensure complete melting as well as destruction of potential nucleation sites and thus reduce crystallization during quenching.

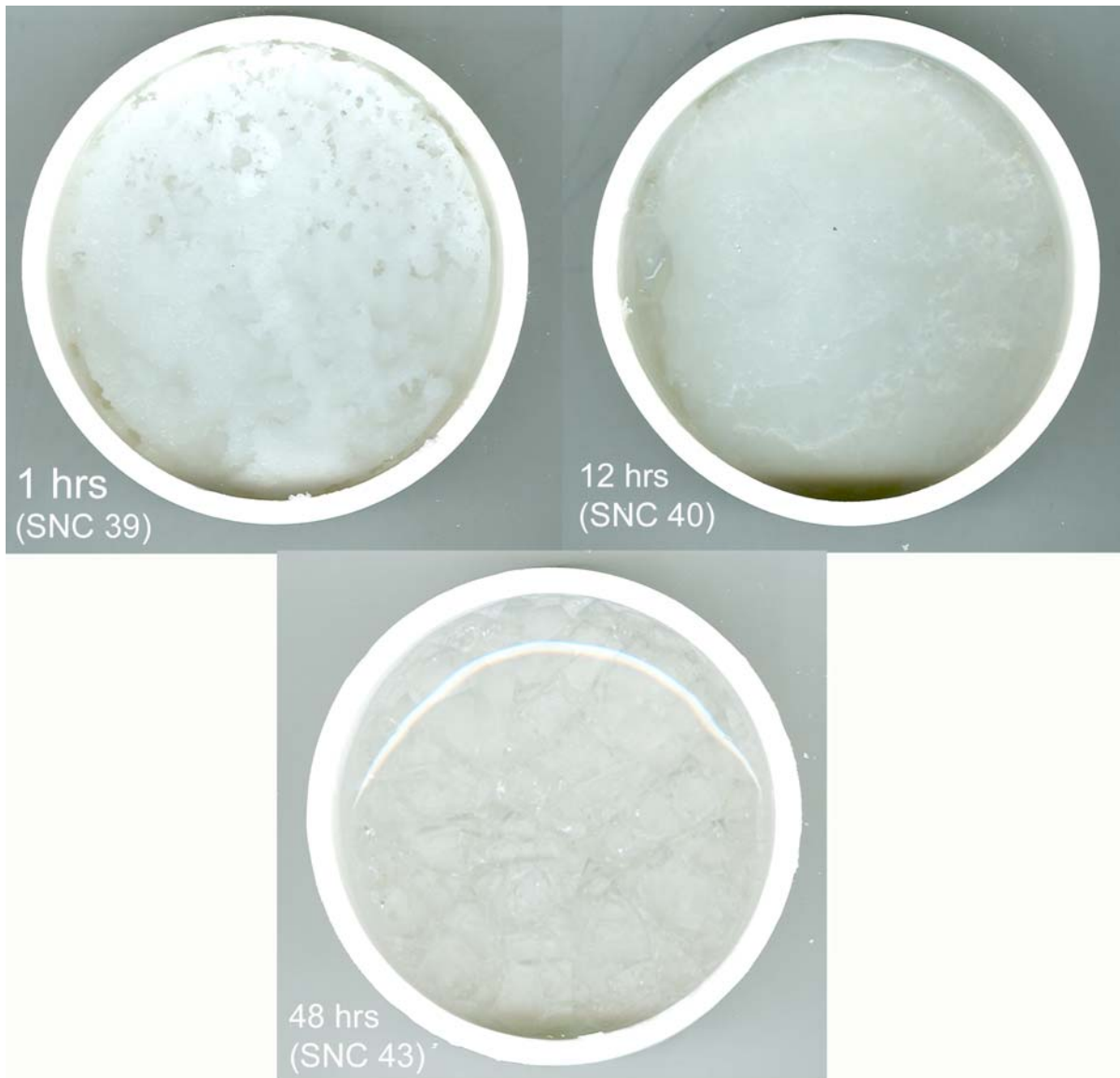


Figure 24. The effect on melting duration at 1300 °C for the same glass composition based of sodium sulfate (see text).

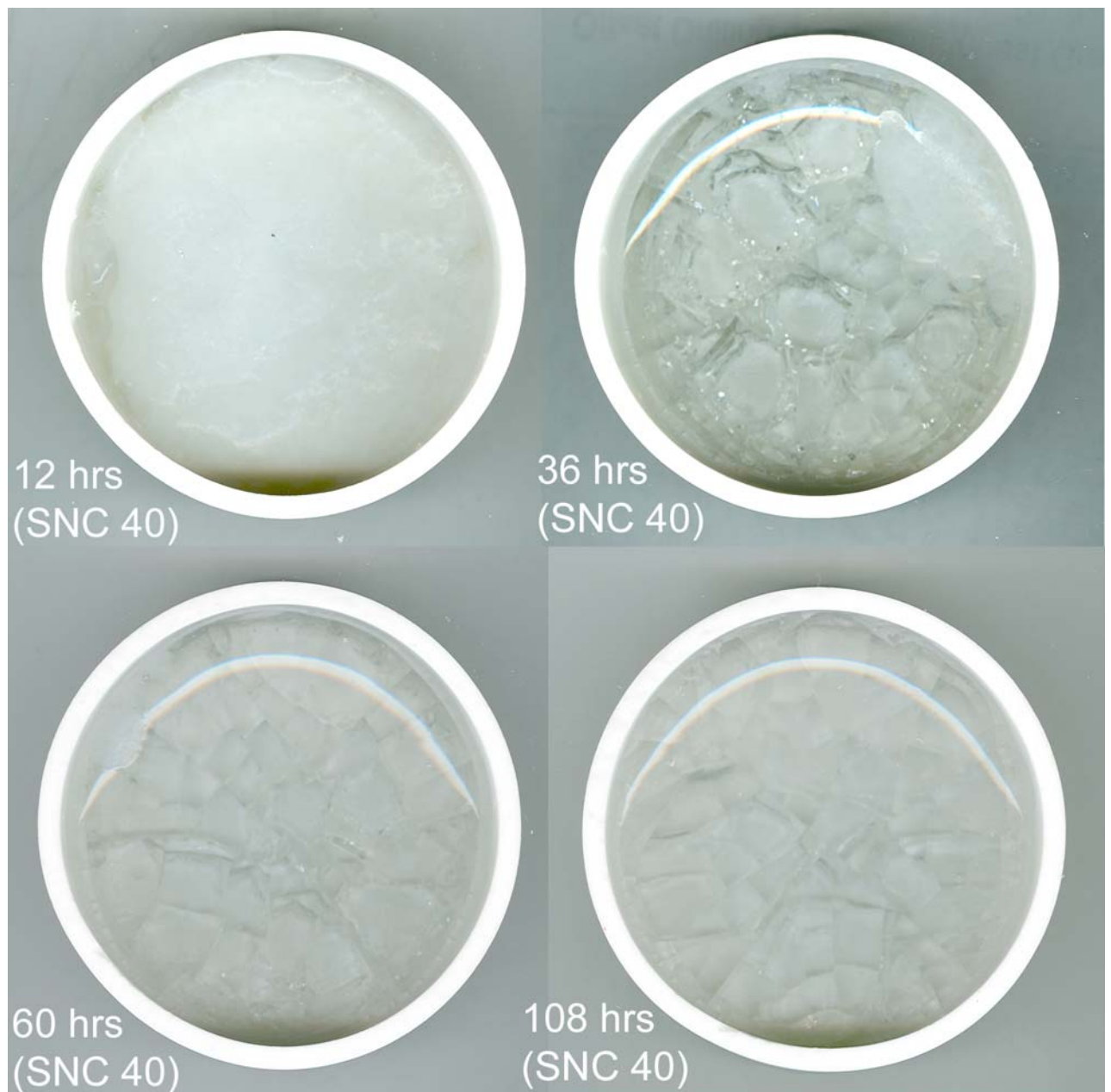


Figure 25. The accumulative effect of remelting the same glass at durations up to 108 hours.

Crystallization and Devitrification

Several experimental products are partially or completely composed of a milky white semitransparent to translucent material. This is particularly well illustrated by SNC-C-16 (Figure 18) that shows an irregular remnant of the original surface as an island in the largely melted glass mass. This suggests that the starting mixture for this experiment was only partially melted.

A back-scattered electron image (BSE) of the white translucent product of SNC-C-16 is shown in Figure 26. It is seen that the material is composed of a fine intergrowth of crystals and presumably glass. An XRD analyses show that the crystals are tridymite (high temperature quartz polymorph) (Figure 27 and Table 11). The XRD analysis also demonstrates the presence of glass as a broad background hump between 2θ of $20\text{--}35^\circ$. There are no indications of the presence of other crystalline phases, including quartz.

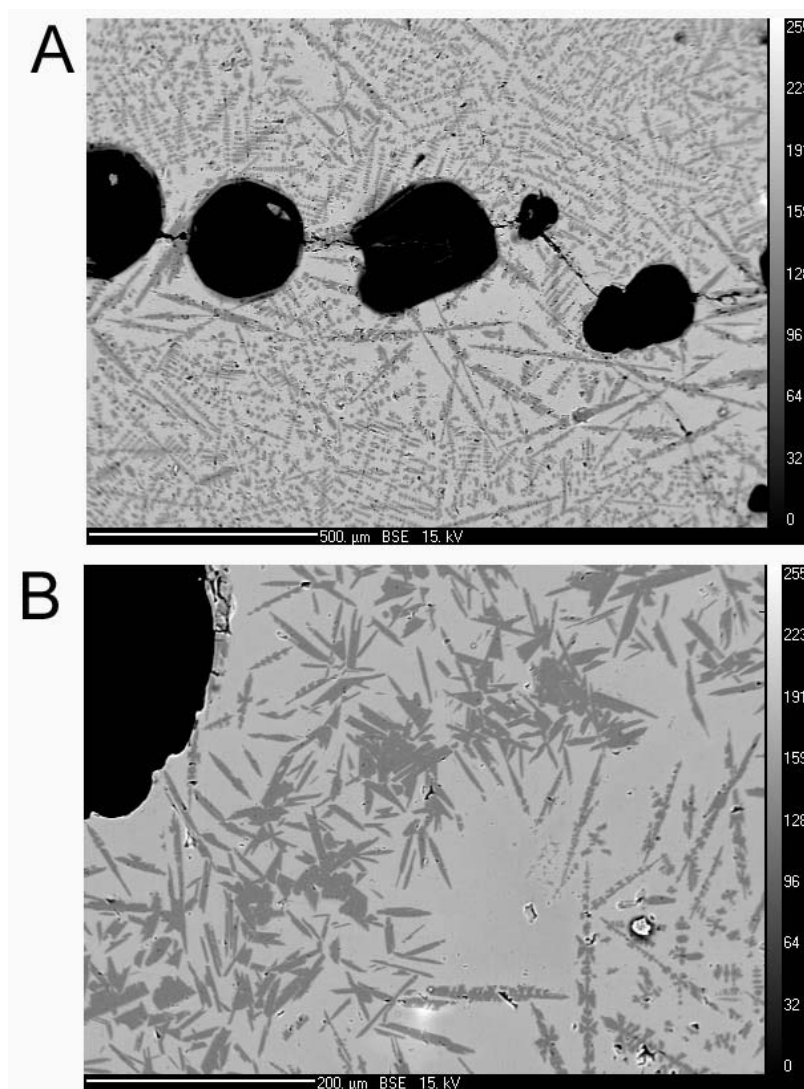


Figure 26. BSE images of the experimental product of SNC-C-16. A. String of early formed vesicles connected by a crack in devitrified matrix. B. Close up of the matrix texture with air bubble in the upper left.

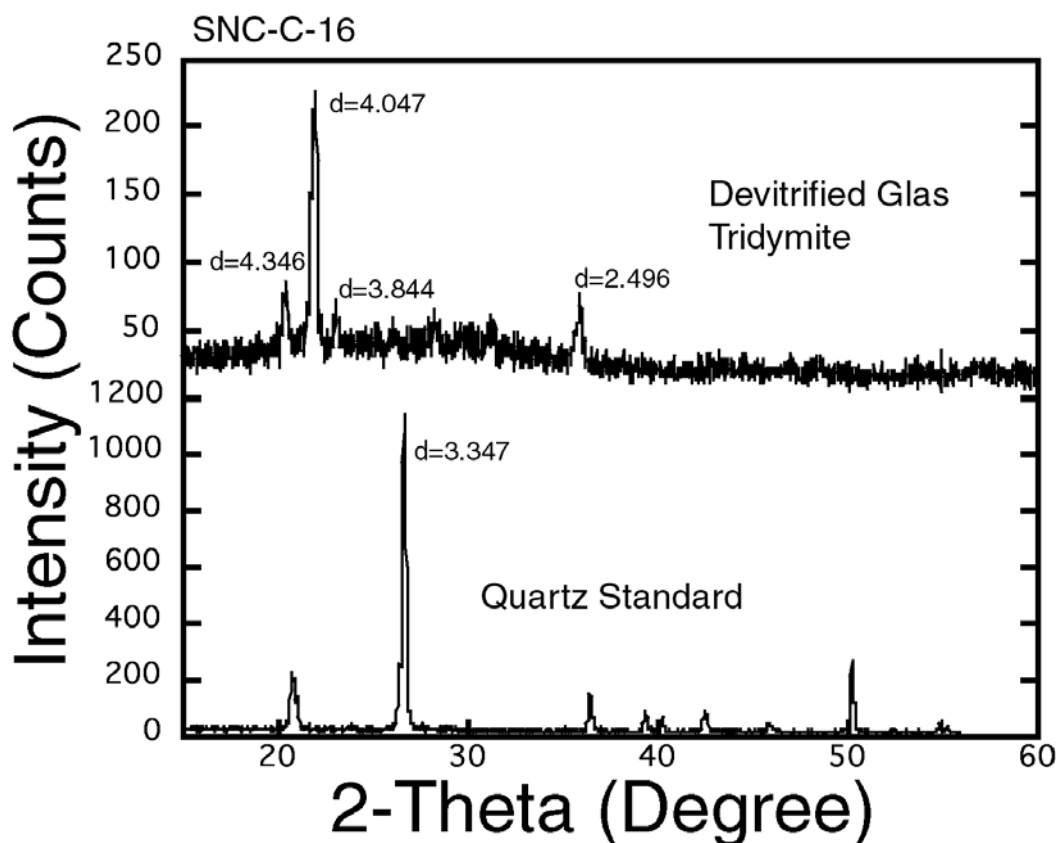


Figure 27. X-ray diffraction patterns for SNC-C-16 shown as total counts against 2-Theta (2θ) with characteristic d-values identified (in Ångstrom). Shown is the characteristic background hump for glass between 20-35° and reflections for tridymite. Lower pattern is for quartz standard.

Table 11. Interpretation of X-ray Diffraction Pattern for Devitrified Glass

#	2-Theta	d(A)	I	I %	Mineral	d(A)	I %	2-Theta
1	20.417	4.346	43	22.9	Tridymite-O	4.285	93	20.713
2	21.940	4.047	188	100.0	Tridymite-O	4.080	100	21.763
3	23.115	3.844	34	18.1	Tridymite-O	3.801	68	23.381
4	35.642	2.517	23	12.2				
5	35.941	2.496	42	22.3	Tridymite-O	2.481	35	36.120

Obtained pattern compared to best fit to expected values for tridymite (orthorhombic).
d(A) - d-spacing in Angstrom; I - intensity in counts; I % - intensity in % relatively to highest peak.

The shape of the tridymite grains vary from angular and tabular ($<20\text{ }\mu\text{m}$) to elongated ($<200\text{ }\mu\text{m}$) needle-shaped and dendritic crystals (Figure 26). The angular and tabular grains show growth forms that indicate equilibrium conditions. Grains with rounded grain boundaries may indicate disequilibrium, but these are not abundant (Figure 28). Thus, there are no strong indications for partial dissolution in the habit of the tridymite grains. There appears to be a bimodal distribution of the tabular and dendritic grains. The tabular and angular grains represent an early generation. Finer and needle shaped grains have partially nucleated and grown on the early tabular grains where present. Very fine-grained, crystallographic orientated overgrowth forms (dendritic) occur further away from the initial tabular grains and appear to have nucleated from the melt (Figure 26a).

The presence of tridymite, as opposed to quartz, restricts the temperature of crystallization to high temperature ($>870\text{ }^{\circ}\text{C}$). For products for which incomplete melting is indicated such as SNC-C-16, this points toward high temperature re-equilibration of the original quartz powder with the melt without reaching liquidus conditions. The dendritic grains may have formed during cooling and quenching of the products as metastable tridymite below $870\text{ }^{\circ}\text{C}$.

The textural evidence thus suggests a progression in the habits of tridymite grains (Figure 26b). The tabular grains were probably in equilibrium with the original melt at the maximum melting temperature of $1300\text{ }^{\circ}\text{C}$. The habit of these early tridymite grains suggests dominating equilibrium growth and to a lesser extent dissolution forms (Figure 28). The next generation of tridymite is angular to needle shaped and appears largely to have nucleated on the earlier grains probably as a result of initiated cooling. The final generation of tridymite grains appears to have nucleated homogeneously from the melt and is characterized by highly elongated dendritic and crystallographic growth forms likely the result of continued progressive cooling that accelerate nucleating and growth rates.

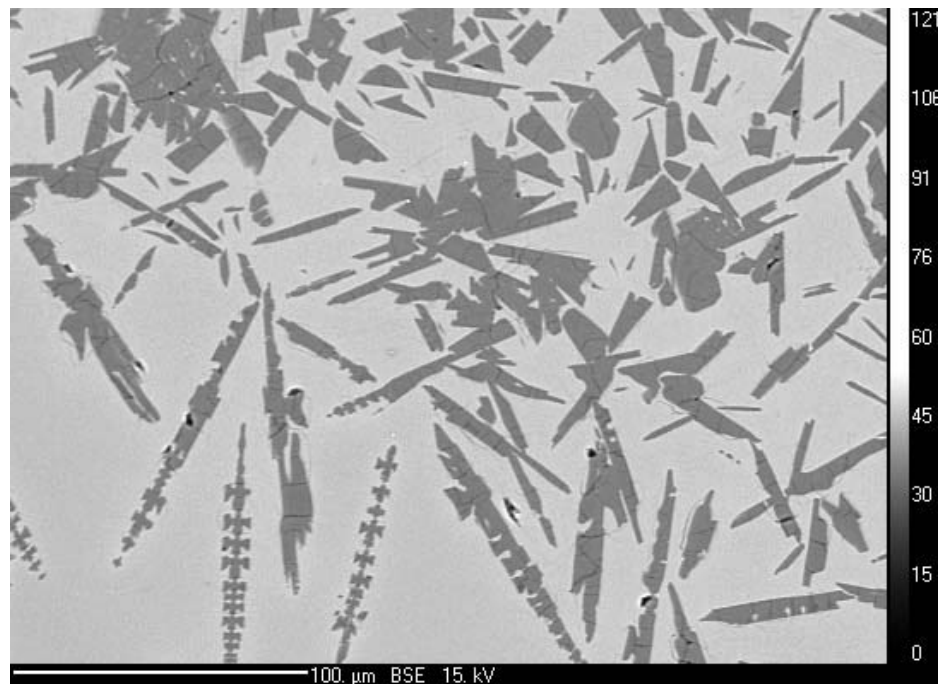


Figure 28. BSE image of tridymite growth forms in SNC-H-23.

It is also interesting to note that there are no indications of nucleation on melt and bubble surfaces or on container surfaces. This rules out the possibility that crystallization occurred on bubble surfaces and that the crystalline material is a scum accumulated on the surface during melting.

The evidence is somehow ambiguous as to when bubble formation occurs. There are signs that tridymite growth was truncated by bubble formation and that tridymite grains restricted bubble growth. There are also signs of elongated tridymite crystals being draped around bubble surfaces (Figure 26b). Although inconclusive, this suggests that bubble formation occurs during growth of tridymite and cooling of the glass. Figure 26a clearly shows that cracking of the glass occurs in the solid stage after formation of tridymite and exsolution of air bubbles.

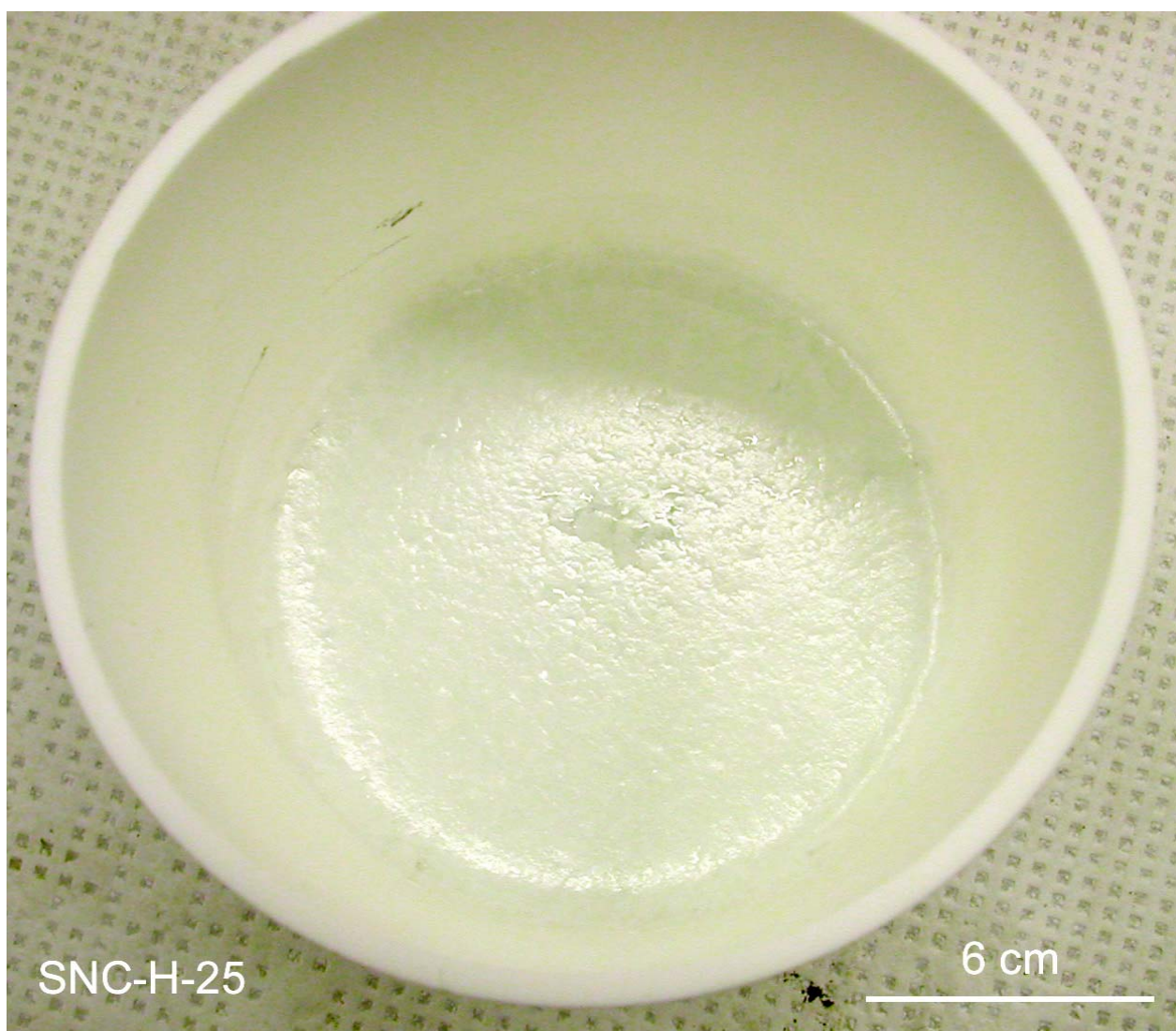


Figure 29. The experimental product SNC-H-25 in a large thin walled alumina container. The results revealed partial devitrification in the glass with clear glass preserved in the center at the surface (see Figure 30).

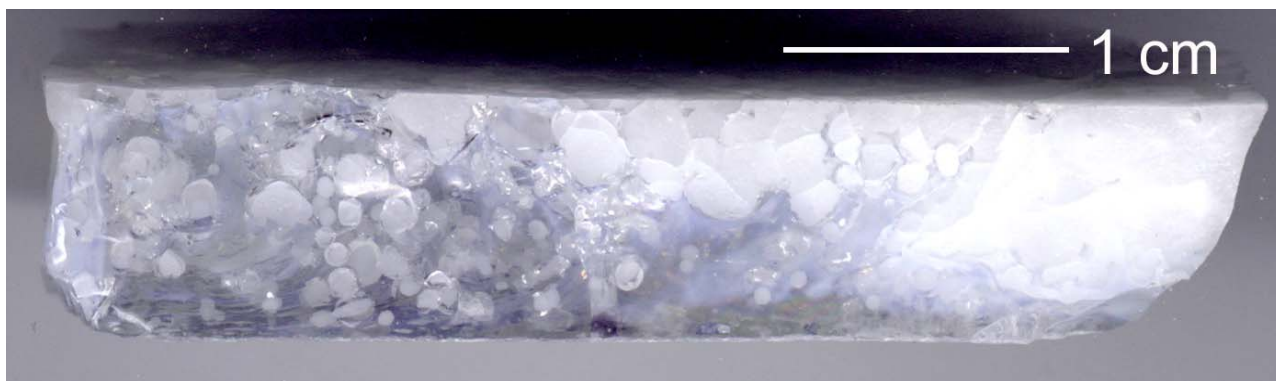


Figure 30. Cross section of partially devitrified glass in SNC-H-25 (see Figure 29). Left is near center, right is the margin of the container. Note the circular devitrification spheres toward the center and that their number increases toward the top and margin where they appear to coalesce to an apparent homogeneous milky white material.

The results of experiment SCN-H-25 is particularly illustrative as to the mechanism of devitrification (Figure 29). This experiment was conducted with a glass mixture prepared with relatively high CaO and Na₂O (Table 10). The experimental product shows partial devitrification (Figure 30) that is seen to be confined to cells (<2-4 mm in diameter) that grow in size eventually to interlock and to transform the whole melt volume to a devitrified glass. The results of SNC-H-25 show that the devitrification cells are most abundant and complete along the margins where the cells interlock and effectively eliminate transparent glass. Toward the center and bottom of the glass there appear to be fewer and also smaller devitrification cells (Figures 29 and 30). This suggests that devitrification is controlled by cooling from the container sides and melt surface. The reason why devitrification cells appear less abundant toward the center of the container is not clear. We speculate that it may be related to the interaction between central convective cooling and radiating cooling along the margins of the melt mass.

A back-scattered electron image of several devitrification cells is shown in Figure 31 from SNC-H-25. The devitrification cells decrease in size with distance from the top surface (see Figure 30). The center of each cell is relatively coarse grained, but the grain size strongly decreases toward the cell margins. Concentric cracks around the cells can often be seen that are probably related to contraction as a result of devitrification.

Figure 32 shows two representative, devitrification cells also from SNC-H-25. Both cells show a concentric pattern with the centers with relatively coarse grains and finer grains towards the margins. The first cell contains angular and tabular grains in the center and elongated grains with dendritic growth forms. Comparisons of electron microprobe analyses of the glass phase in the center of the cell and outside the cell are summarized in Table 12. It is seen that glass in the center is enriched in CaO and Na₂O as result of about 20 % crystallization of tridymite.

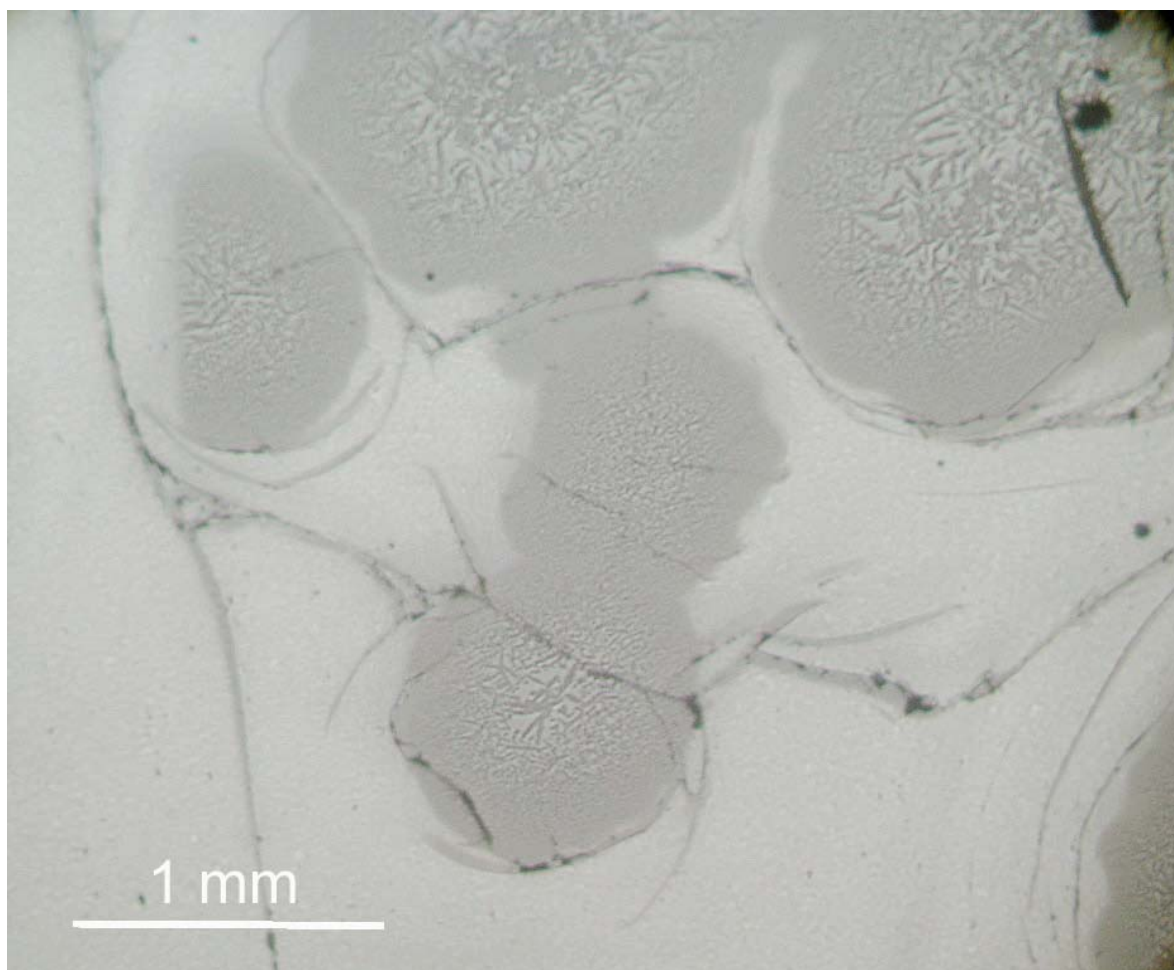


Figure 31. Close-up of the devitrification spheres in SNC-H-25. Top is toward the surface of glass mass. Note the decrease in grain-size from the centers toward devitrification margin (=front) for each cell. Concentric contraction cracks surround the devitrification cells.

Table 12. Effect of Devitrification on Glass Composition (SNC-H-25)

	Bulk Glass		Devitrified Cell	
	Av. (5)	SD (5)	Av. (3)	SD (3)
SiO ₂	69.98	0.32	64.02	0.67
Al ₂ O ₃	1.06	0.20	0.80	0.05
FeO	0.04	0.02	0.07	0.04
MgO	3.37	0.07	4.10	0.06
CaO	15.04	0.67	18.96	0.53
Na ₂ O	8.07	0.76	9.36	0.12
Cl	0.20	0.02	0.24	0.04
SO ₂	0.83	0.04	0.92	0.06
Total	98.58		98.47	
% wt.			19	
Tridymite				

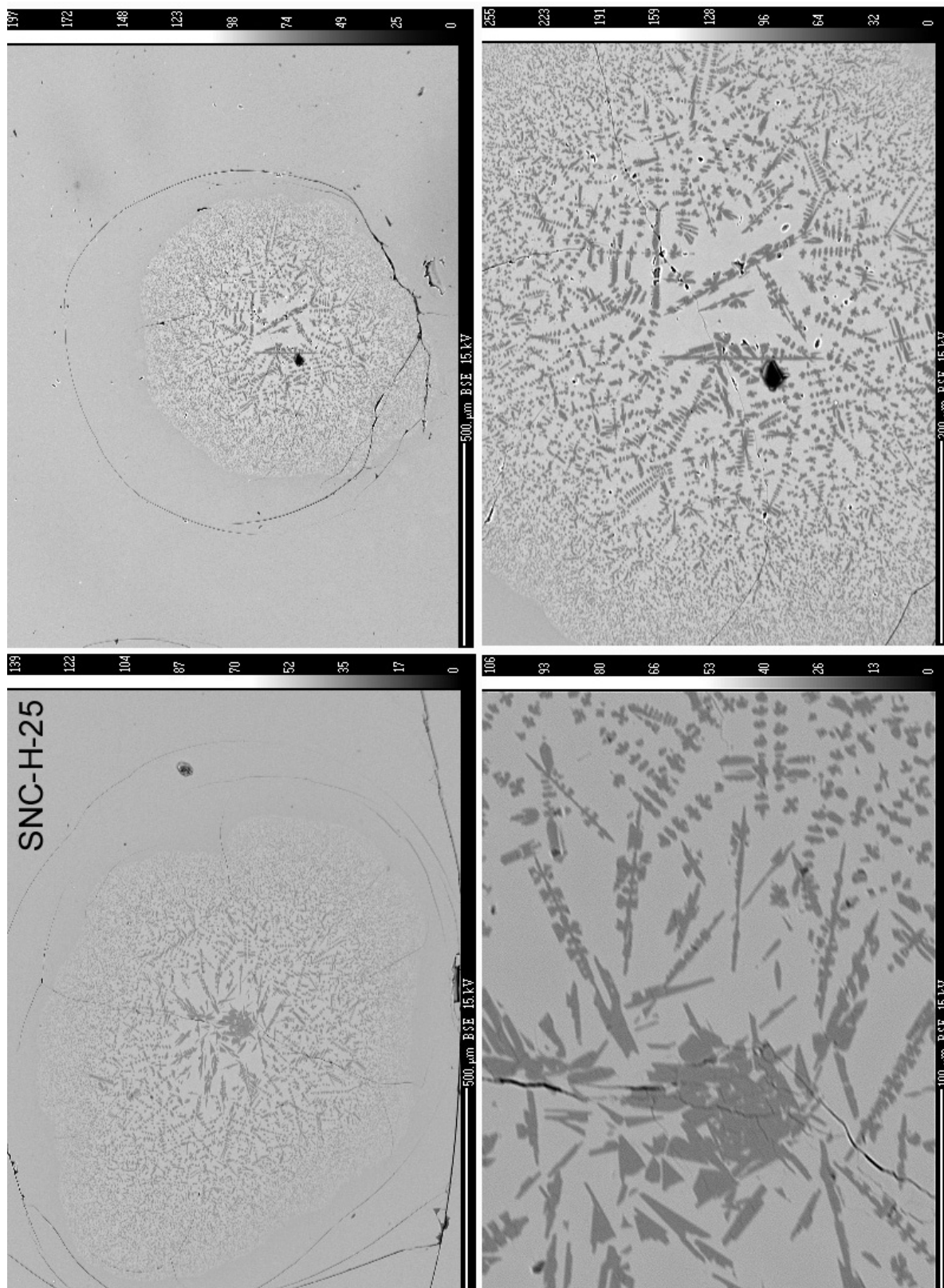


Figure 32. Close-ups of devitrification cells in SNC-H-25.

The next experiment (SNC-D-17) was made in a 100 ml, cylindrical container. The disadvantage of this container was that material during melting was ejected with the release of gas and overflowed and spattered around the container and furnace walls and floor. A thin section through the experimental product (Figure 33) was analyzed with the electron probe from the base to the top. The results are shown in Figure 34. Shown is the composition of the interstitial glass (excluding tridymite grains). It is apparent that Cl and SO₂ show systematic variation and decreases from the bottom to the top of the container. Other elements and oxides show no systematic variation. Mass balance calculations were used to estimate the amount of tridymite grains as 20 %.

We further selected two experimental products for a similar analytical examination: 1) SNC-H-23 made in the thick walled container with a highly crystalline, milky white appearance (similar to product SNC-C-16 in Figure 18, but prepared from mixture H), and 2) SNC-H-22 made in a small thin walled container and composed entirely of clear glass with minor devitrification foam developed along the container margin (Figure 22). For both experimental products, we prepared polished thin sections in order to analyze the vertical composition from top to bottom.

The variation from bottom to top in the clear glass (SNC-H-22) is seen in Figure 35, as wt. % oxides or element. Considerable variation is seen amounting to <3 wt. % SiO₂ and <0.3 wt. % Na₂O. The oxides Al₂O₃, MgO, and CaO appear for unknown reasons slightly to decrease toward the top. There is a small decrease in many oxides, including Na₂O, in the top millimeter. The volatile components Cl and SO₂ show considerable variation, but both lack the systematic decrease toward the top as observed for SNC-D-17 (Figure 35).

The similarly obtained compositional variation seen in the highly crystalline product of experiment SNC-H-23 is illustrated in Figure 36. This product contains numerous vesicles and large cavities. For example, the main mass is lifted up and away from the bottom of the container producing an empty space at the base. Significant contamination is seen near the base from reaction with the alumina container (Figure 36), however, this appears only to affect the lower most part of the product directly in contact with the container (see also Figure 34). The oxides MgO and CaO appear to show a slight increase toward the top, while Al₂O₃ and Na₂O appear to be relatively constant throughout the experimental product. The SiO₂ content shows considerable variation attributed to nucleation of tridymite. The volatile components Cl and SO₂ show a general decline toward the top, but with large local variation that may in part be controlled by the proximity to vesicles and cavities.



Figure 33. SNC-D-17. Experimental product with large vesicles and devitrified glass with quartz grains giving a semitransparent milky white appearance. Sometimes vesicles are filled with sulfate salt.

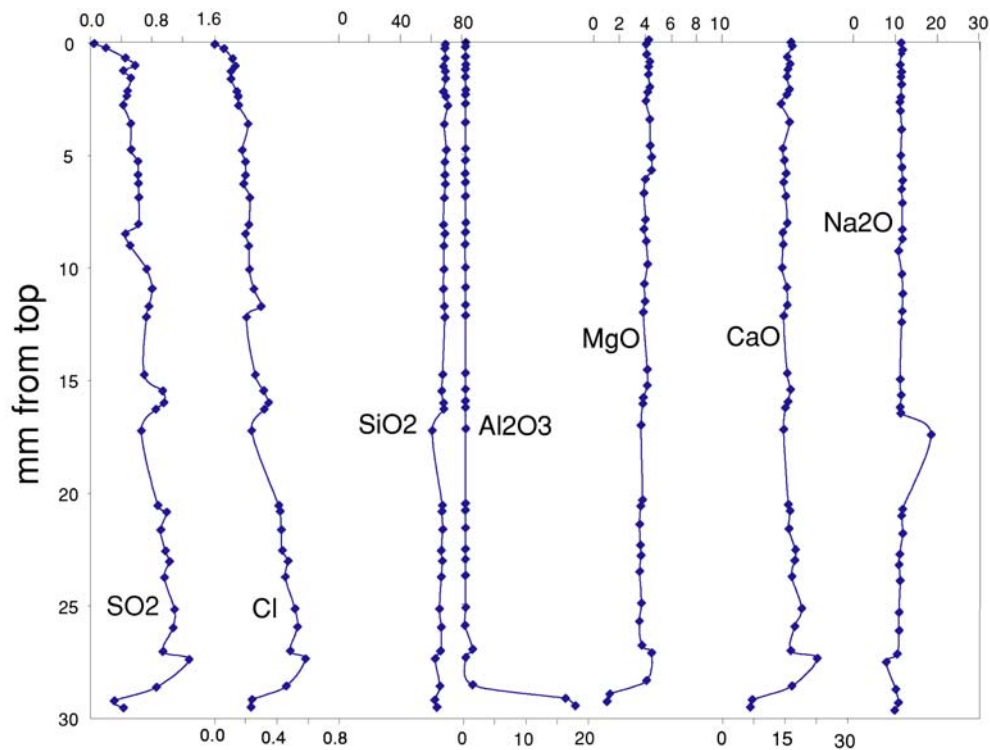


Figure 34. SNC-D-17. Composition of the interstitial glass in devitrified glass from top to bottom of SNC-D-17. Shown are SO₂, Cl, SiO₂, Al₂O₃, MgO, CaO, and Na₂O all as wt. %. Note the large increase in Al₂O₃ toward the bottom of the container is caused by reaction between melt and container wall.

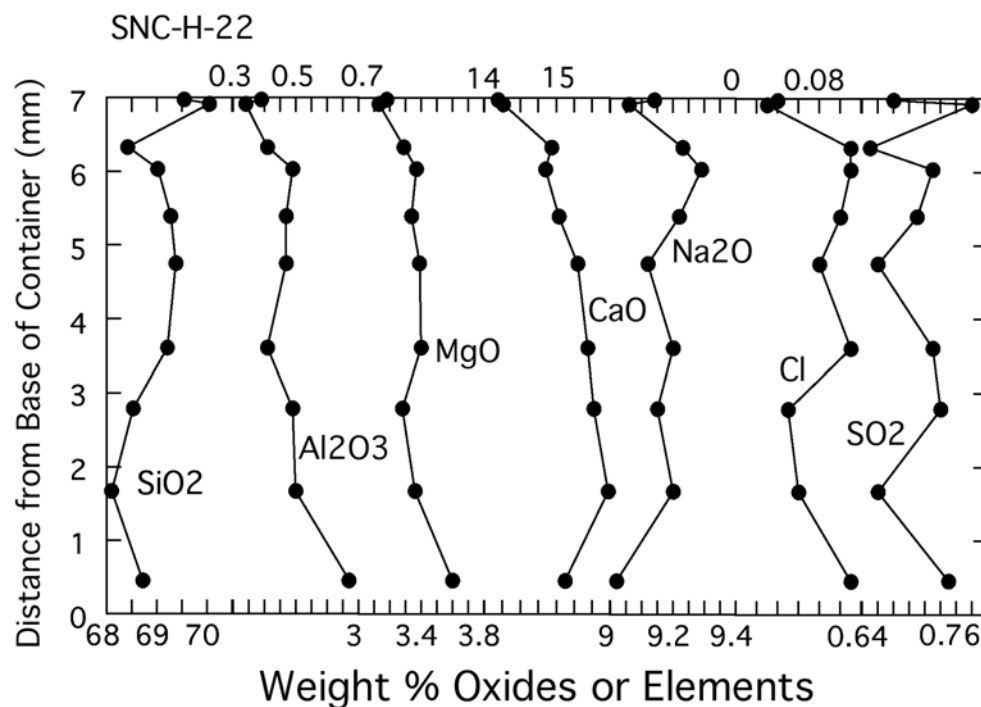


Figure 35. Variation in the major oxides (SiO₂, Al₂O₃, MgO, CaO, Na₂O) and Cl and SO₂ from bottom to top in glass formed in experimental product SNC-H-22.

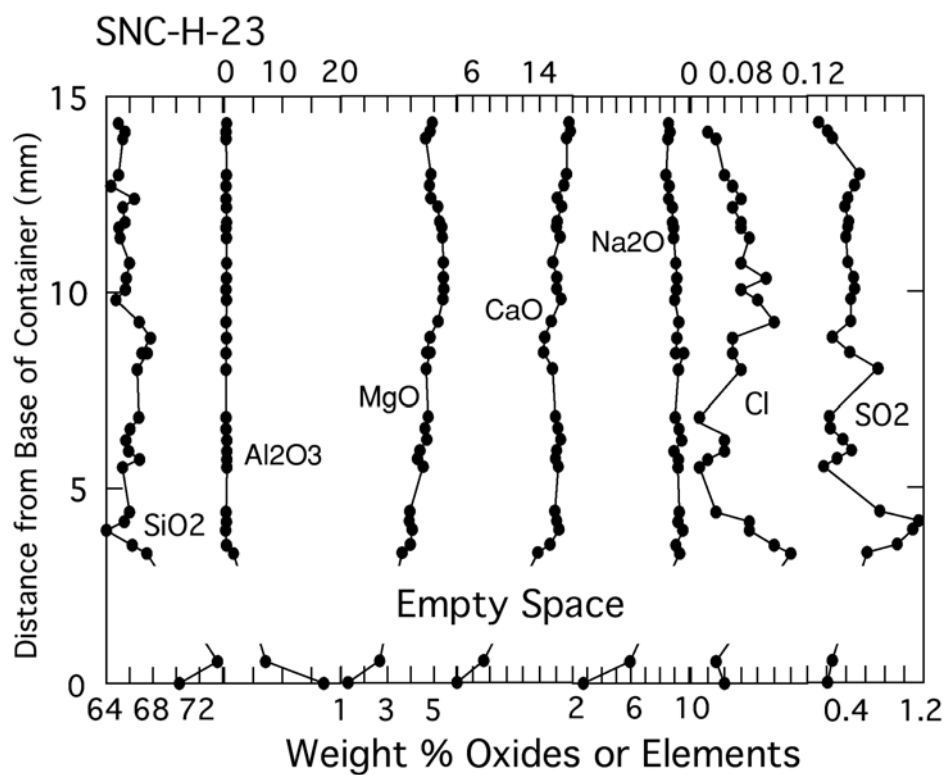


Figure 36. Variation in the major oxides (SiO₂, Al₂O₃, MgO, CaO, Na₂O) and Cl and SO₂ from bottom to top in glass formed in experimental product SNC-H-23. Large empty spaces and vesicles occur in the product. The irregular variation in silica is probably due to variation in tridymite crystallization.

Reaction with Container

Many experiments indicate reactions between melt and containers composed of alumina (or corundum). In some cases it is evident that the amount of melt (glass) increases in proximity to the container. This was particularly observed in SNC-C-16 (Figure 18) and SNC-D-17 (Figure 33), and SNC-H-23 (Figure 37). The reaction is a simple uptake of alumina in the melt (Table 12) that appears to lower melting temperature and to perhaps stabilize glass.

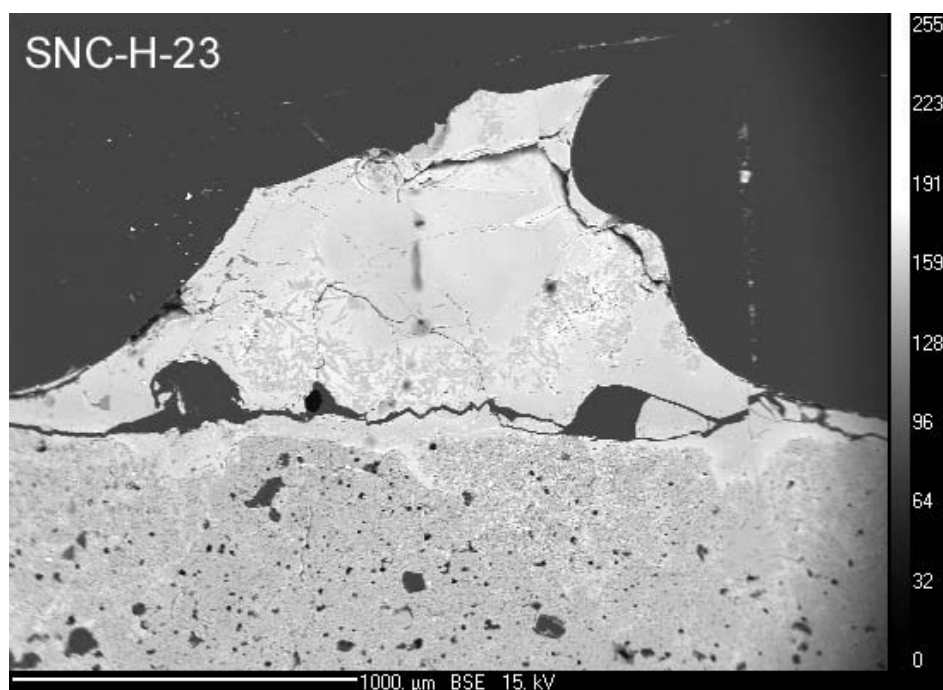


Figure 37. Back-scattered electron image of SNC-C-23. Reaction between alumina container and silica melt.

Table 13. Effect of Reaction With Container (SNC-H-23)

	1	2	Center
SiO ₂	70.30	73.57	65.86
Al ₂ O ₃	17.10	7.13	0.38
FeO	0.03	0.03	0.06
MgO	1.31	2.67	4.79
CaO	6.08	9.29	18.12
Na ₂ O	2.72	5.93	9.05
Cl	0.04	0.03	0.05
SO ₂	0.21	0.26	0.47
Total	97.78	98.90	98.77

1. Near container wall. 2 - 560 microns away from container wall.

Sodium Sulfate Coating

Thin coatings of sulfate appear sometimes on the experimental products (Table 9). This is seen for SNC-C-16 (Figures 18), SNC-D-17 (Figure 33), SNC-G-21 (Figure 22), and SNC-I-26 to SNC-I-27 (Figure 38). The sulfate appears mostly on the top surface of the glass. An example is product SNC-C-16 that had a 1 to 2 mm thick but irregular layer of sulfate. This experiment indicated partial melting with an irregular surface of which only the topographically lower parts were covered with sulfate (Figure 18). A typical appearance of the sulfate coating is shown in Figure 38. The sulfate is crystalline with large grains flattened parallel to the glass surface and often showing dendritic growth forms (Figure 39). The intersection between the glass and sulfate coating shows negative crystal forms indented into the glass. The product of SNC-D-17 has vesicles filled with sulfate (Figure 33). These observations suggest that the sulfate formed as a melt that accumulated on the top of the glass melt and crystallized as a result of cooling together with the transformation of the melt to a glass. This observation is critical for any attempt to make glass, since the removal of sodium from the melt changes the composition of the melt and thereby potentially also its ability to form glass.



Figure 38. Sulfate coating on the surface of experimental glass (SNC-I-27c).

An X-ray diffraction study of product SNC-C-16 showed that the sulfate layer is composed of a mixture of thenardite (Na_2SO_4) and glauberite ($\text{Na}_2\text{Ca}(\text{SO}_4)_2$) (Figure 40 and Table 13). Two unidentified peaks at a 2θ of $24\text{--}26^\circ$ ($d=3.575\text{ \AA}$ and $d=3.411\text{ \AA}$) suggest the presence of dansite ($\text{Na}_{21}\text{Mg}(\text{SO}_4)_{10}\text{Cl}_3$) and thus the retention of chlorite in the sulfate coating. Although this may be possible for experiments based on natural sulfate containing small amounts of halite, this is not likely for products based on synthetic sodium sulfate, like SNC-C-16, without Cl and Mg.

An X-ray diffraction study of a sulfate coating appearing on a product based on natural sulfate (containing small amounts of halite and bloedite with Cl and Mg, respectively) is shown in Figure 41 (SNC-I-26). The result and interpretation are essentially identical to that for the sulfate coating based on synthetic sulfate. The sulfate is composed of a mixture of thenardite and glauberite. Dansite is again suggested by a peak at a 2θ of 24° ($d=3.584\text{ \AA}$). This shows that the original

sodium sulfate used in the glass mixture reacts with calcium carbonate and forms double sulfate salts.



Figure 39. Surface of sulfate coating on surface of experimental glass (SNC-C-16). Note dendritic growth forms. The illustration has been enlarged from Figure 17.

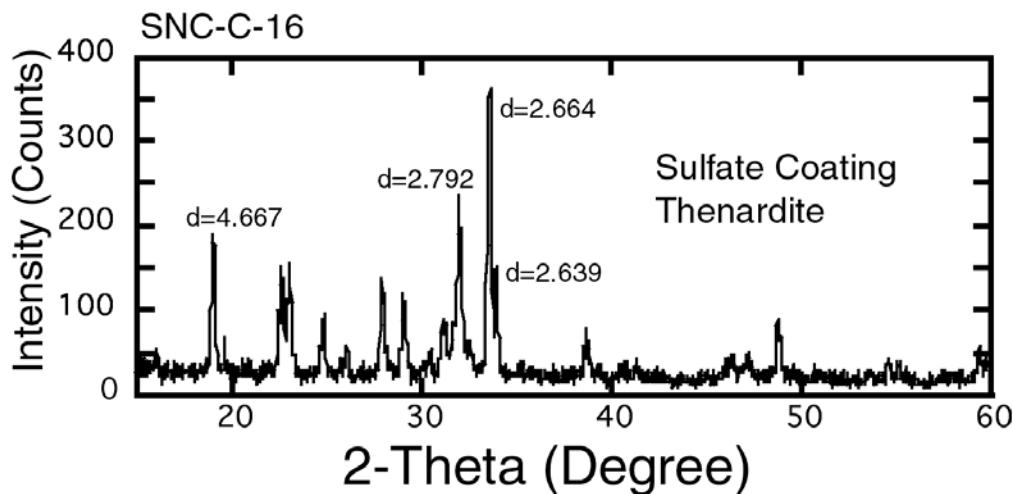


Figure 40. X-ray diffraction pattern for sulfate coating of SNC-C-16 shown as total counts against 2-Theta (2θ) with characteristic d-values identified (in Ångstrom).

After it was discovered that under certain conditions sodium sulfate might form as a coating on the glass after melting at 1300 °C, work was focused on characterizing and analyzing the sodium sulfate coating. It was decided to add additional sodium sulfate to the mixture in order to compensate for the observed loss of sodium. This was achieved by preparing a new mixture I containing excess sodium sulfate compared to mixture H (Table 7). It was expected that this mixture readily would produce a sulfate coating and also that the resultant glass would retain higher proportions of sodium and perhaps restrict devitrification.

As expected, experiments SNC-I-26 and SNC-I-27 produced abundant glass with limited devitrification and a consistent 2-3 mm thick sulfate layer as a cover on top of the glass (Figure 38). The sulfate coating was in addition to the XRF analysis (Figure 41) also examined with the electron microprobe. Back-scattered image and elemental X-ray dot-maps of a grain surface mount are shown in Figure 42. It is seen that the sulfate is composed of a two-phase fine intergrowth on the scale below 10 μm . One phase is Ca-poor or thenardite) while the other phase is calcium-rich or glauberite, as indicated by the XRD analyses.

The fine intergrowth of thenardite and glauberite suggests that the two phases exsolved from a high temperature solid solution to form a mixture of thenardite and glauberite (Müller, 1910).

Table 14. Interpretation of X-ray Diffraction Pattern for Sulfate Coating (SNC-C-16)

#	2-Theta	d(A)	I	I %	Mineral	d(A)	I %	2-Theta
1	15.992	5.537	26	7.7				
2	19.001	4.667	166	49.3	Thenardite	4.658	71	19.035
3	22.640	3.924	126	37.4	Glauberite	3.945	45	22.519
4	23.099	3.847	130	38.6	Thenardite	3.838	17	23.153
5	24.881	3.575	72	21.4	Dansite?	3.561	10	24.985
6	26.100	3.411	34	10.1	Dansite?	3.396	100	26.220
7	27.959	3.188	110	32.6	Thenardite	3.181	52	28.027
8	29.080	3.068	85	25.2	Thenardite	3.077	55	28.990
9	30.456	2.932	27	8.0				
10	31.272	2.857	42	12.5	Glauberite	2.861	50	31.237
11	32.019	2.792	197	58.5	Thenardite	2.784	100	32.123
12	33.617	2.664	337	100.0	Glauberite	2.677	60	33.445
13	33.936	2.639	127	37.7	Thenardite	2.648	52	33.826
14	38.657	2.327	58	17.2	Thenardite	2.330	25	38.615
15	38.872	2.314	36	10.7	Glauberite	2.319	4	38.800
16	46.505	1.951	22	6.5				
17	47.294	1.920	26	7.7				
18	48.818	1.864	58	17.2	Thenardite	1.865	36	48.780
19	54.676	1.677	21	6.2				
20	55.198	1.662	22	6.5				
21	59.383	1.555	41	12.2	Glauberite	1.553	2	59.471
22	59.794	1.545	26	7.7				

Obtained pattern compared to expected values for best fits for dansite, thenardite, and glauberite. d(A) - d-spacing in Angstrom; I - intensity in counts; I % - intensity in % relatively to highest peak.

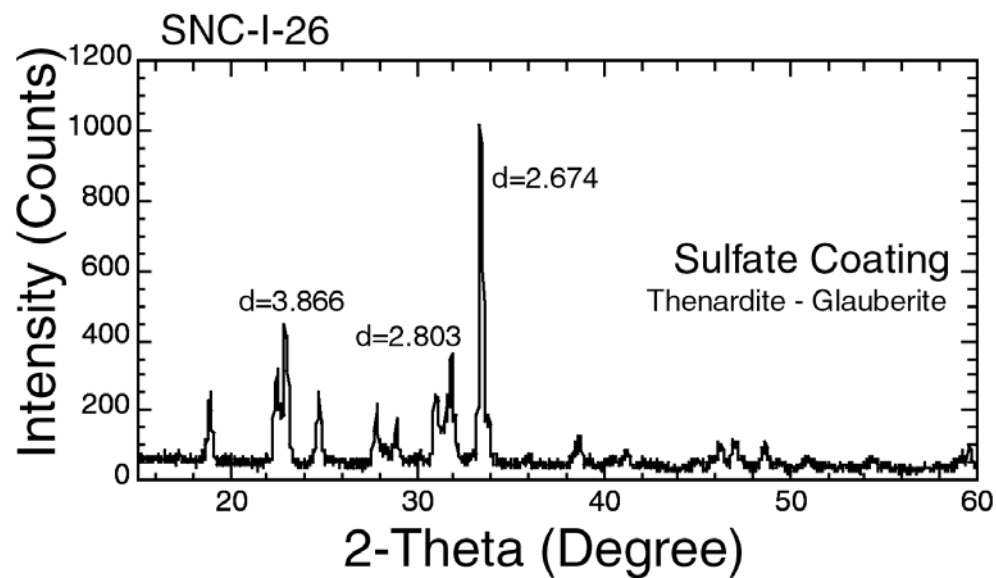


Figure 41. X-ray diffraction pattern for sulfate coating of SNC-I-26 shown as total counts against 2-Theta (2θ) with characteristic d-values identified.

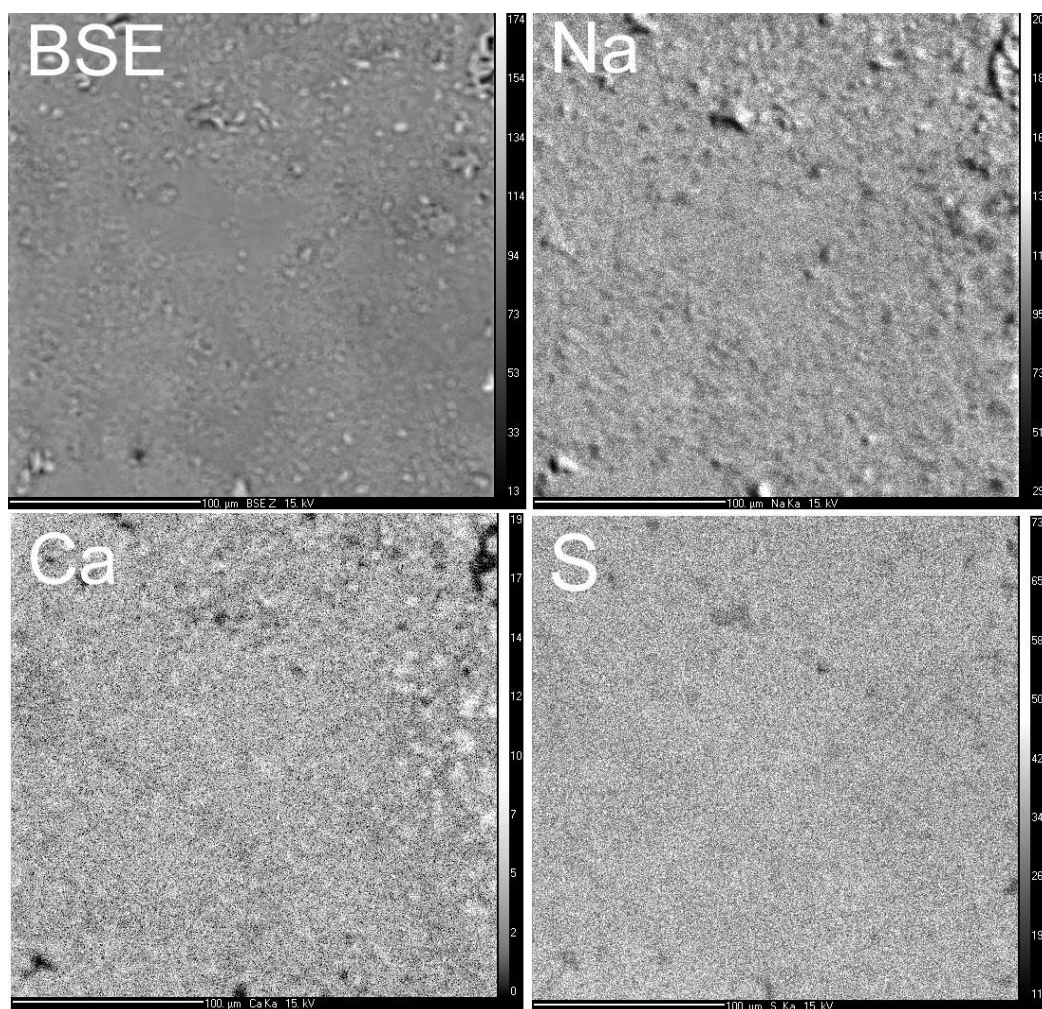


Figure 42. Back-scattered image (BSE) and X-ray elemental dot-maps (Na, Ca, S K_{α}) of a surface grain mount of the sodium sulfate coating obtained in SNC-I-26.

The thenardite-glauberite intergrowth readily dissolved in water and leaves a Ca-rich phase as a solid residue that was not detected by X-ray diffraction. Semiquantitative analyses obtained on grain mounts from the sulfate coating are illustrated in Figure 43 and Table 15. It is seen that the bulk sulfate coating contains dominating sodium and sulfur, but also considerable amounts of calcium (~4 wt. % CaO).

The Ca-rich residual phase appears to be anhydrite. This is demonstrated in Figure 44 by energy-dispersive spectra and in Table 15 by microprobe analyses of separated residual anhydrite grains. Calculated to an ideal sulfate stoichiometry with four oxygens, both the bulk sulfate and the residual anhydrite approximate an ideal sulfate formula by $\text{Na}_{1.83}\text{Ca}_{0.12}\text{S}_{0.99}\text{O}_4$ and $\text{Ca}_{1.01}\text{Na}_{0.01}\text{S}_{0.99}\text{O}_4$, respectively (Table 15). The formula for the bulk sulfate coating suggests a 94 % thenardite and 6 % glauberite mixture.

The analytical results given in Table 15 illustrate that the sulfate coating is composed of a nearly pure mixture of sodium sulfate and calcium sulfate. Elements other than Na, Ca and S are below detection limits with the electron microprobe. This means that MgO, the only other major element of the natural sulfate salt, is completely retained in the glass product. This observation may offer a technique for purifying the natural sulfate salt.

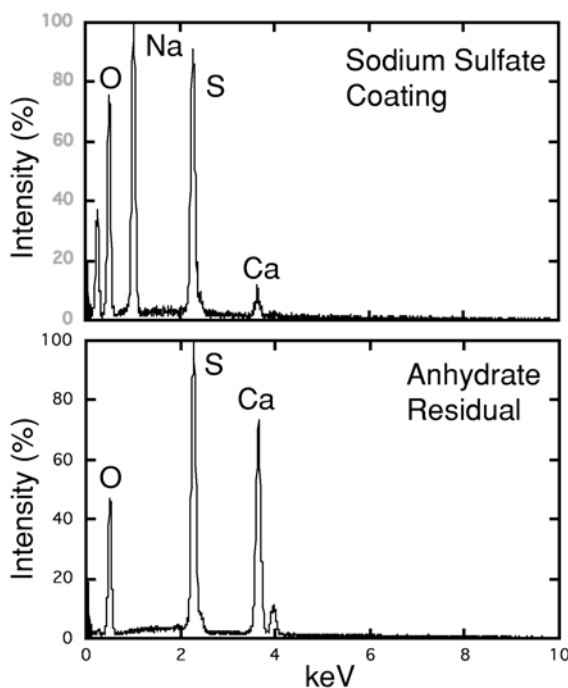


Figure 43. Energy dispersive spectra of bulk sulfate coat (upper) and anhydrite residual grain (lower) after dissolving thenardite in water. Peak at lowermost left is carbon from sample coating

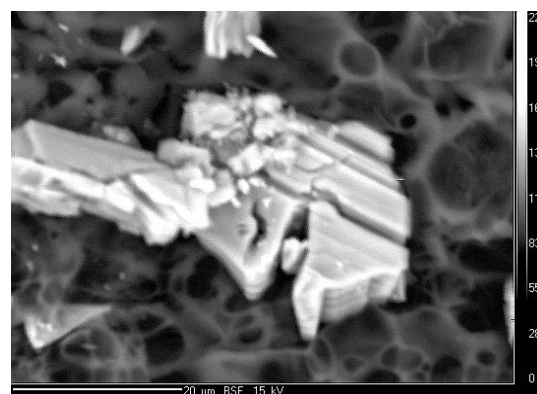


Figure 44. Residual anhydrite grain after dissolving thenardite in water. Analysis of the grain is given in Table 15.

Table 15. Mineralogy of sulfate coating (SNC-I-26)

Wt. % Oxides	Sulfate Coating			Anhydrite Residual		
	AVR	STD (N=6)	Cations/O=4	AVR	STD (N=3)	Cations/O=4
SiO ₂	nd			nd		
Al ₂ O ₃	nd			nd		
FeO	nd			nd		
MgO	nd			nd		
CaO	4.18	0.49	0.117	29.83	2.51	1.012
Na ₂ O	35.95	1.75	1.829	0.21	0.13	0.011
K ₂ O	0.08	0.02	0.001	nd		
P ₂ O ₅	0.07	0.02	0.000	0.28	0.02	0.007
SO ₃	40.11	1.17	0.987	33.25	2.14	0.988
Cl	0.08	0.02		nd		
Total	80.47		2.934	63.57		2.018

Sodium Loss

The loss of Na₂O from the glass during firing is given in Table 10 and has been calculated from the target composition of the glass (Table 7) and the direct microprobe analyses of the resultant product (Table 10). The apparent loss ranges to above 60 % and appears to be correlated with the amount of sodium sulfate in the original glass batch. Figure 45 illustrates the relationship between sodium loss and the amount of sodium sulfate in the original mixture. All experiments with high sodium sulfate (47 %; mixture I) also show a high Na₂O loss (50-63 %). The same products also had a marked sodium sulfate coating, explaining the loss of sodium from the glass that resides in the coating. Two other products indicated sulfate coatings. These are experiments SNC-D-17 and SNC-G-21 (Figure 45). Experiment SNC-D-17 was made in a tall narrow cylindrical container that may have severely restricted air circulation at the surface of the product. Experiment SNC-G-21 was done in a wide-open container and only showed 3-cm circular thin patch of sodium sulfate on the surface. The only other experiment with a significant sulfate coating was SNC-C-16, but the glass product was not analyzed. All the latter three products with sulfate coating were conducted without airflow through the furnace.

A group of experiments showed no or little sodium loss during firing and also no sodium sulfate coating. These are the carbonate based window glass (SNC-E-18) and most experiments conducted on a similar composition, but with sodium sulfate instead of sodium carbonate (SNC-1.0-28, SNC-1.0-30, SNC-0.5-29, and SNC-J-31). There appears to be a correlation between the amount of sodium sulfate in the original mixture and the loss of sodium (Figure 45). This is suggested by SNC-E-18 (no sodium sulfate), SNC-0.5-29 (10 % sodium sulfate), and SNC-1.0-30 (21 % sodium sulfate). However, two experiments with the same mixture and the same conditions resulted in widely different losses (0-20 %) (SNC-1.0-28 and SNC-1.0-30).

There appears in general to be two groupings in Figure 45. One group has high sodium loss and indication for sodium sulfate coating on the surface. The other has low sodium loss and no indication for sodium sulfate coating. There are, however, exceptions since some experiments falling within the

high loss field do not indicate sodium coating. It is uncertain whether this is because the coating has been removed due to decomposition or whether it never existed in the instance.

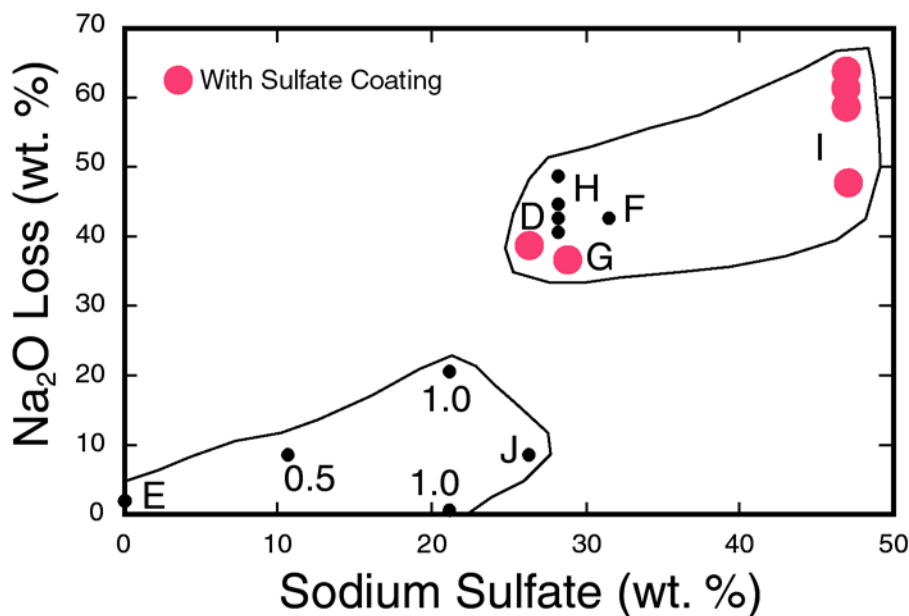


Figure 45. Loss of Na_2O (wt. %) from glass during melting as a function of original sodium sulfate (wt. %). Red dots indicate the detection of sodium sulfate coating.

The results of experiment SNC-I-26 allowed us to perform mass balance calculations since we were able to measure the relative proportions of sulfate coating and glass (Table 7). Experiment SNC-I-26 contained 600 g mixture before melting and 528 g after melting. Of the latter, 172 g was sulfate coating (33 %).

Table 16. Estimated Losses of Sulfur and Sodium (SNC-I-26)

Mixture	Mixture I		Glass		Sulfate Coat		SNC-I-24 Bulk Calculated	Loss/Gain*	
	As mixed	CO ₂ -free	Analyzed	Total to 100	Analyzed	Total to 100		Wt. % Oxides	%
SiO ₂	41.20	43.64	68.37	69.99			43.64		
Na ₂ O	14.18	15.02	12.46	12.75	35.95	44.68	24.77	-9.75	-39
K ₂ O					0.08	0.10	0.04	-0.04	
Al ₂ O ₃			0.78	0.80			0.50	-0.50	
CaO	8.74	9.26	8.82	9.03	4.18	5.19	7.59	1.67	
MgO	3.75	3.97	6.22	6.37			3.97		
P ₂ O ₅			0.07	0.07	0.07	0.09	0.08	-0.08	
Cl	0.59	0.62	0.13	0.13	0.08	0.10	0.12	0.50	
CO ₂	5.28	5.59					0.00		
SO ₃	25.96	27.50	0.84	0.86	40.11	49.84	19.30	8.20	42
Total	99.69	100.00	97.69	100.00	80.47	100.00	100.00		

* Losses/ gains calculated using proportions of 37.6 % sulfate coating and 62.4 % glass result in zero gain/loss for SiO₂.

MgO and Na₂O content of mixture has been adjusted to zero loss/gain for MgO.

Negative values are gained, positive values are lost.

The calculations given in Table 16 balance the compositions of the reactant (Mixture I) with the products of experiment SNC-I-26 (glass and sulfate coating). The calculations assume

that both SiO_2 and MgO are balanced. The latter requires that the MgO content of the reactant mixture is significantly underestimated (3.75 as opposed to 1.26 wt. % MgO). A total of 42 % of SO_3 appear to have been lost from the products during the experiment suggesting that 58 % of SO_3 is retained as solid sulfate in the experimental products. The effect of the sulfate coat thus is to restrict the loss of sulfur to the furnace gas. A small gain of Al_2O_3 can be attributed to reaction with the container, while most chlorine is lost to the vapor. A relatively small loss of CaO may be attributed to an underestimation of anhydrite of the bulk coating.

Physical Properties of Molten Glass and Sodium Sulfate

The relative densities and surface tensions of molten sodium sulfate and coexisting glass melt will indicate whether the accumulation of molten sodium sulfate on top surfaces of the experimental products is feasible.

The density of solid sodium sulfate is 2.66 g/cm^3 (Lide, 1991). Little appears to be known about the properties of molten sodium sulfate. Ueda et al. (1999) determined the density of molten sulfate as 1.97 g/cm^3 (at 827°C). Jaeger (1917) determined the density as a function of temperature (summarized by Stern, 2001). The existing data are summarized in Figure 46. The extrapolation of the existing data to 1300°C suggests a density of molten sodium sulfate around 1.85 g/cm^3 . The compilation of Janz (1967) suggest that the extrapolated surface tension at 1300°C is 0.21 N/m , relatively higher than would have been expected from the result of Ueda et al (1999) that suggests a surface tension of 0.1784 N/m at 827°C .

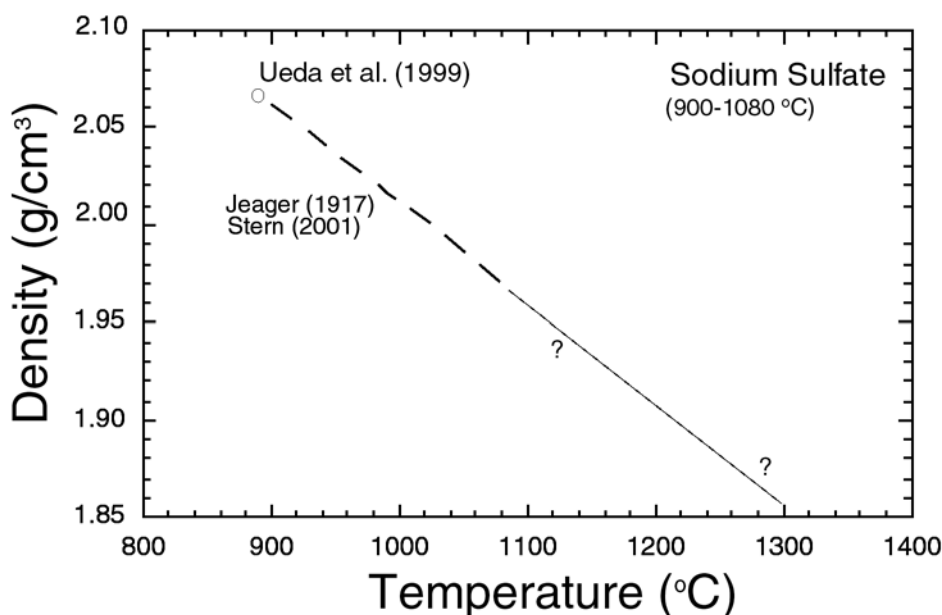


Figure 46. The density of molten sodium sulfate between 900°C and 1080°C as experimentally determined and extrapolated to 1300°C .

Typical window glass has a density of about 2.47 g/cm^3 (Doremus, 1994). The density of molten glass at 1300°C can be estimated from partial molar volumes (Bottinga and Weill, 1970; Bottinga et al., 1982; Lange and Carmichael, 1987). The average values obtained for the glass compositions in Table 10 is 2.38 g/cm^3 that is representative for the compositions used in this study at melting temperature of 1300°C . There is a considerable variation dependent on melt composition (Figure 47) caused by a positive correlation between density and CaO and a negative correlation between density and Na_2O and SiO_2 .

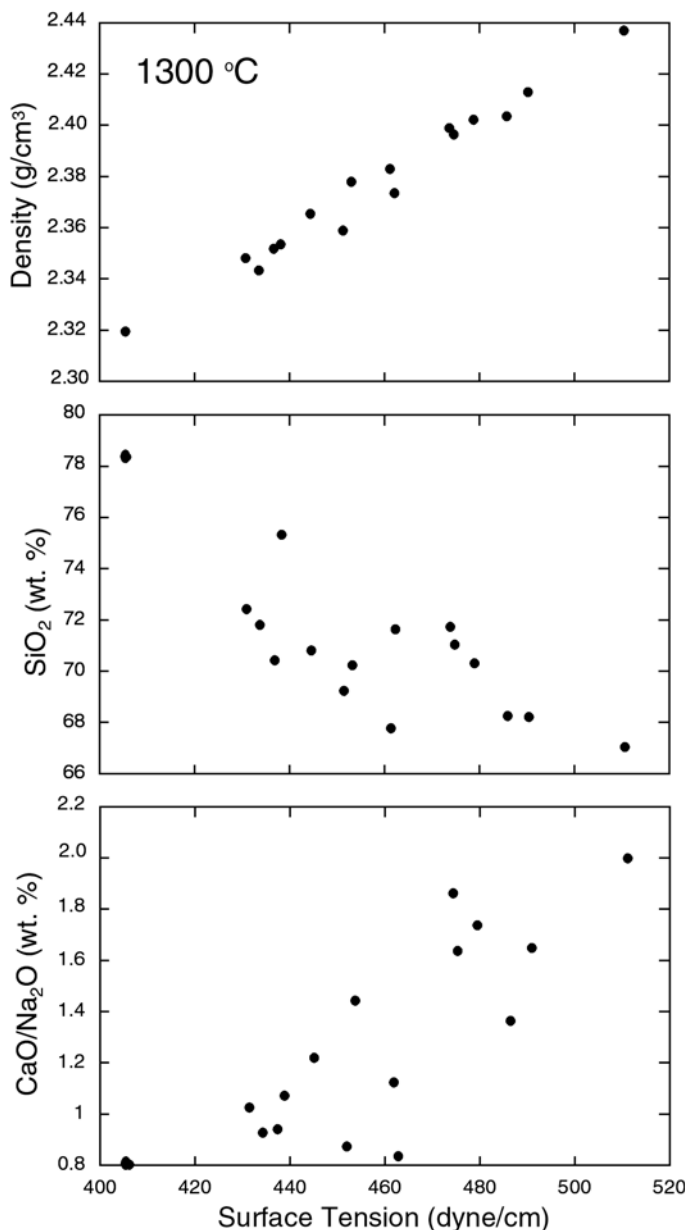


Figure 47. Summary of calculated isothermal physical properties of the glass compositions of Table 10. Shown are the surface tension (dyne/cm) and density (g/cm^3) and their dependencies on SiO_2 content and $\text{CaO/Na}_2\text{O}$ ratio of the glass. All calculations were done for a temperature of 1300°C .

The surface tension for a silicate melt can be calculated using the additive component approach of Boni and Derge (1956) with data from Mills (1986) for Na_2O . The average value for the present glass melts are 458 dyne/cm again at a temperature of 1300 °C. The surface tension is as for the density negatively dependent on SiO_2 and Na_2O and positively dependent on the CaO or the $\text{CaO}/\text{Na}_2\text{O}$ ratio (Figure 47). The surface tension for glass melt is thus significantly higher by a factor of 2-3 compared to the surface tension of molten sodium sulfate determined at 178 dyne/cm (0.1784 N/m) by Ueda et al. (1999) at 1100 °C. The effect of temperature on surface tension is uncertain and often considered to minimal.

The viscosity of molten glass at 1300 °C can be calculated using the additive component approach developed by Bottinga and Weill (1972) and Shaw (1972). The results for the present glass melts show wide variation with an average value of 2.3 log poise and a total range of 1.8-2.9 that apparently is not correlated with chemical composition.

DISCUSSION

Formation of Sulfate Coating

The presence of a sulfate coating on some of the experimental products suggests that sodium together with sulfur can be partially removed from the silicate melt in the form of a sodium sulfate melt. During cooling, this melt crystallizes as a double sulfate salt (Figures 38 and 39) that is effectively isolated from reacting with the main glass melt. At low temperature, probably below 200 °C (Müller, 1910), the solid sulfate exsolves to form a submicroscopic intergrowth of thenardite (Na_2SO_4) and glauberite ($\text{Na}_2\text{Ca}(\text{SO}_4)_2$) (Figure 40; Table 14), with approximately 10 % of the latter. The thermodynamic modeling predicts a mixture of thenardite and anhydrate (Figure 11) and also suggests that the anhydrate component increases as sulfate increases in the starting composition, however, without exceeding 30 % of the total sulfates. Considering that glauberite can be viewed as a solid solution of thenardite and anhydrate, this thermochemical modeling result appears, in general, to be consistent with the experimental findings.

The formation of a sodium sulfate melt is well supported by thermodynamic modeling (Figure 10), which shows that a sulfate melt forms from about 900 °C and remains as a melt until about 1200 °C, at which temperature it starts to decompose to Na_2O and SO_2 as a result of interaction with the silicate melt. The SO_2 is released to the furnace atmosphere, while Na_2O is incorporated into the silicate melt. Our experiments show that in some cases when large amounts of sodium sulfate (synthetic or natural) were present in the original mixture, the sodium sulfate melt segregates to the top of the experimental product as a liquid layer that persists, in closed systems, at least to, or higher than, the maximum temperature of 1300 °C utilized in this study. Thus, the sodium sulfate layer remains at much higher temperatures than suggested by the thermodynamic modeling for equilibrium conditions. We speculate that the main mechanism behind the separation of sulfate melt from the silicate melt is the relatively low density and surface tension compared to the silicate melt.

The formation of sodium sulfate coatings during glass making is not commonly reported in the literature because typically only small proportions of sodium sulfate (1-2 wt. %) as an

additive are used at concentration levels near or slightly above maximum solubility level of Na_2SO_4 (Kim and Hrma, 1991; 1992; Hrma and Kim, 1993; Beerkens, 2003). In our previous study of glasses produced from rice straw ash and natural sodium sulfate (Jenkins et al, 1998), we observed a water soluble coating inferred to be composed of potassium sulfate.

The formation of SO_2 (or SO_3) gas bubbles is used in glass making to accelerate quartz grain dissolution and to remove excess CO_2 from the melt (fining). Foaming, or the preservation of bubbles, at or near the glass surface can be reduced by balancing the heating rate and sulfate content. High sulfate contents and heating rates may result in formation of sulfate melts that can inhibit dissolution and fining (Kim and Hrma, 1991). The high concentrations of sodium sulfate used in this study are well above maximum solubility in the silicate melt allowing sulfate melt to form and as we have observed to migrate and accumulate on the surface of the silicate melt. However, only modest bubble formation and retention in the glass was observed in our study. It is likely that the bubbles can be further removed by lowering the cooling rate during glass formation. It is also significant that we did not observe partially undissolved silica grains in the glass as well as foaming on the surface. This suggests a relatively efficient dissolution of silica as well as removal of gas bubbles.

When sodium sulfate forms a separate layer on top of the molten silicate melt, it is effectively isolated from interacting with the silicate melt. The result is that both the sulfate and the silicate melts cool and solidify to a large extent as isolated systems. Direct experiments on sodium sulfate have shown that this phase melts and remains a melt at temperatures to 1900-2000 °C (Samadhi et al., 2002). If the sodium sulfate melt were not removed from the silicate melt, it would decompose at much lower temperatures of 1200 °C as a result of interaction with the silicate melt. Direct experiments on sodium sulfate have shown that for an open furnace system, with an influx of air, the decomposition of sodium sulfate may occur at 1300 °C leaving a residue of Na_2O . Without being able to react with sample container or a silicate melt, Na_2O is rapidly carbonated and hydrated at low temperature during cooling to thermonatrite ($\text{Na}_2\text{CO}_3 \cdot \text{H}_2\text{O}$) from reaction with furnace air. This suggests that the circulation in the furnace as well as the shape and size of the melting container may in part control the preservation, or demise, of the sodium sulfate coating. The preservation of a sulfate coating will be determined by such factors as the circulation of air in the furnace and shape, size, and surface area directly exposed to the circulating and replenished furnace air. It is possible that these factors may explain why is not observed despite being predicted in some of the experimental products (Figure 45).

Our study suggests that a sodium sulfate layer may form from compositions with above 25 % sodium sulfate in the original glass mixture (Figure 45). There also exists a correlation between the formation of a sulfate layer and the loss of sodium from the product glass. Between 35-65 % of the original Na_2O is lost with a broad positive correlation between Na_2O loss and sodium sulfate in original mixture. It is plausible that high concentrations of sodium sulfate droplets in the melt increase coalescence and the likelihood of gravitational migration to the surface to form a melt layer. Several experiments where a sulfate coating could be predicted, however, lack coatings (Figure 45). Predictions would be that the airflow in the furnace as well as the total duration at maximum temperature would correlate negatively with

the presence (or preservation) of a sulfate coating. The presence of an airflow through the furnace can explain some, but not all, of the anomalies.

Direct measurement of the release of CO_2 and SO_2 during melting of a typical sodium sulfate based window glass mixture shows that CO_2 is released early at 700-800 °C while SO_2 is released at much higher temperatures of 1200-1300 °C (Figure 9). This latter reflects exsolution of a sulfate melt that coexists with the silicate melt from about 900 °C to fairly high temperatures of 1200 °C or higher, well after carbonate decomposes. Sodium carbonate is normally used instead of sodium sulfate for glass making. Direct experiments on the decomposition of sodium and calcium carbonate suggest that both carbonates decompose at about 700-800 °C (Figures 5 and 6). It is possible that a sodium carbonate melt is stable to 800-900 °C in a closed system (Stern, 2001). However, in silicate melts it is plausible that carbonates behave nearly identical and decompose at temperatures below melting of sodium sulfate in a silicate melt (Figure 7).

There is another important observation from the thermodynamic modeling that attests to the different behavior of sulfate and carbonate in glass melts. While the solubility of CO_2 in the silicate melt is very low (Blank and Brooker, 1994), the solubility of SO_2 is much higher (Beerkens, 2003) and markedly is dissolved into the melt during melting. The sulfur content measured as Na_2SO_4 and CaSO_4 increased markedly in the silicate melt to a maximum sulfate total of 13 % at about 1150 °C and, thereafter, decreased to near zero at 1300 °C. Sulfur is detectable in some of the experimental glasses in concentrations below 1.2 wt. % as SO_2 . Likewise, chlorine can be detected in some glasses formed using natural sodium sulfate in concentrations below 0.6 wt. % Cl. The concentration gradients of SO_2 and Cl in these glass batches suggest diffusion out of the silicate melt. By increasing the duration at maximum temperature these components may effectively be eliminated from the glasses.

Glass mixtures based on sodium sulfate as a source for sodium thus melt significantly differently compared to ordinary window glass mixtures. Melting of sodium sulfate occurs after the decomposition of carbonate and presumably the reaction between CaO and SiO_2 to form a melt from 700-800 °C. Sodium sulfate melts at 900 °C and forms droplets in the melt and to a certain extent also is dissolved in the silicate melt. The droplets are in equilibrium with the calcic silicate melt and remain so until about 1200 °C when the decomposition accelerates leading to the removal of SO_2 and the reaction of Na_2O and the CaO-SiO_2 dominated host melt. Concurrently with the increase of Na_2O in the melt, the sulfur solubility in the melt is markedly reduced. If this interpretation is correct, Na_2O is only fully incorporated into the melt from about 1200 °C. The implication is that during the melting interval the CaO content of the melt will be higher and Na_2O lower than the fully melted glass mixture, as also observed in the thermodynamic modeling (Figure 14). This situation will be somehow different if the sodium sulfate melt is gravitationally removed in which case the melt will remain high in CaO and low in Na_2O . It should be noted that this interpretation is largely speculative, as the relevant experiments have not been conducted.

The sulfate coating is composed of sodium, calcium, and sulfur with other elements in very low concentrations. Particularly, magnesium and iron are below detection limits in the sulfate coating despite that at least magnesium is present in the salt in significant concentrations of

3-4 wt. % MgO. This illustrates that the natural salt is purified by the melting process and that some elements like Mg are completely retained in the silicate melt. The intergrowth of thenardite and glauberite can easily be further purified. There are large differences in the water solubility of the various sulfate phases. Thenardite is easily dissolved in water (52 g per 100 cc water at 32°C) while glauberite (12 g per 100 cc water) and gypsum (0.2 g per 100 cc water) have much lower solubilities (Harvie et al., 1984; Spencer, 2000). Furthermore, glauberite dissolves in water leaving gypsum as a residual solid that mechanically can be removed (Figure 44). This allows sodium sulfate to be further purified.

Crystallization and Devitrification

Many experiments exhibit crystallization and devitrification processes that transform the optical and physical properties of the glass. Detailed microscopic and compositional examination has shown that these are caused by the nucleation and crystallization of tridymite. The nucleation appears to occur heterogeneously on preexisting tridymite grains, along the surface, and sides of container. There is no indication that homogeneous nucleation occurs and that the glass should be inherently unstable.

The unexpected appearance of tridymite can be explained by considering the effect of sulfate removal. Partial removal of sodium in the form of sodium sulfate during melting markedly changes the compositions as well as the physical properties of the resultant melt and glass. The effect and magnitude of this removal of sodium (<60 wt. % Na₂O of original target compositions) are illustrated in Figure 46. Because the main loss is Na₂O, the melt compositions are shifted horizontally parallel to the Na₂O-SiO₂ join in the ternary Na₂O-CaO-SiO₂ phase diagram. It is seen that for some compositions also a small loss of calcium also occurs, consistent with analyses of sulfate coatings (~5 % CaO).

Many starting compositions shift from the liquidus fields for Ca-Na silicates into the quartz or tridymite field. By comparing Figure 46 with Figure 16, it can be observed that the main effect, in addition to changing the liquidus mineral from mostly Na₂O.3CaO.6SiO₂ ('devitrifite') to tridymite, is a dramatic increase in the liquidus temperature. This raise in liquidus temperature amounts to 200-400 °C for many glass compositions and occurs when sodium sulfate is separated from the melt and accumulated on the surface. The effect is a liquidus temperature of 1200-1400 °C and a glass melt that is saturated, or near saturated, in tridymite despite that the target liquidus was only 1000 °C and the equilibrium mineral phase would have been sodium-calcium silicates. Tridymite is thus likely to appear in many of these experimental products either as equilibrium liquidus phases or during cooling as metastable quench phases. Experimental products with liquidus near or just below 1300 °C would be expected to show incomplete resorption of tridymite grains and may retain submicroscopic nucleates that may easily act as nucleation and growth sites for tridymite during cooling. This would explain many of the anomalous results where tridymite appears to be stable and/or to easily nucleates during cooling (devitrification).

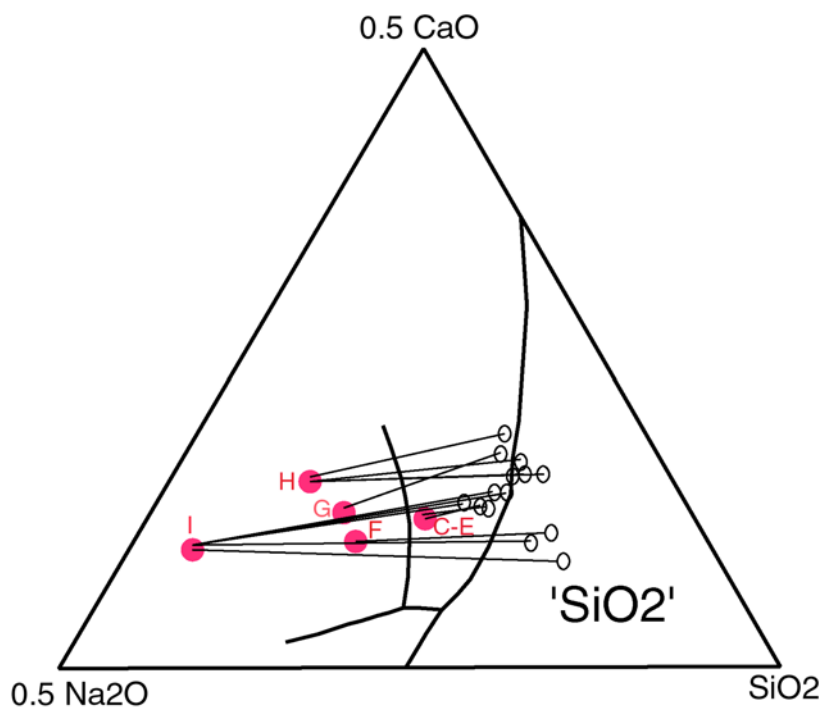


Figure 46. Part of the ternary Na_2O - CaO - SiO_2 system showing the target glass compositions in red (from Figure 15) and the effect of the observed loss of Na_2O and small amounts of CaO . Schematically shown are phase boundaries on the liquidus with the field for silica polymorphs (' SiO_2 ') and various Na-Ca silicates (compare to Figure 15).

There are two other factors that may contribute to differences between the target and the resultant glass compositions. First, the natural sulfate salt contains small amounts of water. The analysis given in Table 2 suggests about 4-5 wt. % H_2O . The use of such a salt in the glass mixture would imply that the sodium content be lower in the resultant glass than anticipated by about 2 %. This amount is, however, insufficient to account for the large losses observed for many starting compositions. Furthermore, analysis of sodium in glasses is complicated by being easily evaporated during electron beam analyses resulting in microprobe analyses that are anomalously low in sodium and high in silica. This evaporation of sodium can easily be controlled by reducing beam current and by analyzing over an enlarged area. Applications of such measures together with control analyses of well-known standards of sodium rich glass has shown that the sodium loss during analyses are minimal. Such an analytical loss is furthermore not plausible due to the presence of tridymite that must have crystallized prior to analysis.

Optimal Conditions for Glass Formation

Several factors influence glass formation and preservation. The composition of a glass mixture determines the overall equilibrium relations, including the liquidus temperature (complete melting), as well as solidus and subliquidus phase relations during both melting and quenching. The glass composition examined in this study is a typical industrial window glass with a liquidus of about 1000 °C. The maximum melting temperature was thus chosen 300 °C higher at 1300 °C. This melting temperature is somehow lower than for many industrial applications, but is still expected to

result in complete melting and also easily to destroy unmelted crystalline particles in the melt that could act as nucleation points during cooling and the transition to glass.

It was, therefore, unexpected to observe ample sign of unmelted material and devitrification for the glass mixtures containing high contents of sodium sulfates. The reason is that changes in glass composition occur during melting as a result of the combined loss from the glass melt of sodium and sulfur. Because of the sharp liquidus rise of the 'silica' field in the Na_2O - CaO - SiO_2 ternary phase diagram (Figure 16), a partial loss of sodium easily shifts the glass composition toward increasing SiO_2 with constant CaO , well within the quartz and tridymite field below liquidus conditions. This will result in partial melting and will also likely increase the ease with which devitrification occurs during cooling because of the presence of abundant nucleation sites in the melt. Large sodium loss do not occur in a standard glass composition, based on sodium carbonate, because carbonate decomposes at low temperature and do not form a high temperature immiscible melt that is preserved to very high temperature and also able to segregate from the silicate melt.

Many of the unexpected results showing partial melting and strong devitrification can clearly be explained by such an unintentional rise in liquidus temperature and a consequent change in the stable liquidus assemblage. Attempts to compensate for the sodium loss by increasing sodium content in the glass mixture were unsuccessful and caused increased sodium loss without clear indications that a higher proportion of sodium was retained in the silicate melt as intended. A further attempt to compensate for the raise in liquidus was to raise the melting temperature. Melting an example of a partial unmelted and devitrified product between 1300 °C and 1450 °C increased the melt fraction still without reaching liquidus conditions.

The melt duration was shown to have some effect on devitrification. Experiments to 100 hours clearly showed a marked decrease in the amount of devitrification. This is expected since increased duration will increase the destruction of remaining nucleation sites in the melt and thus inhibits nucleation and crystal growth during cooling and glass formation. Long melting duration at high temperature may also decompose sodium sulfate remaining in the silicate melt. It is thus plausible that the combined effect of increased melting temperature (~1500-1700 °C) as well as extended melting duration (20-100 hours) will increase the likelihood of complete melting and glass preservation. However, such solutions require high power and/or fuel consumption that make them technological and economical unattractive.

Restricting the amount of sulfate in the glass mixture to below 25 % appears to eliminate the separation of sulfate from the silicate melt and thus to restricts the loss of sodium. Therefore, raising the melting temperature to 1500 °C and optimizing duration to eliminate devitrification should produce clear glass for most typical industrial glass compositions with below 25 % sodium sulfate.

However, the ease with which devitrification occurs in most of the examined compositions suggests that interaction between sodium sulfate melt and quartz and tridymite grains during melting may severely restrict dissolution and thus promote nucleation during cooling. Devitrification may thus be a fundamental property of sulfate rich glass mixtures that should be further explored. It is possible that properties of the devitrified material for some applications might be advantageous, as has been proven for some glass ceramic materials recently developed.

SUMMARY AND CONCLUSIONS

The effects of substituting natural and synthetic sodium sulfate for sodium carbonate in a typical soda-lime glass recipe were investigated in this study using thermodynamic and experimental techniques.

Both sodium and calcium carbonates decompose in a standard glass composition at about 800 °C. In contrast, sodium sulfate forms an immiscible melt that is stable in silicate melt to 1200-1300 °C, well above the liquidus temperature of the glass mixture (~1000 °C). The result is that melting behavior, melt composition, and physical melt properties during reaction and melting depend on whether sulfate or carbonate is used as source for sodium.

We have shown that sodium sulfate melt can segregate from molten glass forming a stable sulfate melt crust. The sulfate coating is composed of a mixture of thenardite and glauberite resulting from the high temperature crystallization and low temperature exsolution from an original sulfate melt. The preservation of the sulfate coating is controlled by the rate of decomposition that can be increased by a flow of air through the furnace as well as by the shape of container. Strong circulation and replenishment of the furnace gas along the melt surface will increase decomposition rate of sodium sulfate with the result that the sodium sulfate coating may be reduced or not preserved.

The most significant effect of this is a change in melt composition from the removal of sodium together with sulfate from the glass melt. This results in a marked rise in liquidus temperature and the appearance of tridymite as a stable liquidus phase for melt compositions that was expected to be completely melted at the chosen temperature of 1300 °C. The result is restricted melting and a strong devitrification effect during cooling with abundant nucleation of tridymite transforming the glass to a milky white, translucent, glass-ceramic material.

Glass mixtures with above 25-30 % sodium sulfate content may restrict segregation of sodium sulfate from the molten glass and therefore devitrification. Further, longer melting duration increases the likelihood of devitrification by destruction of potential nucleation sites in the melt.

The ease with which devitrification occurs suggests that interaction between sodium sulfate melt and crystalline grains during melting may severely restrict dissolution and thus promotes nucleation during cooling. Devitrification may thus be a fundamental property of sulfate-rich glass mixtures that should be further explored. It is possible that properties of the glass ceramic material for some applications might be advantageous.

REFERENCES

- Babcock, C.L., 1977. *Silicate Glass Technology Methods*. Wiley, New York.
- Bale, C.W., Chartrand, P., Degterov, S.A., Eriksson, G., Hack, K., Mahfoud, R.B., Melancon, J., Pelton, A.D., and Petersen, S., 2002. FactSage thermochemical software and databases. *Calphad* 26, 189-228.
- Bansal, N.P. and Doremus, R.H., 1986. *Handbook of Glass Properties*. Academic Press, San Diego.
- Beerkens, R.G.C., 2003. Sulfate decomposition and sodium activity in soda-lime-silica glass melts. *J. Am. Ceram. Soc.* 86, 1893-1899.
- Beerkens, R.G.C., 2003. Sulfate decomposition and sodium oxide activity in soda-lime-silica glass melts. *J. Am. Ceram. Soc.* 86, 1893-1899.
- Blank, J.G. and Brooker, R.A., 1994. Experimental studies of carbon dioxide in silicate melts: solubility, speciation, and stable carbon isotope behavior. In (Carroll, M.R. and Holloway, J.R., eds.) *Volatiles in Magma*, 157-186. *Reviews in Mineralogy* 30, Mineralogical Society of America, Washing DC.
- Boni, R.E. and Derge, G., 1956. Surface tensions of silicates. *J. Metals* 8, 53-59.
- Bottinga, Y. and Weill, D.F., 1972. The viscosity of magmatic silicate liquids: a model for calculation. *American Journal Science* 272, 438-475.
- Bottinga, Y. and Weill, D.F., 1970. Densities of liquid silicates systems calculated from partial molar volumes of oxide components. *American Journal Science* 269, 169-182.
- Bottinga, Y., Weill, D., and Richet, P., 1982. Density calculations for silicate liquids. 1. Revised method for aluminosilicate compositions. *Geochimica Cosmochimica Acta* 46, 909-919.
- Burnett, D.G. and Douglas, R.W., 1970. Immiscibility, nucleation and crystal growth in the soda-baria-silica system. *Discussions Faraday Society* 50, 200-205.
- Cervinka, V., Diener, J., Erickson, J., Finch, C., Martin, M., Menezes, F., Peters, D., and Shelton, J., 1999. Integrated system for agricultural diainage management on irrigated farmland. Final Report, Grant Number 4-FG-20-11920, US Department of the Interior, Bureau of Reclamation, Fresno, California.
- Copper, A.R., 1986. Glass melting. In (Bever, M.B., ed.) *Encyclopedia of Materials Science and Engineering*, Vol. 3, 1986-1989. Pergamon Press, Oxford.
- Doremus, R.H., 1994. *Glass Science*. 2nd Edition. John Wiley, New York.
- Hardie, L.A., Moller, N., and Weare J.H., 1984. The prediction of mineral solubilities in natural waters: The Na-K-Mg-Ca-Cl-SO₄-OH-HCO₃⁻-CO₃-H₂O system to high ionic strengths at 25 oC. *Geochim. Cosmochim Acta* 48, 723-751.
- Hrma, P. and Kim, D., 1994. Sulfate mass balance and foaming threshold in a soda-lime glass. *Glass Technology* 35, 128-134.
- Janz, G.J. and Lorenz, M.R., 1961. Molten carbonate electrolytes: physical properties, structure, and mechanism of electrical conductance. *J. Electrochemical Society* 108, 1052-1058.
- Janz, G.J., 1967. *Molten Salts Handbook*. Academic Press, New Youk.
- Jenkins, B.M., Sun, G., Cervinka, V., Faria, J., Thy, P., Kim, D.H., Rumsey, T.R., and Yore, M.W., 2003. Salt separation and purification concepts in integrated farm drainage management systems. ASAE Paper No. 032236, ASAE Annual Meeting, Las Vegas, Nevada.
- Jenkins, B.M., Thy, P., Liu, P.Y., Leshner, C.E., Beland, A., and Cervinka, V., 1998. Preliminary investigarion into the vitrification of salt from evaporation drain water. Final Report, Westside Resource Conservation District and California Department of Water Resources, Sacramento.
- Jones, G.O., 1956. *Glass*. Methuen, London.

- Kim, D.-S. and Hrma, P., 1991. Foaming in glass melts produced by sodium sulfate decomposition under isothermal conditions. *J. Am. Ceram. Soc.* 74, 551-555.
- Kim, D.-S. and Hrma, P., 1992. Foaming in glass melts produced by sodium sulfate decomposition under ramp heating conditions. *J. Am. Ceram. Soc.* 75, 2959-2963.
- Lange, R.A. and Carmichael, I.S.E., 1987. Densities of Na_2O - K_2O - CaO - MgO - FeO - Fe_2O_3 - Al_2O_3 - TiO_2 - SiO_2 liquids: new measurements and derived partial molar properties. *Geochimica et Cosmochimica Acta* 51, 2931-2946.
- Lide, 1991. *CRC Handbook of Chemistry and Physics*. CRC Press, Boca Raton.
- Mills, K.C., 1986. Estimation of physicochemical properties of coal slags and ashes. In (Vorres, K.S., ed.) *Mineral Matter and Ash in Coal*, 195-214, ACS Symposium Series, Am. Chem. Soc., Washington D.C.
- Morey G.W. and Bowen, N.L., 1925. The ternary system sodium metasilicate-calcium metasilicate-silica. *J. Soc. Glass Technology* 9, 226-264.
- Morey, G.W., 1930. The devitrification of soda-lime-silica glass. *J. Am. Ceram. Soc.* 13, 683-713
- Morey, G.W., 1954. *The Properties of Glass*. 2nd Edition. Reinhold, New York.
- Müller, H., 1910. Binary systems of the sulfates of alkalis and calcium. *Nues Jahrb. Min. Geol. (Beil. Bd.)*, 30, 1-54 (in German).
- Palache, C., Berman, H., and Frondel, C., 1951. *The System of Mineralogy*. Seventh Edition, John Wiley, New York.
- Pearce, M.L., 1964. Solubility of carbon dioxide and variation of oxygen ion activity in soda-silica melts. *J. Am. Ceram. Soc.* 47, 342-347.
- Rekhson, S.M., 1986. Glass transition. In (Bever, M.B., ed.) *Encyclopedia of Materials Science and Engineering*, Vol. 3, 2008-2011. Pergamon Press, Oxford.
- Samadhi, T.W., Elliott, J.C., Jones, L.E., and Clare, A.G., 2001. Sodium decomposition in dry atmospheres. *Glastech. Ber, Glass Sci. Technol.* 74, 47-56.
- Shaw, H.R., 1972. Viscosity of magmatic silicate liquids: an empirical method of prediction. *American Journal Science* 272, 870-893.
- SJVDIP, 2000. Evaluation of the 1990 drainage management plan for the Westside San Joaquin Valley, California. Final Report, San San Joaquin Valley Drainage Implementation Program (SJVDIP). California Department of Water Resources, Sacramento.
- Spencer, R.J., 2000. Sulfate minerals in evaporate deposits. In (Alpers, C.N., Jambor, J.L., Nordstrom, D.K., eds.) *Sulfate Minerals. Crystallography, Geochemistry, and Environmental Significance*. Reviews in Mineralogy and Geochemistry 40, 173-192. Mineralogical Society of America, Washington D.C.
- Stern, K.H., 2001. *High Temperature Properties and Thermal Decomposition of Inorganic Salts with Oxyanions*. CRC Press. Boca Raton.
- Stookey, S.D. and Maurer, R.D., 1962. Catalyzed crystallization of glass – theory and practice. *Progress Ceramic Science* 2, 77-101.
- Strnad, Z., 1971. Determination of the solubility of carbon dioxide at various partial pressures in soda-silica melts using gas chromatography. *Physics Chemistry Glasses* 12, 152-155.
- Swartz, E.L., 1986. Fining of glass. In (Bever, M.B., ed.) *Encyclopedia of Materials Science and Engineering*, Vol. 3, 1769-1771. Pergamon Press, Oxford.
- Tanji, K.K., Ong, C.G.H., Dahlgren, R.A., and Herbel, M.J., 1992. Salt Deposits in evaporation ponds: an environmental hazard? *California Agriculture* 46, 18-21.

- Ueda, T., Tanaka, T., and Hara, S., 1999. Thermodynamic evaluation of surface tension of molten salt mixtures in alkali halides, nitrate, carbonate and sulfate systems. *Z. Metallkd.* 90, 342-347.
- USDOI/CRA, 1990, A management plan for agricultural subsurface drainage and related problems on the Westside San Joaquin Valley. Final Report, San Joaquin Valley Drainage Program. US Department of Interior and California Resources Agency, California Department of Water Resources, Sacramento.
- Wicks, G.G., 1986. Glasses: structure. In (Bever, M.B., ed.) *Encyclopedia of Materials Science and Engineering*, Vol. 3, 2020-2025. Pergamon Press, Oxford.



Close-up of contact between glass and container wall (see Frontispiece)